Reconstructing Baltic Sea hypoxia from sediment cores

Supervisors:
dr. T.J. Jilbert
dr. C.P. Slomp

Simon Veldhuijzen

Master Thesis

Department of Earth Sciences
Faculty of Geosciences
University of Utrecht
Wednesday June 11^{th} 2014

Abstract

The establishment of hypoxia (oxygen concentrations of <2 ml L^{-1}) and associated dead zones in coastal marine systems is receiving increasing attention. The Baltic Sea may be a good target for extensive research into present-day hypoxia as well as hypoxia throughout the Holocene. While several hypoxic periods in the Baltic Sea have been identified (such as the Holocene Thermal Maximum (HTM) and the Medieval Climate Anomaly (MCA)), most of these studies use low-resolution records. In this study, hypoxia at F80 in the Baltic Sea and SR5 in the Bothnian Sea has been reconstructed on a high, sub-annual resolution using Laser Ablation-Inductively Coupled Plasma-Mass Spectrometry. Onset of hypoxia in the Baltic Sea requires a complex interplay of several different forcings such as precipitation, internal and external nutrient loading and inflow through the Danish Straits to influence nutrient availability and stratification. Hypoxia during the MCA may have been forced – in part – by anthropogenic influences. Anthropogenic influences on modern hypoxia are virtually certain. Correlations with climatic records throughout Europe show the important role of large-scale multi-decadal climatic variability such as the North Atlantic Oscillation.

Contents

1 Introduction **5**
- 1.1 Hypoxia in the Baltic Sea . . . 5
- 1.2 Unanswered questions about past hypoxia in the Baltic Sea . . 7
- 1.3 Redox sensitive behaviour of selected elements . . . 8
  - 1.3.1 Manganese (Mn) . . . 8
  - 1.3.2 Iron (Fe) . . . 10
  - 1.3.3 Molybdenum (Mo) . . . 11
  - 1.3.4 Uranium (U) . . . 12
  - 1.3.5 Vanadium (V) . . . 13
  - 1.3.6 Bromine (Br) . . . 13
- 1.4 Relevant techniques . . . 14
  - 1.4.1 Laser Ablation-Inductively Coupled Plasma-Mass Spectrometry (LA-ICP-MS) . . . 14
  - 1.4.2 Wavelet and spectral analysis . . . 15

2 Methods **21**
- 2.1 Sediment coring . . . 21
- 2.2 Discrete samples . . . 21
- 2.3 Resin embedding and LA-ICP-MS . . . 22
- 2.4 LA-ICP-MS data calibration . . . 22

3 Results **28**
- 3.1 Identification of hypoxic events in discrete sample profiles and LA-ICP-MS data . . . 28
  - 3.1.1 F80 . . . 28
  - 3.1.2 SR5 . . . 29
- 3.2 High-resolution LA-ICP-MS profiles of selected intervals . . . 30
  - 3.2.1 Holocene Thermal Maximum at SR5 . . . 30
  - 3.2.2 Holocene Thermal Maximum at F80 . . . 33
  - 3.2.3 Medieval Climate Anomaly at F80 . . . 36
  - 3.2.4 Modern hypoxic event at F80, LL19 and BY15 . . . 39
- 3.3 Spectral analysis results . . . 41

4 Discussion **47**
- 4.1 Techniques . . . 47

4.1.1 Laser Ablation-Inductively Coupled Plasma-Mass Spectrometry . . . 47
4.1.2 Calibration of the LA-ICP-MS (trace) elemental records 48
4.2 Critical assessment of Mo/Al peak counting as a dating technique . . . 50
4.2.1 Mo/Al peak counting . . . 50
4.2.1.1 Validation of Mo/Al peak counting approach: modern hypoxic interval . . . 50
4.2.1.2 Application of Mo/Al peak counting to construct age models for older intervals . . . 51
4.2.1.3 Possible future improvements to dating approach . . . 53
4.2.2 Sedimentation rates . . . 53
4.2.2.1 Influence of detrital versus non-detrital material on sedimentation rates . . . 53
4.2.2.2 Comparison of methods for inferring sedimentation rates . . . 55
4.3 Euxinia and redox conditions recorded in Baltic Sea high-resolution (trace) elemental records . . . 59
4.3.1 Validity of molybdenum as redox proxy . . . 59
4.3.2 Reorganisation of hypoxic events . . . 60
4.3.3 Baltic Sea hypoxic intervals throughout the Holocene . 60
4.3.4 Causes of onsets and terminations of Baltic Sea hypoxia 61
4.3.4.1 Nutrient loading as driver of Baltic Sea hypoxia 61
4.3.4.1.1 Internal forcings on Baltic Sea nutrient loading . . . 62
4.3.4.1.2 External forcings on Baltic Sea nutrient loading . . . 65
4.3.4.2 Stratification of the water column as driver of Baltic Sea hypoxia . . . 68
4.3.4.3 Combinations of different forcings as triggers of hypoxic events . . . 71
4.3.5 Rapidity of onsets of hypoxic events . . . 72
4.3.6 Fe/Al as indicator of regional-scale hypoxic conditions 76
4.3.7 Multi-decadal to centennial cycles and patterns in Baltic Sea hypoxia . . . 79
4.3.7.1 Internal variability . . . 80
4.3.7.2 Climatological variability . . . 80

4.4 Evolution of Baltic Sea hypoxia during the Holocene 85

5 Conclusions **87**
5.1 Techniques and age model 87
5.2 Hypoxic events in the Baltic Sea during the Holocene 87
5.3 Suggestions for the future 90

6 Acknowledgements **91**

7 References **92**

1 Introduction

1.1 Hypoxia in the Baltic Sea

The Baltic Sea is a large body of brackish water between Sweden, Finland, Poland and the Baltic States (Figure 1.1). After its shift from fresh water to brackish water about 8 kyr ago (Berglund *et al.*, 2005) the Baltic Sea has been periodically hypoxic (Zillén *et al.*, 2008). Hypoxia describes the depletion of oxygen in the bottom waters and is often associated with bottom water oxygen concentrations lower than $2mLL^{-1}$. As a result of hypoxia, dead zones establish (Diaz and Rosenberg, 2008), leading to the extinction of benthic life (Vaquer-Sunyer and Duarte, 2008). In the Baltic Sea, hypoxia is currently present in about 20% of the total sea area, although this has been as low as 5% and as high as 27% between 1970 and 2000 (Conley *et al.*, 2002). Since the start of the twentieth century, hypoxia in the Baltic Sea has been increasing rapidly in intensity as well as in affected area (Fonselius and Valderrama, 2003).

Figure 1.1: Overview map of the Baltic Sea basin, indicating the sampled locations (A) and surface and deep water flows (B).

The only connection between the Baltic Sea and the North Sea is through the Danish Straits. Water inflow into the Baltic Sea through these Danish

Straits is slow. This slow inflow of water combined with strong stratification due to high differences in salinity leads to low ventilation rates throughout the Baltic Sea as well as long residence times of the deeper water (Gustafsson, 2012). The average residence time of deep Baltic waters is about 33 years (Omstedt and Hansson, 2006). On a decadal timescale, Major Baltic Inflows (MBIs) through the Danish Straits can ventilate the whole water column (Matthäus and Franck, 1992). Although this periodically decreases the hypoxia, with these MBIs large amounts of salt are transported from the North Sea to the Baltic Sea, causing enhanced stratification in the Baltic Sea (Reissmann *et al.*, 2009).

Hypoxic conditions are reached when the demand for oxygen exceeds the supply of oxygen, such as when high primary productivity in the surface waters causes large amounts of organic material to settle through the water column. It is possible for oxygen concentrations to be negative, indicating free sulphides are present. In this case oxygen conditions are said to be euxinic. Increased primary productivity in the Baltic Sea is thought to be caused by basin-wide eutrophication due to increasing nutrient input of anthropogenic origin during most of the twentieth century (Savchuk *et al.*, 2008). After this initial start of modern Baltic hypoxia, these hypoxic conditions are probably maintained by natural processes within the phosphorus (P) and nitrogen (N) cycles (Jilbert and Slomp, 2011).

Baltic Sea hypoxia is receiving increasing attention, and different studies are being undertaken to find a solution (Conley *et al.*, 2009a). Before any steps can be taken to reverse twentieth century eutrophication of the Baltic Sea a thorough understanding of processes related to hypoxic conditions is required (Conley *et al.*, 2009b). Investigating past periods of Baltic Sea hypoxia such as during the Holocene Thermal Maximum (HTM, 8–4 ka BP) and the Medieval Climate Anomaly (MCA, 950–1250 AD) would help increase this understanding. The behaviour of trace elements under hypoxic conditions could provide new insight into how hypoxic events in the past are recorded in sediment cores. A study by Jilbert and Slomp (2013a) shows that Molybdenum (Mo) to Aluminium (Al) ratios faithfully record the HTM, MCA and modern hypoxic intervals. These hypoxic intervals experienced high-amplitude variability of a frequency of multiple centuries (Jilbert and Slomp, 2013a). Furthermore, these intervals are characterised by the deposition of sapropels (layers of high organic carbon concentration). These sapropels are thought to be an effect of both increased primary production in the surface waters (Savchuk *et al.*, 2008) and increased organic carbon

(C_{org}) preservation due to low oxygen availability (Moodley *et al.*, 2005). High-frequency variability during Baltic Sea hypoxia in the HTM and the MCA could be related to climatic influences, such as changes in the North Atlantic Oscillation (NAO) influencing the ventilation rate of the Baltic Sea (Jilbert and Slomp, 2013a). Hypoxic conditions during the MCA were likely reached by (a combination of) increased nutrient loading of anthropogenic origin (Zillén and Conley, 2010) and/or increased sea surface temperatures (Kabel *et al.*, 2012).

1.2 Unanswered questions about past hypoxia in the Baltic Sea

This study will use high-resolution trace elemental records from three sediment cores to investigate how the chemistry of laminated Baltic Sea sediments records modern short-timescale climate and oceanographic variability, and to compare these signals to signals of past variability during the Holocene. To accomplish this, variability of different (trace) elements (most notably molybdenum and iron, but also vanadium, uranium and manganese) will be examined for the modern hypoxic event. These trace elemental records will be compared to bottom water oxygen data from the same sites to infer the response of these elements to changing redox conditions.

(Trace) elemental profiles of older hypoxic events during the HTM and MCA provide meaningful information that could not be gained from the modern hypoxic event alone. For example, research into the required conditions for termination of a hypoxic event benefits from reconstructions of past hypoxic events. The longer timespans present in older records allow for analysis of timescales typically related to hypoxic events as well as cyclicities that may be present. Last, Holocene records of hypoxia in the Baltic Sea can be compared with records of other climatic parameters to assess the relative importance of internal and external forcings on hypoxic events. Records of the older hypoxic events will therefore be used to try to distinguish internal and external influences on Baltic Sea hypoxia and provide their possible driving mechanisms. Onsets and terminations of these hypoxic events will be analysed to try to explain the conditions needed for the system to shift to and from hypoxia.

In addition to analysis into the causes of onsets and terminations of hypoxic events, a basin-scale reconstruction will be made of the modern hypoxic

event in the Baltic Sea. This will give insight into the evolution of a single hypoxic event through time and space. On a broader scale such a comparison can also be made between the Baltic Sea and the Bothnian Sea for the hypoxic events during the HTM. Such information on spatial variability of hypoxia during a hypoxic event can help in the identification of important processes playing a role during a hypoxic event.

The main aims of this study will therefore be to

- investigate how the chemistry of laminated Baltic Sea sediments records modern short-timescale variations in redox conditions;
- reconstruct the development of a single hypoxic event on a basin-scale;
- find the relative importance of both internal and external forcings and
- try to explain the mechanisms behind the onsets and terminations of hypoxic events.

1.3 Redox sensitive behaviour of selected elements

1.3.1 Manganese (Mn)

The naturally occurring valency states of manganese in seawater are $Mn(II)$, $Mn(III)$ and $Mn(IV)$. Under oxic conditions, $Mn(II)$ is usually dissolved as Mn^{2+} or $MnCl^{+}$ while $Mn(III)$ and $Mn(IV)$ are mostly in the form of insoluble Mn-oxyhydroxides. However, $Mn(II)$ is unstable under oxic conditions and is slowly oxidised to $Mn(III)$ and (dominantly) $Mn(IV)$ oxides (Calvert and Pedersen, 1993). Under anoxic conditions this process is reversed, and Mn-oxyhydroxides are reduced back to Mn^{2+}. This leads to an accumulation of dissolved $Mn(II)$ in deep, sulphidic waters (Spencer and Brewer, 1971).

Highest Mn concentrations in the water column can generally be found just above and just below the chemocline (i.e., the depth in the water column of the transition from oxic to sulphidic conditions) (Calvert and Pedersen, 1996). Here Mn-oxyhydroxides just above the chemocline settle down to be reduced in the sulphidic waters, producing dissolved Mn. This dissolved Mn then diffuses upward (and downward) to be oxidised again to Mn-oxyhydroxides (Figure 1.2). This self-maintaining cycle of Mn transport

across the chemocline plays an important role in the transport of trace metals from the water column to the sediment (Tribovillard *et al.*, 2006). Even under anoxic conditions Mn-oxyhydroxides can reach the sediment-water interface given their rapid settling rates. Any trace metals adsorbed onto these Mn-oxyhydroxides are released upon reduction in the sediment and become available for further reactions.

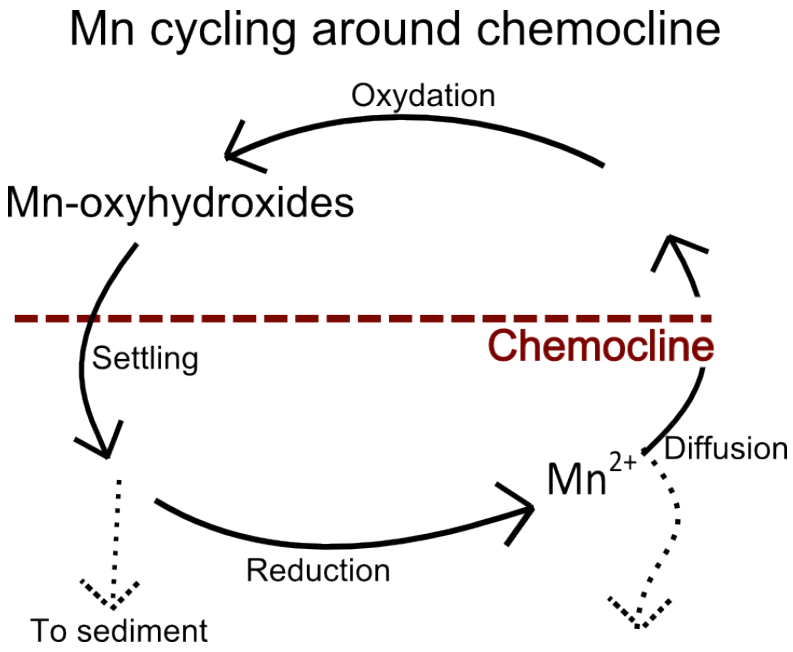

Figure 1.2: Manganese cycling around the chemocline.

Despite accumulation in anoxic bottom waters, Mn^{2+} concentrations don't reach levels permitting Mn-carbonates to form (Calvert and Pedersen, 1993). Euxinic sediments however could facilitate the precipitation of Mn-carbonates if pore water alkalinity is increased sufficiently as a result of sulphate reduction (Richards, 1965). Despite this possibility Mn-carbonates are mainly formed in anoxic sediments beneath oxic bottom waters. Oxic conditions in the bottom waters enable sedimentation of Mn-oxyhydroxides. Upon burial, these Mn-oxyhydroxides eventually pass the limit of the oxygen penetration depth, leading to reduction and subsequent release of dissolved Mn^{2+} (e.g., Middelburg *et al.*, 1987; Rajendran *et al.*, 1992). This released Mn^{2+} then diffuses both upward and downward. Dissolved Mn can freely diffuse partly because it is rarely taken up by organic or sulphidic phases

(Huerta-Diaz and Morse, 1992). Upward diffusion leads to either precipitation of Mn-oxyhydroxides (upon reaching pore water oxygen) or escape of Mn^{2+} to the water column (Cruse and Lyons, 2004). Downward diffusion can lead to precipitation of Mn-carbonates if the pore water is supersaturated in Mn^{2+} with respect to rhodochrosite (i.e., the "pure" Mn-carbonate) (Pedersen and Price, 1982).

In short, manganese plays an important role as "shuttle" transporting trace metals from the water column to the sediment-water interface. The occurrence of Mn-carbonates in the sediment is mostly indicative of oxic bottom waters overlying anoxic sediments at time of precipitation.

1.3.2 Iron (Fe)

Behaviour of iron (Fe) is very similar to that of manganese when comparing its pattern of cycling around the chemocline (Tribovillard *et al.*, 2006). However, while manganese is dominantly precipitated as a Mn-carbonate, the contribution of Fe-carbonates is very low (Canfield *et al.*, 1993). Instead, iron mainly precipitates as an iron-sulphide under anoxic sediment and bottom water conditions, as opposed to oxic bottom waters for Mn-carbonate precipitation. When oxygen concentrations are sufficiently high iron will precipitate as Fe-oxyhydroxide instead.

In oxic waters, the dominant valency state of iron is $Fe(III)$. Around 92% of all inorganic iron species is in the form of the $Fe(OH)_3$ complex (Raiswell and Canfield, 2012). Under anoxic conditions iron is reduced to $Fe(II)$, with the Fe^{2+} ion as main species. Iron can precipitate in solid form under both oxic (Fe-oxyhydroxides, nanoparticulate ferrihydrites) and euxinic (pyrite) conditions (Raiswell and Canfield, 2012). This leads to the possibility of a lateral "shuttle" for iron developing from shelves to deeper parts of the sea (Lyons and Severmann, 2006). If oxygen concentrations are too low to form Fe-oxyhydroxides and H_2S concentrations are too low to form pyrite, iron can be released from the sediment by diffusion and transported laterally. Upon reaching either more oxidised or more sulphidic waters the iron can precipitate again. These specific conditions for mobilisation of iron from the sediment can be seen as a "window of opportunity" for the transport of iron from one site to another.

Iron can act as a trap for phosphorus reaching the sediment, since phosphorus is strongly adsorbed to iron oxyhydroxides (Jensen *et al.*, 1995; Ruttenberg, 1993). This relationship between Fe-oxyhydroxides and phospho-

rus causes an "Fe-cap" (Raiswell and Canfield, 2012), stopping phosphate from diffusing into the water column from the sediments as long as Fe-oxyhydroxides are present beneath the sediment-water interface. When oxygen concentrations drop, the Fe-oxyhydroxides are reduced and the phosphate bound to the iron is released. A positive feedback loop may follow from this process (van Cappellen and Ingall, 1997), where an initial decrease in bottom water oxygen levels is accompanied by reduction of Fe-oxyhydroxides, releasing phosphate. Released phosphate can then enable increased primary productivity in the surface waters, increasing the flux of organic matter to the sediment-water interface, further decreasing bottom water oxygen levels. Upon recovery of the system, the formation of Fe-oxyhydroxides traps phosphate, possibly leading to more rapid decrease in primary productivity.

1.3.3 Molybdenum (Mo)

Under oxic conditions, molybdenum mainly occurs in its $Mo(VI)$ valence state, with MoO_4^{2-} (molybdate) as the main species. Due to the nonreactive nature of this dissolved species, molybdenum is conservative in oxic waters (Calvert and Pedersen, 1993). Although molybdenum does not adsorb onto iron oxyhydroxides, it does do so with manganese oxyhydroxides (Tribovillard *et al.*, 2006). These Mn-oxyhydroxides act as shuttles transporting molybdenum from the water column to the sediment-water interface (Morford and Emerson, 1999). Upon reaching anoxic conditions in the sediment, the Mn-oxyhydroxides are reduced, releasing the molybdate. This essentially causes accumulation of Mo in surficial sedimentary pore waters and bottom waters (Berrang and Grill, 1974).

Accumulation of conservative dissolved molybdenum species in anoxic bottom and pore waters does not yet explain their fixation into the sediment. Because of the lack of any correlation between dissolved molybdenum concentrations and dissolved sulphide concentrations, it was thought that molybdate was scavenged directly from the water column and pore waters to co-precipitate with FeS (Bertine, 1972). When FeS was then converted to pyrite, it was thought molybdenum formed a separate insoluble sulphide phase (i.e., MoS_3) (Korolev, 1958). Helz *et al.* (1996) proposed a more direct role for H_2S, where the oxygen atoms in MoO_4^{2-} were sequentially replaced by sulphur. This ultimately (and relatively quickly) leads to the formation of thiomolybdates (MoS_4^{2-}) (Erickson and Helz, 2000).

These thiomolybdates are then scavenged by iron sulphides (Vorlicek *et*

al., 2004), metal-rich particles (most importantly Fe) and sulphur-rich organic molecules (Helz *et al.*, 1996). In the case of iron sulphide scavenging, this leads to the formation of compact Fe-Mo-S clusters (Helz *et al.*, 1996). Organic matter will scavenge molybdenum either indirectly through metal-rich particles carried by the OM or directly through O-S groups attaching to the molybdenum species (Tribovillard *et al.*, 2006). Note that, regardless of the process, consistent euxinic conditions are necessary to fix molybdenum in the sediment (Calvert and Pedersen, 1993; Erickson and Helz, 2000).

Although molybdenum is commonly used as proxy for benthic redox conditions, possible effects of basin reservoir ages should always be considered (Algeo, 2004). If the rate of molybdenum removal is higher than the rate of supply, accuracy of molybdenum reconstructions will decrease. This is especially likely in restricted, anoxic basins such as the Baltic Sea.

1.3.4 Uranium (U)

As with molybdenum, uranium acts conservatively under oxic conditions. With a valence state of $U(VI)$ it is present mainly as the nonreactive $UO_2(CO_3)_3^{4-}$ species. Although uranium seems to stay conservative in some anoxic basins (e.g., Todd *et al.*, 1988), most of these basins experience (slight) decreases in uranium concentrations over time (e.g., Anderson *et al.*, 1989).

Although laboratory experiments prove the labile nature of $U(VI)$ under anoxic conditions by showing that it can reduce to $U(IV)$, $U(VI)$ still seems conservative in anoxic waters (Anderson *et al.*, 1988). Kochenov *et al.* (1977) proposed that this was due to the need for particle surfaces catalysing the reduction process. Later research showed the catalysing role of bacterial sulphate reduction reactions in reduction of $U(VI)$ (Zhang *et al.*, 2002). The reduced uranium then precipitates (or adsorbs) as uraninite (UO_2) (Barnes and Cochran, 1991). Since the abundance of reactive organic matter is an important control on the intensity of sulphate reduction, a good correlation can usually be found between uranium abundance, and organic carbon rain rate (McManus *et al.*, 2005) and organic carbon abundance in anoxic sediments (Algeo and Maynard, 2004).

Since enrichment of solid-state uranium occurs only in the sediment, sedimentation rate may play an important role, since slow sedimentation rates would allow uranium more time to diffuse into the sediment (Crusius and Thomson, 2000). It is possible for uranium to remobilise in the sediment, when a deepening of the oxygen penetration depth causes uraninite to come

in contact with oxygen.

1.3.5 Vanadium (V)

Present in the $V(V)$ valence state in oxic waters, vanadium mainly forms the vanadate oxyanions HVO_4^{2-} and $H_2VO_4^-$. These species are almost conservative in oxic waters, although they do adsorb to manganese and iron oxyhydroxides (Wehrli and Stumm, 1989). Even though vanadium concentrations in deep waters are constant, a slight depletion can be seen in surface waters correlated to phosphate depletions, suggesting involvement in biogeochemical cycles (Collier, 1984).

Under mildly reducing conditions, $V(V)$ is reduced to $V(IV)$, forming VO^{2+}. This VO^{2+} is then hydrolysed to $VO(OH)_3^-$ or the insoluble $VO(OH)_2$ (Van der Sloot *et al.*, 1985). Because of this, small vanadium enrichments can be found in the sediment even when conditions are not euxinic. VO^{2+} and $VO(OH)_3^-$ can also be removed from anoxic bottom waters, probably by surface adsorption (Emerson and Huested, 1991). In the presence of free sulphides, vanadium is further reduced to $V(III)$, which precipitates as V_2O_3 or $V(OH)_3$ (Wanty and Goldhaber, 1992). This two-step reduction process of vanadium can sometimes cause the formation of different vanadium carrier phases between anoxic and euxinic conditions (Calvert and Pederson, 1993).

A strong correlation has been found between V/Fe ratios and organic carbon levels (Francois, 1988), possibly related to observed coprecipitation of vanadium with iron oxyhydroxides (Rudnicki and Elderfield, 1993). Apart from precipitating as vanadium species, V can also associate with clay minerals (Breit and Wanty, 1991).

1.3.6 Bromine (Br)

Present conservatively in seawater as Br^-, bromine is completely controlled by the organic fraction in marine sediments and diagenetic reactions during degradation of organic matter (Calvert and Pedersen, 1993). In sediments, bromine is closely related to organic matter in both oxic and anoxic circumstances, mainly through incorporation in geomacromolecules (e.g., humics) (Leri *et al.*, 2010). Because of this close coupling of bromine with organic matter, Br has been proposed and investigated as a possible proxy for marine organic carbon (e.g., Ziegler *et al.*, 2008).

1.4 Relevant techniques

1.4.1 Laser Ablation-Inductively Coupled Plasma-Mass Spectrometry (LA-ICP-MS)

Laser Ablation-Inductively Coupled Plasma-Mass Spectrometry (LA-ICP-MS) was first developed in the mid-eighties (Gray, 1985). Since then, many studies have utilised this technique to create high-resolution (trace) elemental records of geological samples. A LA-ICP-MS system typically consists of three components (Figure 1.3). The first of these components is the Laser Ablation (LA). A laser beam is "shot" at a certain frequency at the sample stored in an airtight chamber. Each time the laser beam hits the sample surface, part of that surface is ablated, forming aerosols within the chamber. These aerosols are transported by a carrier gas (mostly a combination of argon and helium) through tubing to the second component of the LA-ICP-MS system. By (slowly) moving the sample at a constant speed beneath the laser beam a track is formed on the sample surface, leading to a constant supply of new sample aerosols trough the tubing.

The second component of the LA-ICP-MS system is the Inductively Coupled Plasma (ICP). Aerosols being transported to the ICP through the tubing are being ionised here for measurement on the mass spectrometer. Ionisation is achieved by electrically heating the argon-helium carrier gas to high temperatures, forming a plasma. Plasma can be described as a fluid that is in many ways similar to a gas, but with significant amounts of free electrons and ions. The ions created this way are transported further to the third component, which is the Mass Spectrometer (MS). The MS separates the ions based on their mass/charge ratio, although the charge of an ion is often 1, with the exception of some rare earth elements. In practice, most ions are therefore separated based on their mass alone. Many different mass spectrometers are available, although most are based on deflection of ions when travelling through a magnetic field.

Measurements by an LA-ICP-MS system on a sample need to be calibrated using a standard reference (often the reference glass NIST-610), since the LA-ICP-MS system may be more or less sensitive to certain elements compared to others. This phenomenon is referred to as elemental fractionation (Fryer *et al.*, 1995; Figure 1.4). Fryer *et al.* (1995) continuously ablated a standard material for four minutes and plotted, for 60 different elements, the ratio of signals during the second two minutes (minutes 2–4) to the sig-

nals during the first two minutes (minutes 0–2). This was all normalised to calcium. The resulting ratios are therefore an indication of the fractionation factor of different elements relative to calcium. Figure 1.4 demonstrates the wide range of sensitivities of different elements under LA-ICP-MS. Sensitivity factors are calculated for each set of LA-ICP-MS measurements by repeated analyses of NIST-610, and used to correct sample data.

1.4.2 Wavelet and spectral analysis

Time series analysis is a useful approach to reconstruct environmental variability from sediment chemical records. Any time- or depth-domain dataseries is comprised of several cyclical components. The main component is a sum of any amount of cyclicities. In other words, a time- or depth series can be split in several sine waves of different periods. These sine waves can therefore be seen as the "building blocks" of a time- or depth series, and adding them up will result in that series. The amplitude of these sine waves is then an indication of the importance of that period to the original record. For this reason the importance of different cyclic periods within a certain range of periods can be plotted using the amplitude (mostly indicated as the "power" of a certain frequency or period) of these sine waves. Such a plot is also called a "power spectrum" (Figure 1.5). As an example, the original record in the top of Figure 1.5 is a reconstruction of Earth's eccentricity (which is a measure for the shape of Earth's orbit around the sun) for the past 5 Myr (Laskar *et al.*, 2011). The power spectrum for this record (middle of Figure 1.5) shows that the record is build up of a combination of 100-kyr, 125-kyr and 400-kyr cyclic periods (the three peaks in the power spectrum).

Certain periods or frequencies can subsequently be "filtered out", meaning that all other frequencies are removed from the original record. This filter then gives an indication of the importance of that frequency or period through time in the form of the amplitude of variability. In addition, variability in the filtered frequency (i.e., timing of peaks and troughs) can be compared to the original record. For example, one may want to further investigate the 400-kyr period found by the power spectrum in the middle of Figure 1.5. By filtering out this 400-kyr period, the influence of this period on the original record can be assessed (bottom of Figure 1.5). Peaks and troughs between the filter and the record align, indicating that this period is indeed an important component of the record. Note that the amplitude of the filter is only a measure of the importance of that period at that point in

time. As an example, the low peak around 2.5 Myr has the highest amplitude in the filter. Indeed, variability of the 100-kyr periods is very low here.

On top of this sum of different cycles there are some other components of a time- or depth series. For example, an (often linear) trend may be superimposed on the variability, and random noise may also be present. Influence of these other components needs to be reduced as much as possible before trying to create a power spectrum, since they may influence the result. Linear detrending is often easy to accomplish, although certain pitfalls may be present when one part of the record "weighs down" the rest of the record (Figure 1.6). Random noise superimposed on the natural variability of a record may be removed by applying smoothing techniques. Care should be taken though, since too much smoothing will also remove high-frequency natural variability.

Another method to unravel the importance of different cyclic periods in a record is the application of a wavelet transform (Figure 1.7). The advantage of a wavelet transform is that it will not only generate the powers of different cyclic periods, but that it adds a time component as well. As a result, a wavelet diagram can be seen as a stack of power spectra, showing the changing influence of different natural cycles over time. A disadvantage of wavelet diagrams is that they are less precise, disallowing high-resolution determination of the magnitudes of important periods. A wavelet is most commonly constructed by moving a range of sine waves, each with a different period, over the record. Power of a period is then calculated through the correlation between the record at that point and the corresponding sine wave. Other waves may also be used, varying the sine wave in amount of phases or using a completely different curve such as a Gaussian.

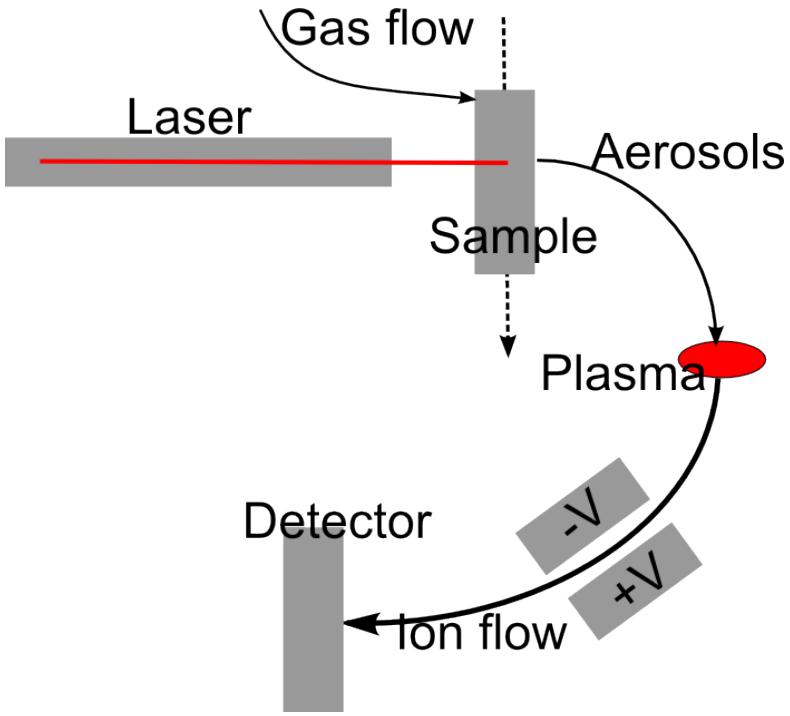

Figure 1.3: Simplified model of the LA-ICP-MS system.

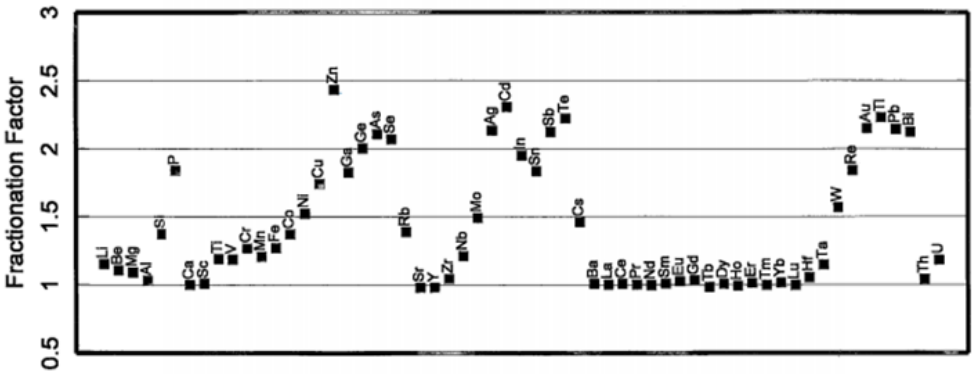

Figure 1.4: Relative fractionation of elements relative to calcium. Calculated by taking the ratio of signals during the second two minutes (minutes 2–4) to signals during the first two minutes (minutes 0–2) relative to calcium, during a 4-minute LA-ICP-MS run on a glass standard (Fryer et al., 1995).

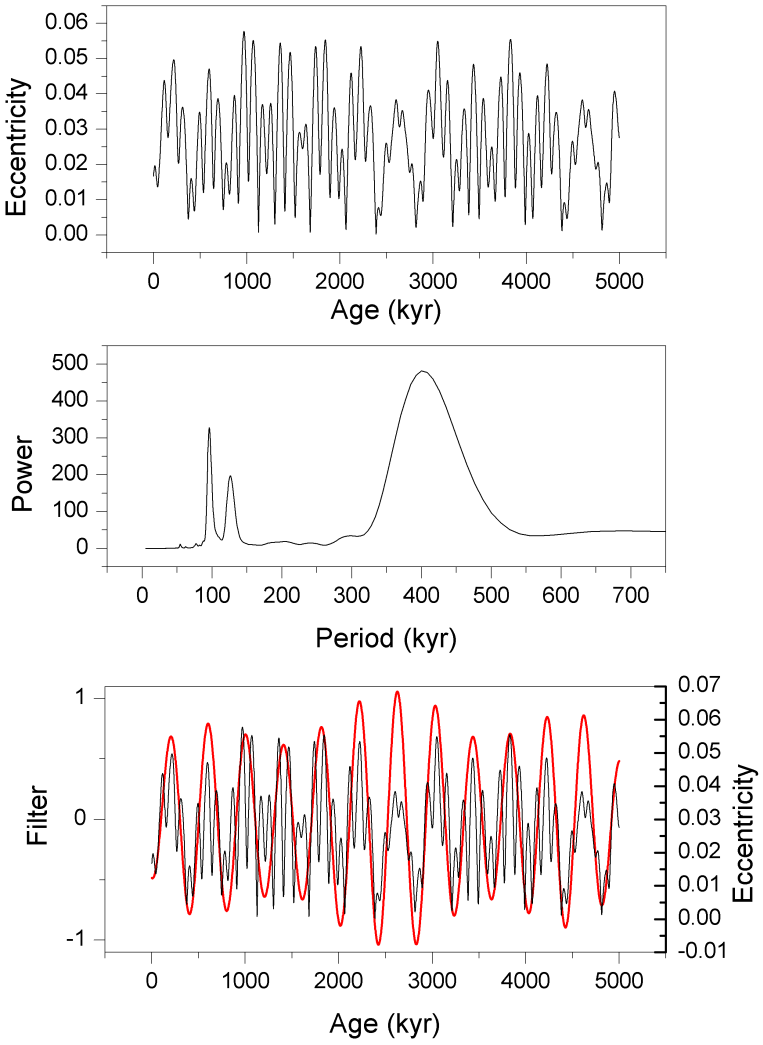

Figure 1.5: Example of the different steps involved in the creation and application of a power spectrum.

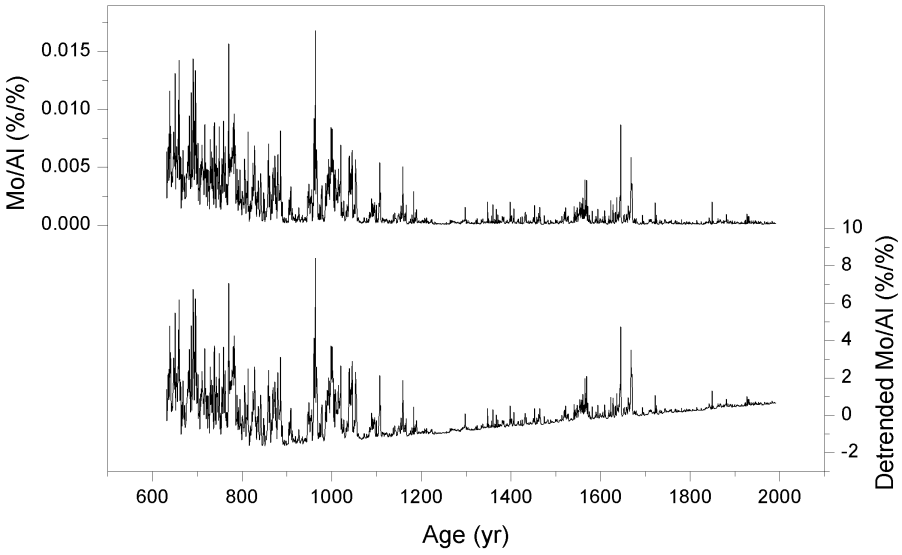

Figure 1.6: Example of an incorrect detrending application on the Mo/Al record of the MCA at F80. Due to the large difference in nature of the record during the older and newer part the more elevated last few centuries "weigh down" the rest of the record, artificially introducing a trend in the older part of the record.

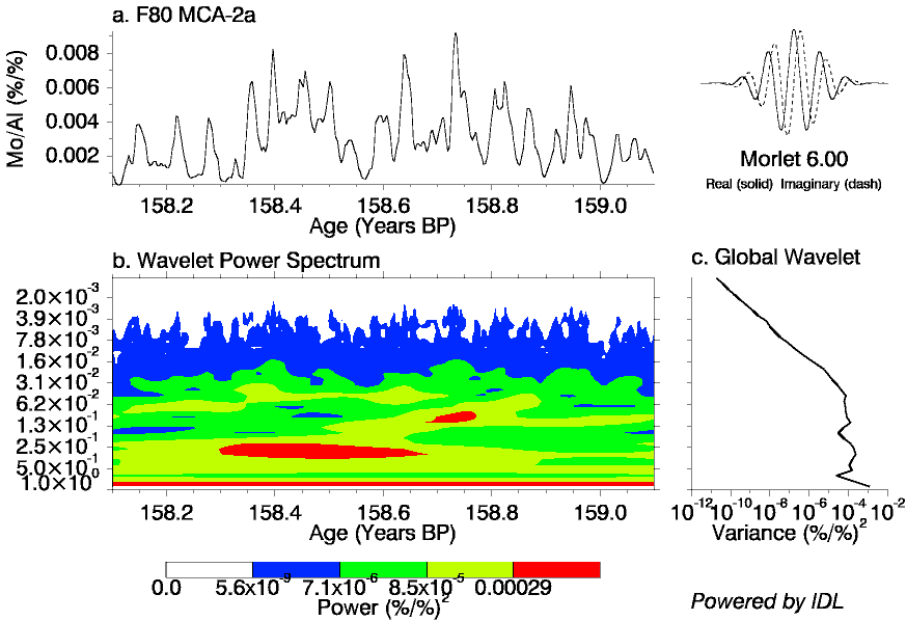

Figure 1.7: Example of a wavelet transform on a record of Earth's eccentricity over the past 5 Myr (the same record was used for Figure 1.5). Note that the y-scale (for periods) is less precise than the period scale of Figure 1.5. The same periodicities can be found in this record though, with strong representation of the 400-kyr period, visible as a red band. Furthermore, the 100 kyr cycles can be seen as a more yellowish band with red spots. The low-intensty peak around 2.5 Myr as identified in Figure 1.5 is characterised by less intense colours in the 100-kyr band.

2 Methods

2.1 Sediment coring

Three sediment multicores (top 50 cm of the sediment, two cores per location) were taken from sites LL19 in the Nothern Gotland Basin, F80 in the Fårö Deep and BY15 in the Gotland Deep during a cruise across the Baltic Sea with R/V Aranda in September 2013 (Figure 1.1; Table 2.1). Furthermore, gravity cores (top 5 m of the sediment) from site SR5 in the Bothnian Sea and site F80 were taken during a cruise with R/V Aranda in May and June of 2009.

Table 2.1: Depths and locations of coring sites.

Site	Depth	General location	Coordinates
LL19	169 m	Northern Gotland basin	58 °52.84'N 20 °18.65'E
F80	191 m	Fr Deep	58 °00.00'N 19 °53.81'E
BY15	238 m	Gotland Deep	57 °32.00'N 20 °05.00'E
SR5	126 m	Bothnian Sea	61 °05.00'N 19 °35.00'E

2.2 Discrete samples

The collected multicores were sliced anoxically at a 0.5 to 2 cm resolution in a glovebag filled with nitrogen gas. The cores all had to remain in a vertical position during slicing due to the low firmness of the sediment. The gravity cores from the 2009 cruise had been sliced horizontally. The obtained discrete samples were weighted before and after freeze-drying to allow for a determination of water content. After freeze-drying, the samples were crushed anoxically in a glovebox filled with nitrogen gas. A subsample of 1 to 1.5 g was weighted in a Teflon bomb and dissolved in 2.5 mL HF (40%) and 2.5 ml of a mixture of $HClO_4$ and HNO_3 at 90 $°C$ for 12 hours. After evaporating the acids at 190 $°C$ the resulting gel was dissolved in 1M HNO_3. Using an ICP-OES, these gels were measured for Al (308.215 nm), Ba (455.404 nm), Ca (315.887 nm), Fe (259.941 nm), Mn (257.611 nm), Mo (202.095 nm), P (178.287 nm), S (182.034 nm) and V (292.402 nm). A second set of subsamples was decalcified using 1M HCl by shaking for 12 hours.

After these 12 hours, fresh acid was added before shaking for another 4 hours. After drying and crushing, the subsamples were analysed for C_{org} by combustion by Fisons NA 1500 NCS, using an atropine/acetanilide standard and an internal laboratory standard.

2.3 Resin embedding and LA-ICP-MS

Parallel to the discrete sample profiles high resolution profiles were created using LA-ICP-MS (Laser Ablation-Inductively Coupled Plasma-Mass Spectrometry) line scanning of resin-embedded subcores. These 7 cm long subcores (1 cm diameter) were taken during slicing along the length of the same multicores using 15 mL greiner tubes with the tip sawn off. Since the gravity cores were sliced horizontally, subcores for these cores could be taken using aluminium trays, creating 20 cm long subcores instead. After embedding these subcores in resin (Jilbert *et al.*, 2008) they were sawn in half and polished to expose the sediment sample surface. Furthermore, they were sawn in blocks of at most 3.5 cm long, in order for them to fit in the sample stage.

An Excimer laser beam (193 nm with spot size of 120 μm, 10 Hertz, 8 J cm^{-2}) was aimed at the sample surface, ablating the material. This material was transported to a Thermo Element 2 high mass resolution ICP-MS using a helium-argon carrier gas to measure counts of the same elements as measured on the discrete samples by ICP-OES, and additionally of Br, Re and U. However, counts of Re rarely exceeded the detection limit. By moving the sample stage at a constant speed of 0.04 mm sec^{-1} the laser beam ablated a "track" from one end of the block to the other, causing a constant supply of ablated material to the ICP-MS. The resolution of the generated depth series is limited by the spot size of the laser beam (i.e., 120 μm). An (external) glass standard (NIST-610) was used to correct the raw counts for element-specific sensitivities and isotopic abundances. Furthermore, all elements were normalised to aluminium (Al).

2.4 LA-ICP-MS data calibration

Correction of raw counts for element-specific sensitivities and isotopic abundances was performed using a relative sensitivity factor (RSF, relative to Al). The RSF was generated for every sample using the NIST-610 glass standard. After subtracting the background counts, counts on the standard

were averaged and compared to known ppm values of the elements in the glass (Equation 2.1).

$$Sensitivity\ factor = \frac{standard * isotopic\ abundance}{100 * (average\ counts - background)} \tag{2.1}$$

The RSF was then computed by dividing the sensitivity factor of the element by the sensitivity factor of Al. The obtained RSF was subsequently used to correct the counts of the elements before normalising to Al (Equation 2.2).

$$Ratio\ \frac{element}{Al} = \frac{(C_e - B_e) * RSF_e * \frac{100}{I_e}}{(C_{Al} - B_Al) * RSF_{Al} * \frac{100}{I_{Al}}} \tag{2.2}$$

C_e *and* C_{Al} = *Raw counts element and Al*
B_e *and* B_{Al} = *Background element and Al*
RSF_e *and* RSF_{Al} = *Relative Sensitivity Factors element and Al*
I_e *and* I_{Al} = *Isotopic abundance element and Al*

After applying this procedure to all blocks, these blocks were combined back into their original subcores (either 7 cm long or 20 cm long) based on elemental profiles (most notably the Mo/Al, V/Al and U/Al profiles). However, shrinkage effects due to the methods of vertical slicing as well as due to the resin embedding procedure caused the apparent length of these subcores to be around 10% less than their length in the original core. To reverse this effect, apparent depths in the subcores were multiplied by a constant factor to set the length back to the original length. To complete the depth series, the individual subcores were connected based on elemental profiles.

The obtained ratios of elements to Al were further calibrated using the discrete sample profiles. Geometric means were calculated from depth intervals in the high-resolution data corresponding to the depth intervals of the discrete samples. These binned means were then correlated to the discrete samples. Offsets of the correlation line from the x = y line were corrected for by applying the regression formula to the high-resolution samples and their binned means (Figure 2.1). This procedure was necessary to correct for potentially variable sensitivity factors between heterogeneous sediment samples and the glass standard used in the first stage of the data calibration.

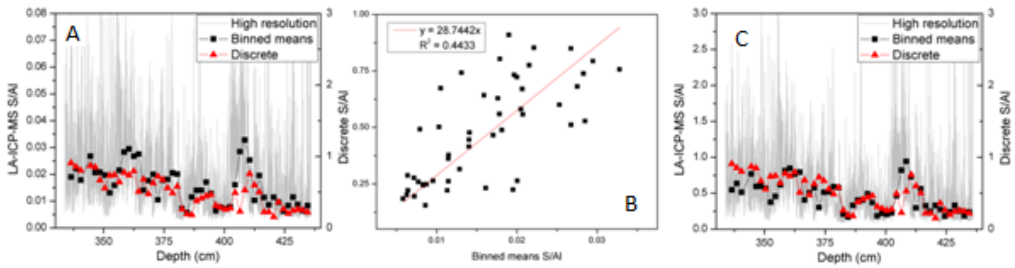

Figure 2.1: Calibrating the LA-ICP-MS record to the discrete samples (ICP-OES record). Offset between the binned means and discrete samples (A) is corrected for by regressing these two against each other (B) and applying the slope of the regression to the binned means and high-resolution record (C). Note the changing y-axis for the LA-ICP-MS record between A and C.

For the modern interval (i.e., the upper multicore sediments), the obtained elemental series in the depth domain were initially tuned to the bottom water oxygen time series for the relevant sites, where more positive oxygen concentrations correlated to low Mo/Al troughs (Figure 2.2). In addition, the onset of the hypoxic event was tuned to the shift to euxinic conditions in the bottom water oxygen record. This resulted in a number of tie-points for the first order age model. This age model was further refined by counting Mo/Al peaks between these tie-points, assuming an annual cycle of Mo/Al concentrations related to changing inputs of organic matter. A strong negative correlation between Mo/Al and raw Al counts was present, possibly due to sequences of high organic matter (high Mo/Al) and low organic matter concentrations (high Al counts) within the laminations (see also Section 4.2.1.1 and Figure 4.3). This was used to more confidently identify yearly peaks in the Mo/Al record. The amount of these peaks present in the records was similar to the length of the modern hypoxic interval, indicating that Mo/Al peaks could indeed reflect a yearly cyclicity (Figure 2.3).

The indication that Mo/Al peaks could reflect yearly cyclicity was then used to construct an independent age model for the older hypoxic intervals (i.e., the Medieval Climate Anomaly (MCA) and the Holocene Thermal Maximum (HTM)) present in the gravity core samples. For F80, the total number of years likely to be covered in these intervals was taken from an earlier age model (Lougheed *et al.*, 2012). The full 68.2% confidence envelope of poten-

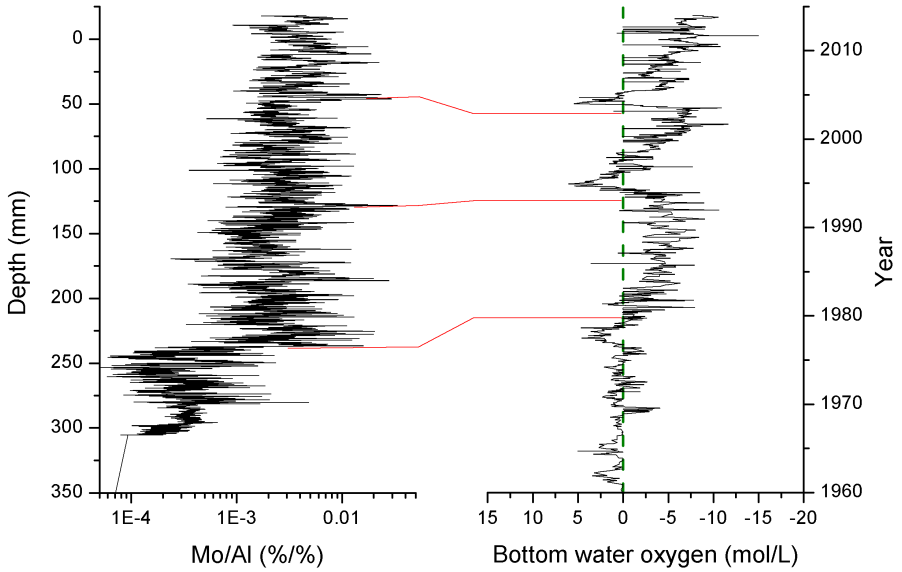

Figure 2.2: Tuning of the Mo/Al record at BY15 to the bottom water oxygen record since 1960. Mo/Al has been plotted on a logarithmic scale to emphasise the shift from hypoxic to euxinic bottom water oxygen conditions. Red lines indicate tuning points between the Mo/Al and the bottom water oxygen record, related to onset of hypoxia and inflow events. A vertical green line is added to the bottom water oxygen record to indicate the zero-oxygen level.

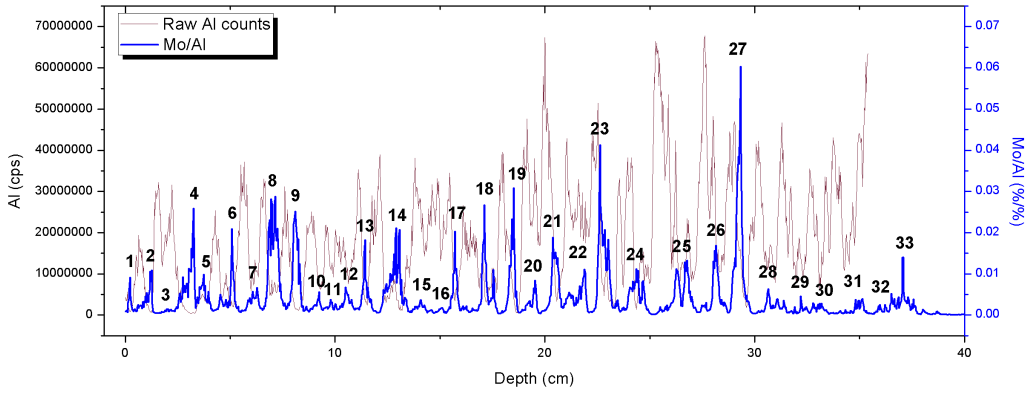

Figure 2.3: Counting of yearly Mo/Al peaks from 2013 back to 1981 (33 years). Peaks were selected based on a combination of Mo/Al peaks and troughs in raw Al counts.

tial ages in that age model indicated a total length of 1000–1600 years for the MCA and 2000–2600 years for the HTM hypoxic intervals, respectively. By dividing the envelope of the likely duration of each interval by its total length in cm, an upper and lower boundary for average years per cm was calculated. Sliced power spectra of the Mo/Al depth series were then generated over 1 cm intervals in the depth domain. All generated 1-cm sliced power spectra were analysed to identify candidate frequencies for the 1-year cyclicity and hence give an estimation of sedimentation rate.

To pass the test to be a candidate frequency, the peak had to satisfy three conditions. First, it had to fall within a frequency band based on the upper and lower boundaries of the 68.2% confidence envelope of Lougheed *et al.* (2012). The exact frequency band was extended slightly beyond this range by five years per centimeter. Second, it could not be a harmonic or other artefact of another frequency. Third, the peak had to be the only significant peak within the frequency band. When no peak in the 1 cm slice satisfied these conditions, no sedimentation rate was recorded. Depth series of identified candidate frequencies were overlain onto the corresponding 1-cm slices of the Mo/Al record to check their relation to the Mo/Al peaks.

Using the candidate frequencies in the full series of 1 cm slices, sedimentation rates were estimated for past hypoxic intervals. The upper and lower bases of the peaks (i.e., the width of the peak in the frequency domain) were used to estimate the error bar (Figure 2.4). These sedimentation rates were interpolated to cover the sections for which no candidate frequency was identified, and used to construct a floating timescale for the records of the HTM and the MCA. From Lougheed *et al.* (2012), the most centric depth-to-age tie point for each of the two hypoxic intervals was used to fix the floating timescales. Although the same procedure was used for SR5 the resulting floating timescale could not be fixed since no independent age model was available.

It should be noted that since the uncertainties in this age model are still rather large, the original PSV-based age model was used for most analyses (see also Section 4.2). This includes the presentation in the results (Section 3).

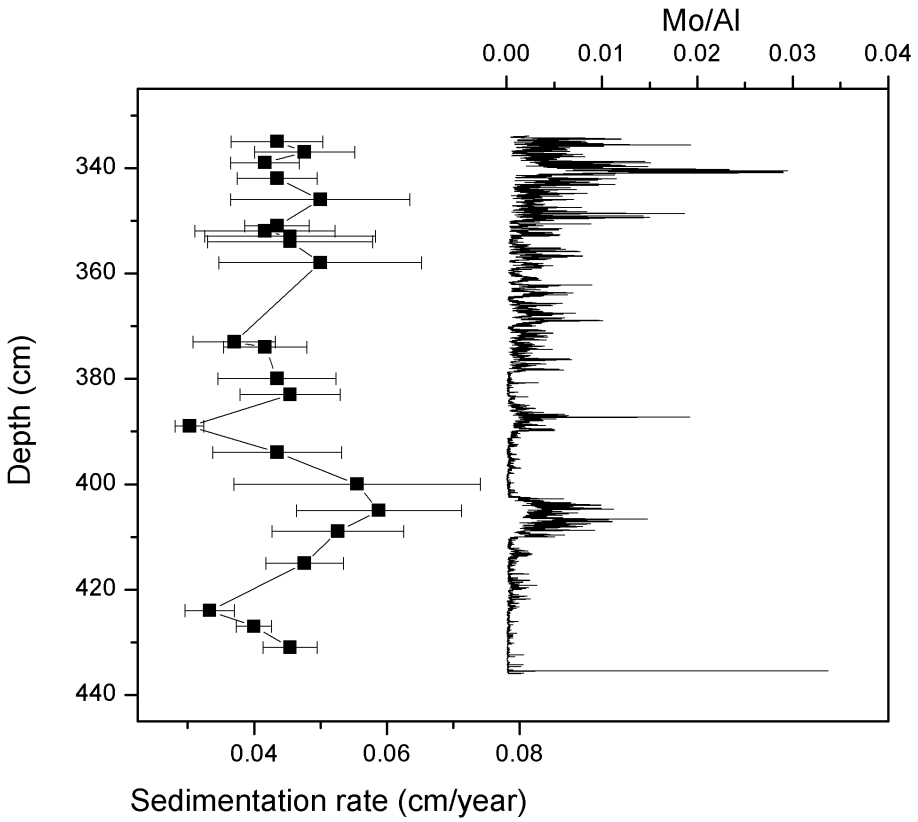

Figure 2.4: Reconstruction of sedimentation rates during the HTM at F80.

3 Results

3.1 Identification of hypoxic events in discrete sample profiles and LA-ICP-MS data

3.1.1 F80

Based on discrete sample profiles of Mo/Al, C_{org} and C/P, several hypoxic events throughout the last 8 kyr can be indentified at F80 (Figure 3.1). Each of these events is characterised by in-phase excursions of molybdenum, organic carbon and C/P ratios. At F80, seven of these hypoxic events can be identified during the HTM and two hypoxic events during the MCA. The last excursion corresponds to the current hypoxic interval. These have all been numbered according to the identification used by Jilbert and Slomp (2013a). Duration of events is typically in the order of a few centuries, although events during the HTM last longer than more recent excursions. Apart from one outlier during HTM-7, Mo/Al and organic carbon levels seem to reach an upper limit of ~ 0.005 and ~ 11, respectively. Increased organic carbon levels at the top of the core could be related to decaying organic aggregates in the top layer (Jilbert and Slomp, 2013a). Although subsequent analyses will all be on hypoxic events, it should be noted that under "normal" conditions, Baltic Sea deep waters are oxygenated.

The response of iron enrichments to hypoxic events on the larger timescales captured by discrete samples differs between the HTM, the MCA and modern hypoxic event. During the HTM, Fe correlates well with Mo enrichments, except near the end of HTM-7. This does not apply to the MCA, however. Around the onset of the MCA Fe peaks are relatively high compared to Mo peaks, quickly decreasing in intensity to reach relatively low levels during MCA-2. In addition to this, a significant iron peak is present before the MCA concurrent with a small increase in C_{org}. This pattern of a "bulge" of iron around the onset of the MCA is even more apparent in the modern interval, where the onset of this interval is characterised by a large peak in Fe of the same intensity as those at the start of the MCA. Shortly after, Fe drops back to pre-event levels although Mo/Al and Corg stay elevated.

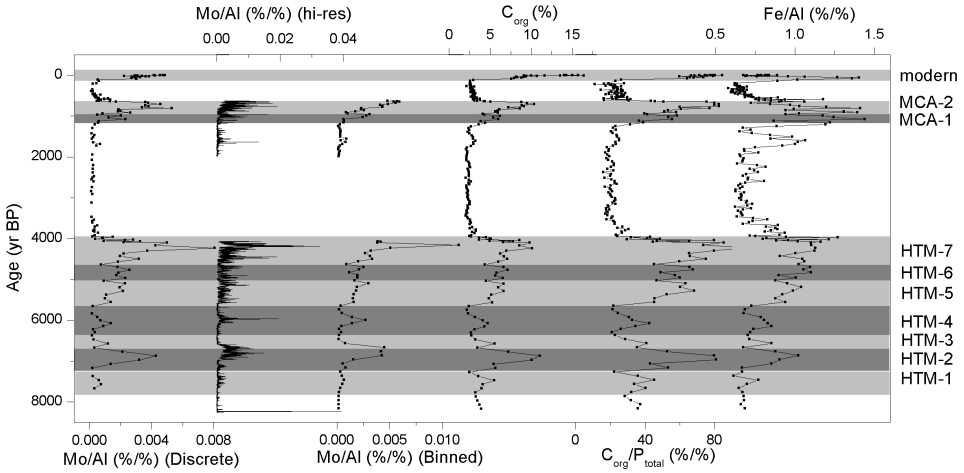

Figure 3.1: Comparison of discrete sample profiles, high-resolution profiles and binned means of Mo/Al at F80 over the last 8 kyr. Included are C_{org}, C_{org}/P_{tot} and Fe/Al profiles. Different events are indicated by alternating light and dark grey bands, named on the right. The age model was constructed using the PSV-based method.

3.1.2 SR5

At SR5 in the Bothnian Sea only the Holocene Thermal Maximum has been sampled, since no enrichments occur during younger intervals (Figure 3.2). Based on the discrete sample profiles, six events can be discerned. To avoid confusion with events at F80, these events at SR5 have been named differently. Although events have been determined based on the discrete Mo/Al record, correlation between this record and the LA-ICP-MS record is weak, and stronger correlation can be found between the LA-ICP-MS record and the C_{org} record. Distinct differences are observed in intensities and durations between events SR5-1 to SR5-3 and SR5-4 to SR5-6. While the first three events last around 500–1200 kyr with molybdenum concentrations of up to 0.009, the second three events reach molybdenum maxima of 0.002 for a duration of two or three centuries. Highest iron concentrations occur during the onset of the second event although significant peaks are still present during the later molybdenum enrichments.

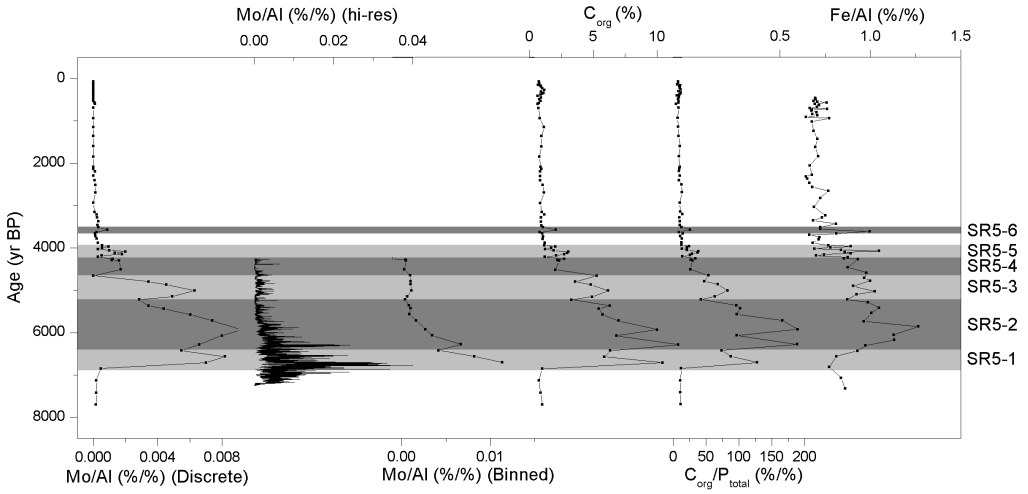

Figure 3.2: Comparison of discrete sample profiles, high-resolution profiles and binned means of Mo/Al at SR5 over the last 8 kyr. Included are C_{org}, C_{org}/P_{tot} and Fe/Al profiles. Different events are indicated by alternating light and dark grey bands, named on the right.

3.2 High-resolution LA-ICP-MS profiles of selected intervals

The LA-ICP-MS data provides a long high-resolution record throughout the HTM, MCA and the modern interval, allowing detailed investigation of individual events. In the following, a number of events showing distinctly different characteristics will be reviewed in higher detail.

3.2.1 Holocene Thermal Maximum at SR5

From the start of hypoxic events around 7.2 ka the system at SR5 never fully recovered to oxic conditions until 5.3 ka. For this reason, although several events can be identified during this time interval, none of these are associated with an onset from (or termination to) near-zero Mo/Al enrichments. Regardless, variability in Mo/Al is observed and three hypoxic events have been selected from this time interval, based on their Mo/Al excursions above background values. Two of these fall within the SR5-1 interval (SR5-1a and SR5-1b; Figures 3.3 and 3.4, respectively) while the third occurs at the start of SR5-2 (Figure 3.5).

With the exception of SR5-1b onset of these events is mostly gradual. This is especially the case for SR5-2, where background levels, peak maxima and amplitudes of variability all show constant increase over a period of around 60 years. Timing of onset of SR5-1a is hard to pinpoint, due to a steady increase in Mo/Al from the first small enrichment until the most intense period. Amplitude of variability in all events is relatively high, with Mo/Al values shifting from close to depletion to enrichments of at least 0.015 to 0.02 within years. Uranium profiles tend to have good correlation with molybdenum. Using uranium, the most intense part of SR5-1a can be dated at around 6.8 ka. Despite concurrent, rapid enrichments in molybdenum and uranium at the start of SR5-1b, correlation between the two records during the rest of the event is weak. This sharp increase in molybdenum levels at the start of SR5-1b can be seen in the vanadium and iron records as well, although it is not present for bromine.

In general, good correlation can be found between vanadium, bromine and molybdenum, with the exception of SR5-1b. Aside from a small enrichment in iron at the start of SR5-1a around 7.2 ka this record stays relatively constant throughout all three events. Just before initial molybdenum enrichments start at 7.2 ka a significant manganese peak occurs. Throughout SR5-1a several weaker manganese peaks are present. However, SR5-1b only contains one weak manganese excursion, and none can be identified for SR5-2. Fe/Al enrichments increase more gradual than Mo/Al, reaching its maximum during SR5-2 and gradually decreasing after that. A final peak in Fe/Al is present coincident with the Mo/Al peak of SR5-6.

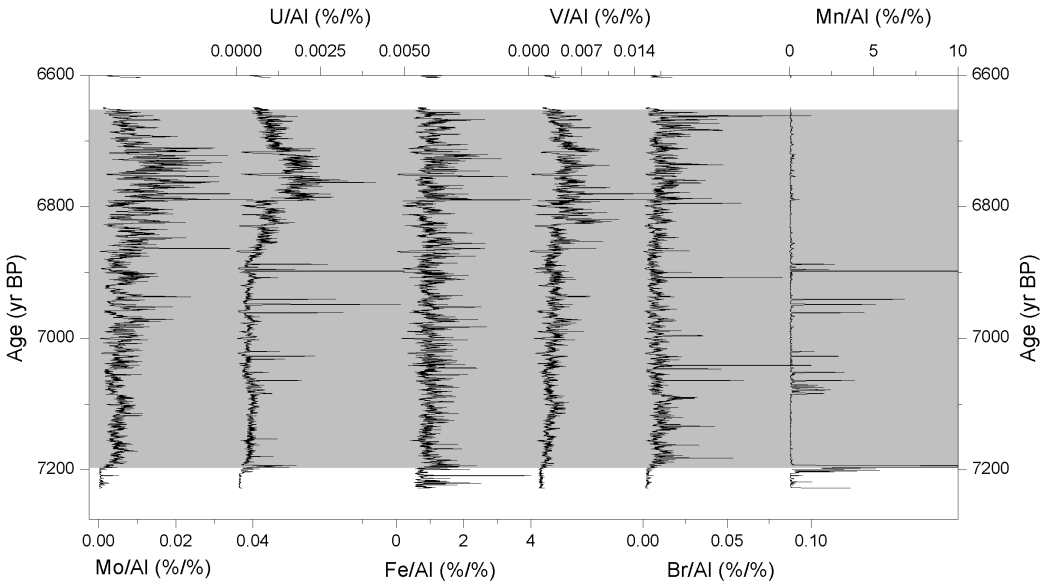

Figure 3.3: LA-ICP-MS records of several (trace) elements during SR5-1a at SR5 in the Bothnian Sea. The grey area indicates the duration of the event.

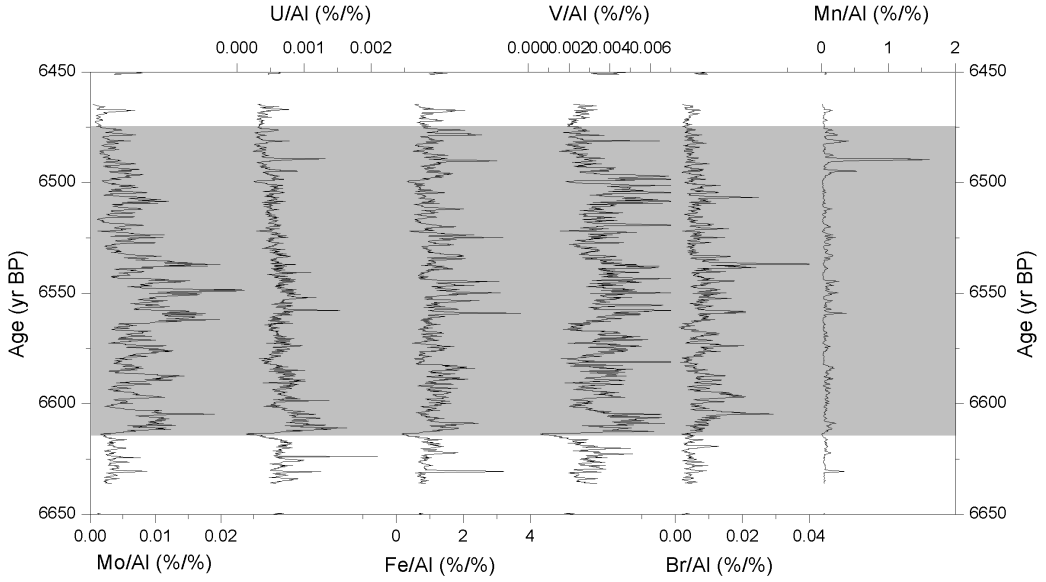

Figure 3.4: LA-ICP-MS records of several (trace) elements during SR5-1b at SR5 in the Bothnian Sea. The grey area indicates the duration of the event.

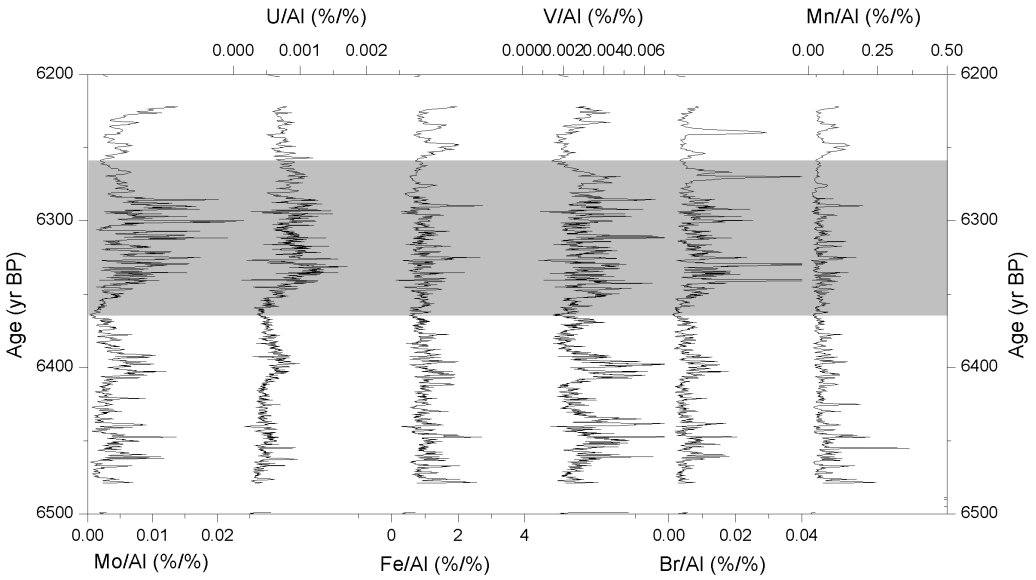

Figure 3.5: LA-ICP-MS records of several (trace) elements during SR5-2 at SR5 in the Bothnian Sea. The grey area indicates the duration of the event.

3.2.2 Holocene Thermal Maximum at F80

Three different Mo/Al excursions have been selected for the HTM at F80, each showing different characteristics. These three events include HTM-2 (Figure 3.6), one excursion from the combined HTM-5+6 (Figure 3.8) and the most intense part of HTM-7 (Figure 3.9). HTM-5+6 is different from the other events, since it consists of a sequence of smaller events (Figure 3.7). These smaller events are characterised by rapid onsets and terminations, with enrichments typically lasting for around 30 to 40 years and durations of depletions ranging from a few years to two decades.

Onset of HTM-2 is characterised by a abrupt initial enrichment in Mo/Al within one year, after which Mo/Al enrichments continued increasing throughout the following two centuries. Termination was also quite gradual, with the final drop to pre-event background levels, again, quite sudden. The same applies to the onset and termination of the short events during HTM-5+6 and the termination of HTM-7, although the system never fully recovered around these hypoxic events. The only exception could be the onset of HTM-7, which was more gradual although it did experience rapid increase in Mo/Al levels

going into the more intense hypoxic period. Amplitude of variability within events is high, although minima during the events are relatively higher than those during events at SR5.

Especially during HTM-7 did uranium background values enrich during an event. During the other selected events, uranium backgrounds stayed closer to pre-event values, although with slight increases in the baseline U/Al values. Some U/Al peaks especially during the short events during HTM-5+6 may be associated with Mn/Al peaks. Vanadium generally correlates well with bromine and molybdenum.

During the HTM at F80, iron enrichments correlate better with onsets and terminations of events than at SR5. At all events an increase in iron can be seen at or just after the onset as determined by the molybdenum record. Some events, such as HTM-2, also see a drop in iron enrichments at their termination. Only during the excursion during HTM-6 are iron peaks significantly higher around the onset of the excursion than during the rest of the hypoxic interval. Intensity of manganese peaks decreases over time, although frequency remains relatively constant. The only exception to this is the excursion during HTM-6, which only has a few manganese peaks.

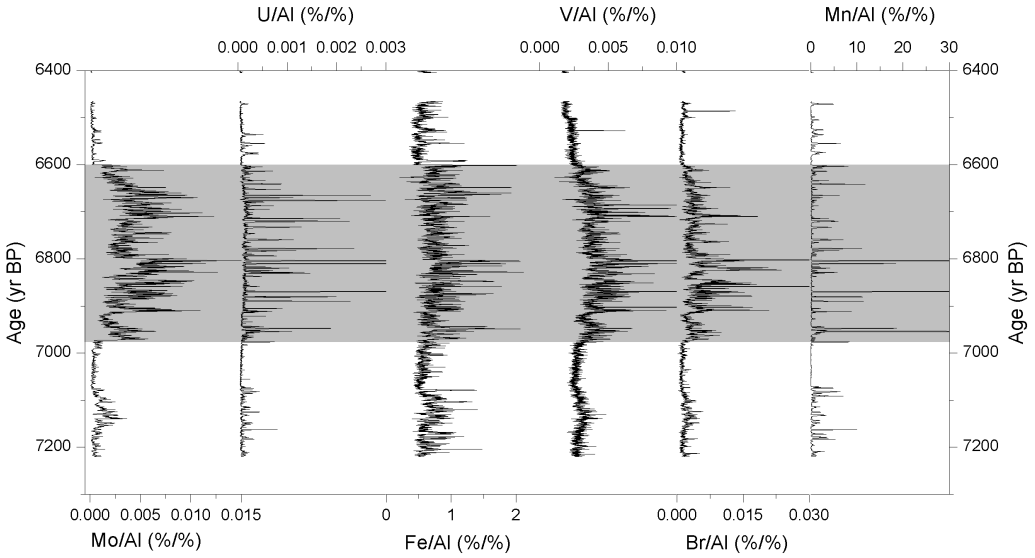

Figure 3.6: LA-ICP-MS records of several (trace) elements during HTM-2 at F80. The grey area indicates the duration of the event. The age model was constructed using the PSV-based method.

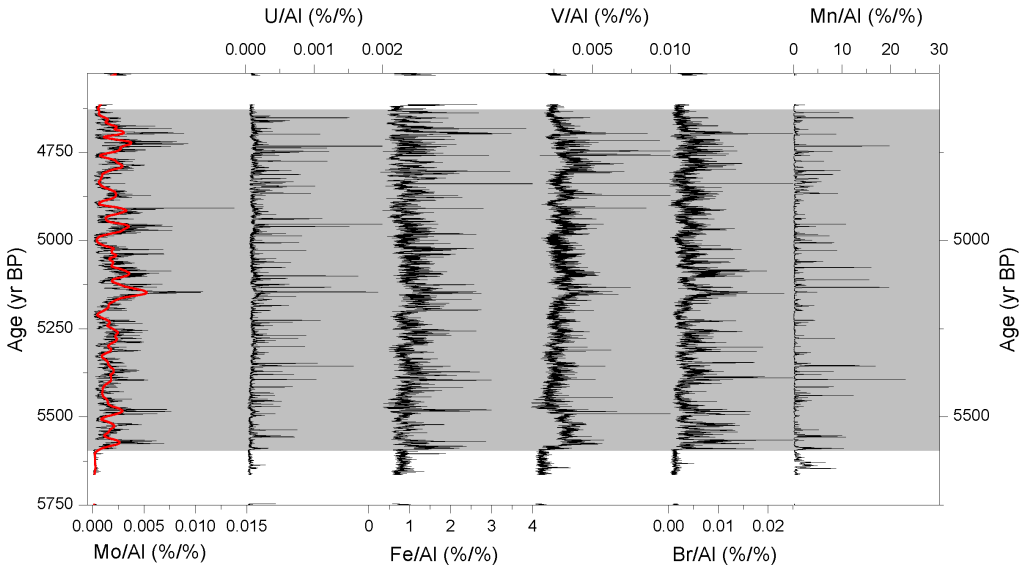

Figure 3.7: LA-ICP-MS records of several (trace) elements during HTM-5 and HTM-6 at F80. The red overlay of the Mo/Al record is a 100-point moving average. The grey area indicates the duration of the events. The age model was constructed using the PSV-based method.

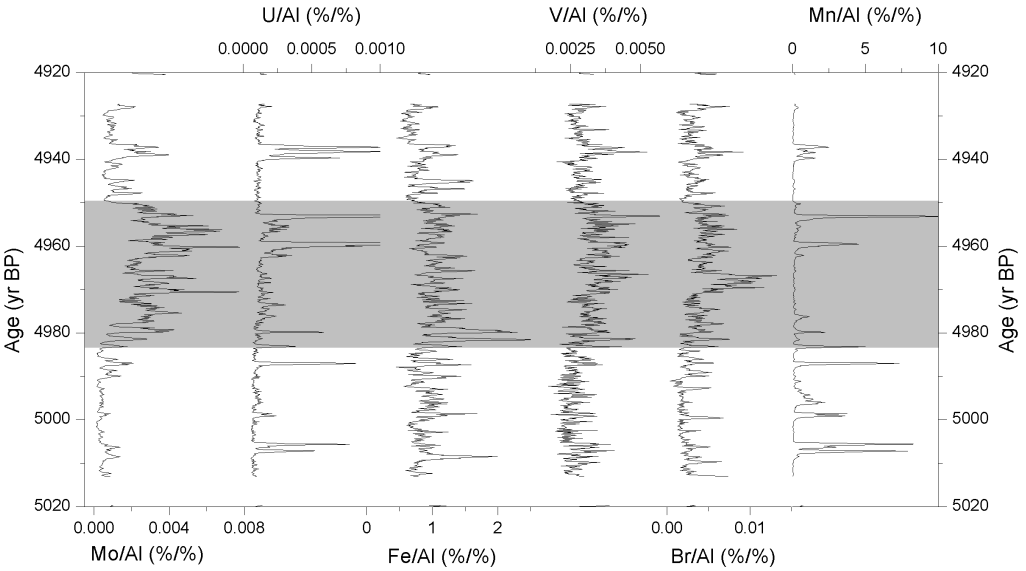

Figure 3.8: LA-ICP-MS records of several (trace) elements during one molybdenum excursion during HTM-5 and HTM-6 at F80. The grey area indicates the duration of the excursion. The age model was constructed using the PSV-based method.

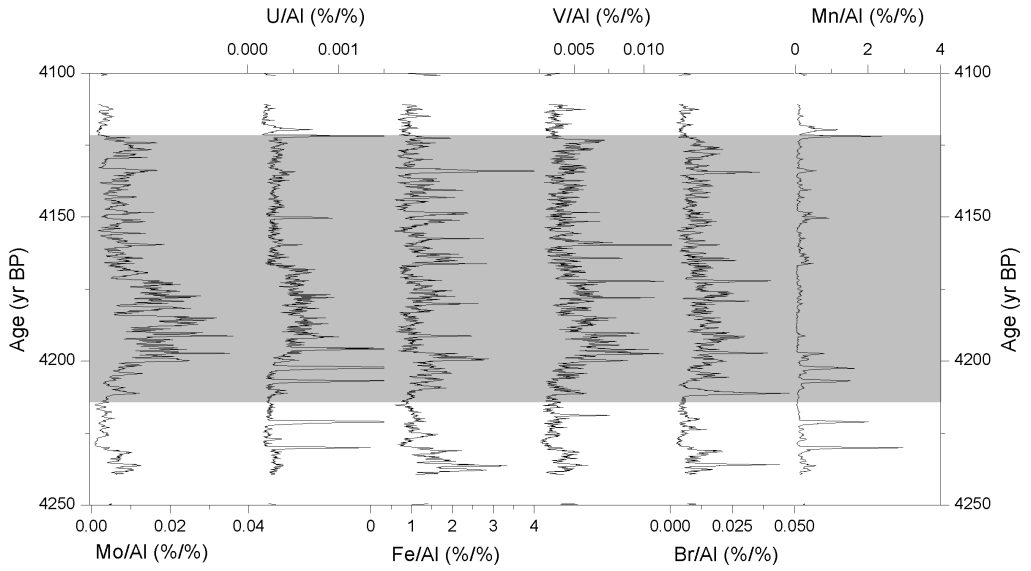

Figure 3.9: LA-ICP-MS records of several (trace) elements of the most intense part of HTM-7 at F80. The grey area indicates the duration of the period. The age model was constructed using the PSV-based method.

3.2.3 Medieval Climate Anomaly at F80

Although not captured well by the discrete samples profile, a small event occurred around 1.5 ka, half a millennium before the onset of MCA-1 (Figure 3.10). Apart from this pre-MCA event, two other events have been selected from the MCA at F80. Of these two events, one occurs during MCA-1 (Figure 3.11) and the other during MCA-2 (Figure 3.12).

The hypoxic events at F80 during the MCA (i.e., MCA-1 and MCA-2) as identified by Jilbert and Slomp (2013a) each contain several individual hypoxic (sub)events. A gradual increase in Mo/Al enrichments can be identified for both MCA-1 and MCA-2, reaching maximum Mo/Al values after at least one century. Superimposed on this general trend of gradually increasing hypoxia, onset and termination of individual hypoxic events during MCA-1 and MCA-2 at F80 is rapid, with Mo/Al enrichments and depletions occurring within one to three years. In addition, the system was already unstable in the decades running up to the pre-MCA event, with occasional enrichments lasting no more than two years. Amplitude of variability was

high, with Mo/Al values shifting to pre-event background levels in between most peaks.

Overall Mo/Al trends are replicated to a large extent by the V/Al and U/Al records. U/Al enrichments at the pre-MCA event started one year before molybdenum enrichments. Large differences between Mo/Al peaks and troughs at the pre-MCA event allow precise determination of the length of this event at 15 years. Despite this inferred length of the pre-MCA event, the age model suggests that the pre-MCA event lasted ∼10 years longer. See Section 4.2.2.2 for an explanation for this discrepancy.

Good correlation is visible between iron and molybdenum, with both the onset and termination of most events coinciding. During the course of the MCA, iron enrichments during events decrease from Fe/Al = 10 at the pre-MCA event down to Fe/Al = 4 during MCA-2a. During the pre-MCA event and MCA-1, manganese peaks are more abundant during events than just before or after events. The opposite is true for events during MCA-2, which see strong decline in manganese peak frequency during hypoxic intervals. As with iron, intensity of manganese enrichments declines throughout the MCA.

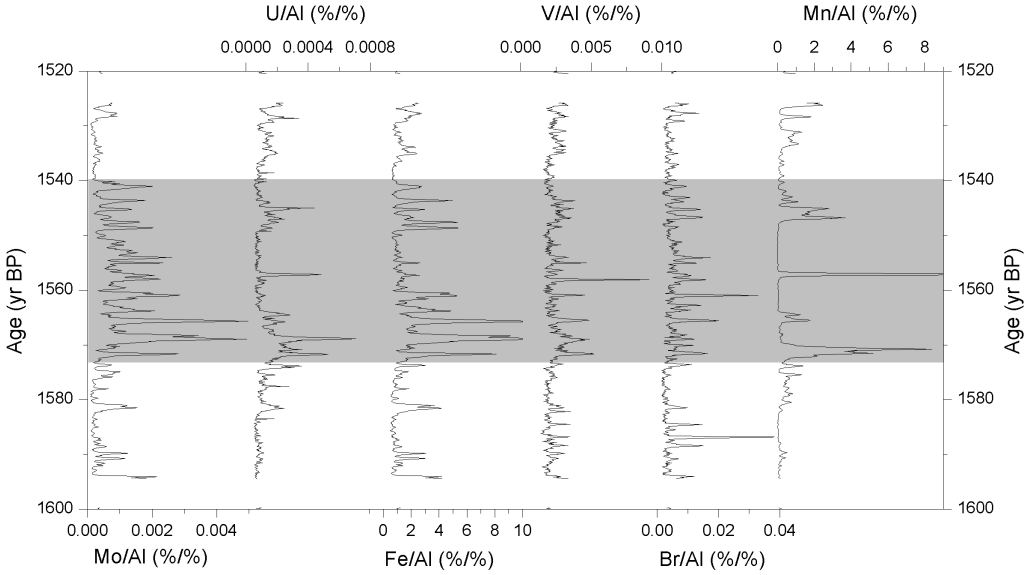

Figure 3.10: LA-ICP-MS records of several (trace) elements during the pre-MCA event at F80. The grey area indicates the duration of the event. The age model was constructed using the PSV-based method.

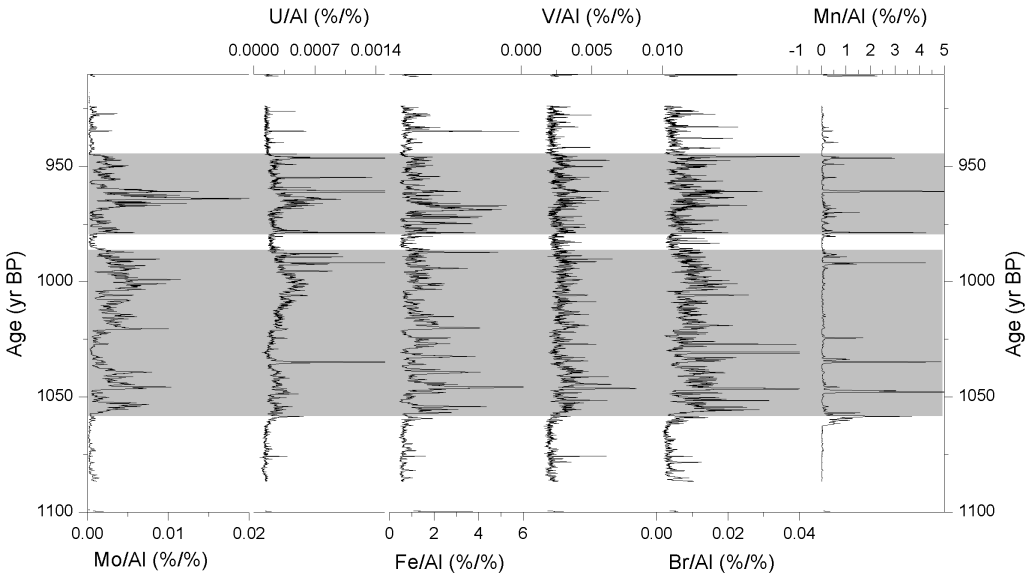

Figure 3.11: LA-ICP-MS records of several (trace) elements during a single hypoxic (sub)event during MCA-1 at F80. The grey area indicates the duration of the event. The age model was constructed using the PSV-based method.

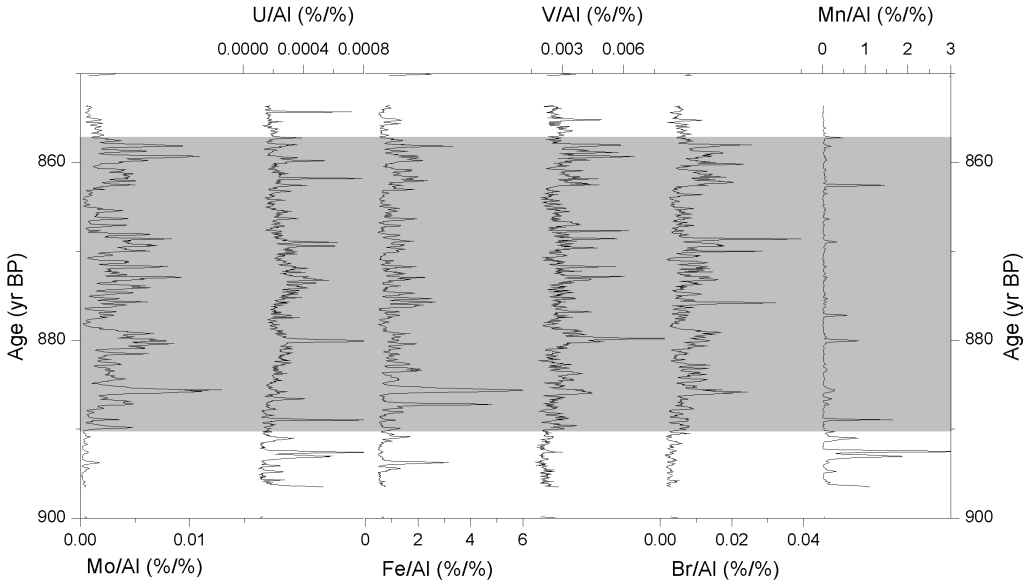

Figure 3.12: LA-ICP-MS records of several (trace) elements during a single hypoxic (sub)event during MCA-2 at F80. The grey area indicates the duration of the event. The age model was constructed using the PSV-based method.

3.2.4 Modern hypoxic event at F80, LL19 and BY15

Onset of the modern hypoxic event at all three analysed locations (Figures 3.13, 3.14 and 3.15, respectively) indicates that this event started suddenly, with rapid enrichments in molybdenum concurrent with a shift in bottom water oxygen levels to permanently euxinic levels. At all three sites this happened around 1980, although enrichments at F80 occur one year before those at LL19, in turn occurring one year before those at BY15. The start of the modern event at BY15 was slower than at the other two locations, with molybdenum levels going back to pre-event background levels for prolonged times (up to three years) during the first seven to eight years. A strong seasonal signal is visible in all three records, indicated by Mo/Al values going back down to pre-event levels between most peaks.

Location of vanadium peaks tends to correlate well with those of molybdenum, although general trends are more related to bromine. This is especially visible at BY15, with a "bulge" of vanadium and bromine around 2000. Although mean molybdenum enrichments stay relatively stable, uranium enrichments continue to increase throughout the events. This is visible in an increase in background levels, with LL19 and BY15 experiencing increased intensity of uranium peaks in more recent years as well.

At F80, iron enrichments occur before onset of the event as indicated by the molybdenum record. These enrichments quickly decline after onset of the event to reach pre-event background levels around 1990. Although iron enrichments at LL19 do not start until onset of the event, the same rapid decrease in Fe/Al occurs, reaching pre-event background levels just after 1990. Iron peak intensities at BY15 do not decrease over time, although their frequency does. The last recorded iron peak at BY15 occurs in 2005.

Up until onset of the event at F80 manganese peaks are abundant and intense. After onset of the event only a few manganese peaks appear, roughly correlated with inflow events in 1993 and 2003. During the event at LL19 only three manganese peaks appear, all during the first ten years of the event. No peaks occur before the hypoxic event at LL19. On the other hand, several intense manganese peaks are present throughout the hypoxic event at BY15, increasing in intensity throughout the years. The last of these peaks occurs just before 2000.

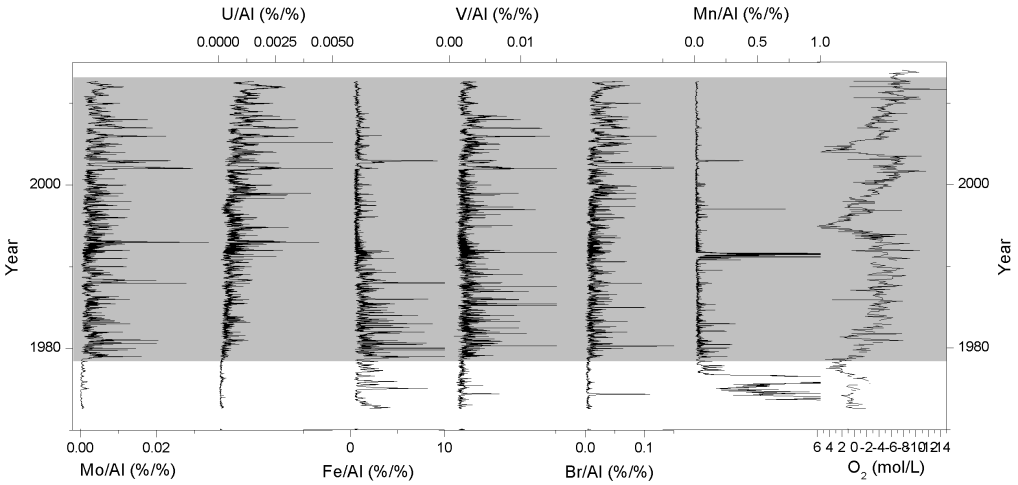

Figure 3.13: LA-ICP-MS records of several (trace) elements during the modern event at F80. The grey area indicates the duration of the event. The age model was constructed using the peak-counting method.

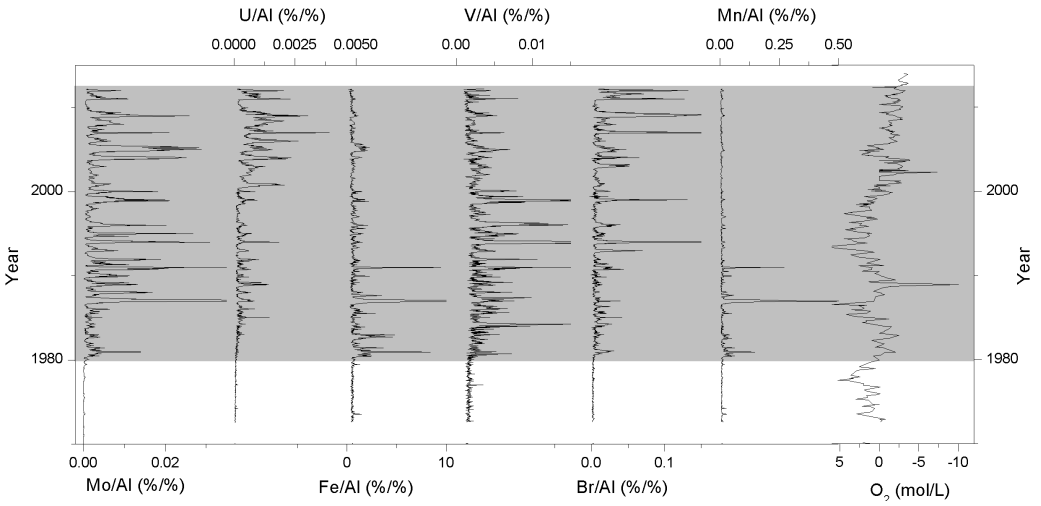

Figure 3.14: LA-ICP-MS records of several (trace) elements during the modern event at LL19. The grey area indicates the duration of the event. The age model was constructed using the peak-counting method.

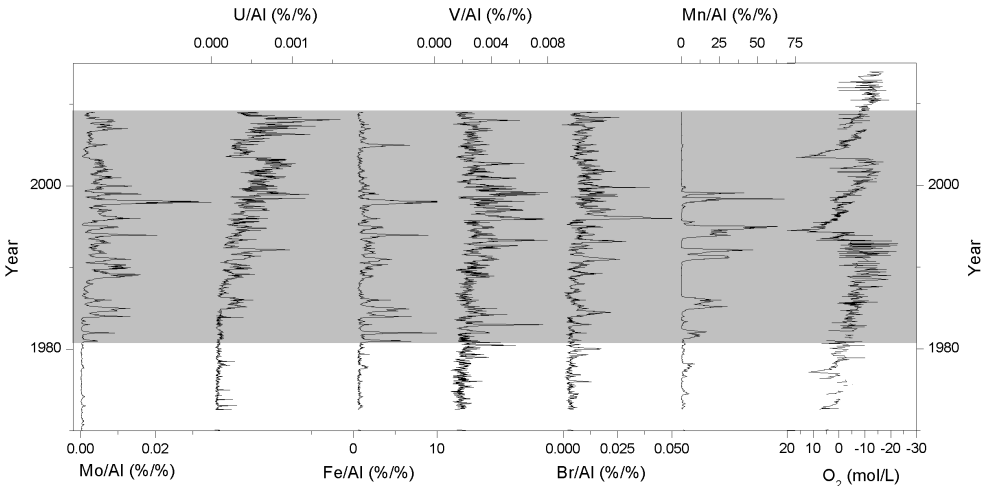

Figure 3.15: LA-ICP-MS records of several (trace) elements during the modern event at BY15. The grey area indicates the duration of the event. The age model was constructed using the peak-counting method.

3.3 Spectral analysis results

Based on the full LA-ICP-MS records of the HTM at F80 and SR5, and the MCA at F80 several power spectra were produced of selected elements. These power spectra reveal several multi-decadal cycles influencing the different records. During the HTM at F80 (Figure 3.16) a strong 50-year cycle is suggested by the power spectra of molybdenum, vanadium and uranium. Filtering this frequency indicates that the strongest representation of this cyclicity is during HTM-2, although HTM-5 to HTM-7 show influence of this 50-year cycle as well (Figure 3.17). Filters of the significant 100-year peaks in the power spectra of molybdenum and vanadium do not correlate well with their respective records.

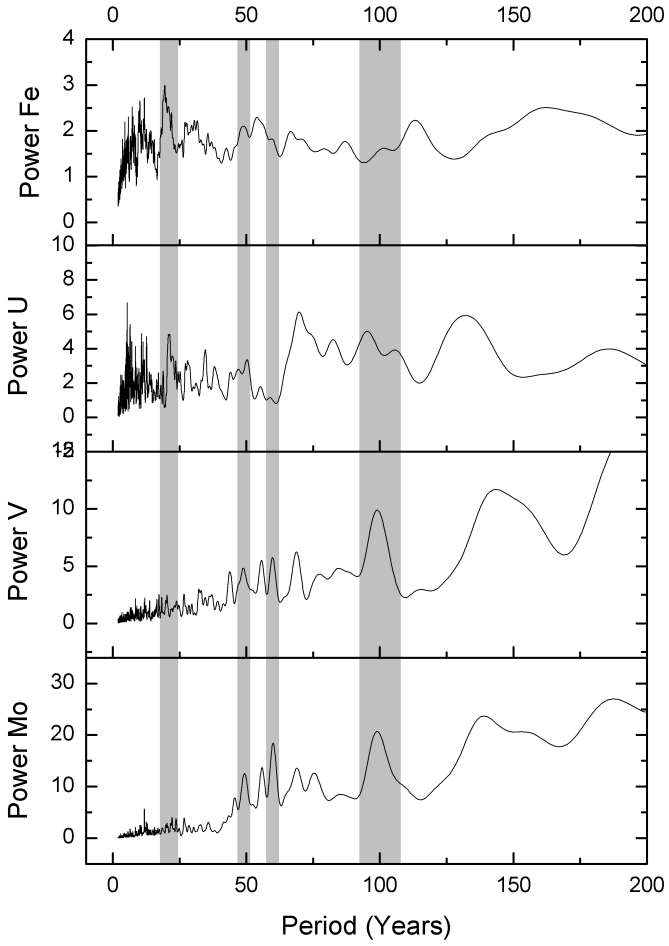

Figure 3.16: Power spectra for iron, uranium, vanadium and molybdenum at F80 during the HTM. Grey bands indicate cyclic periods shared between (some of) the elements.

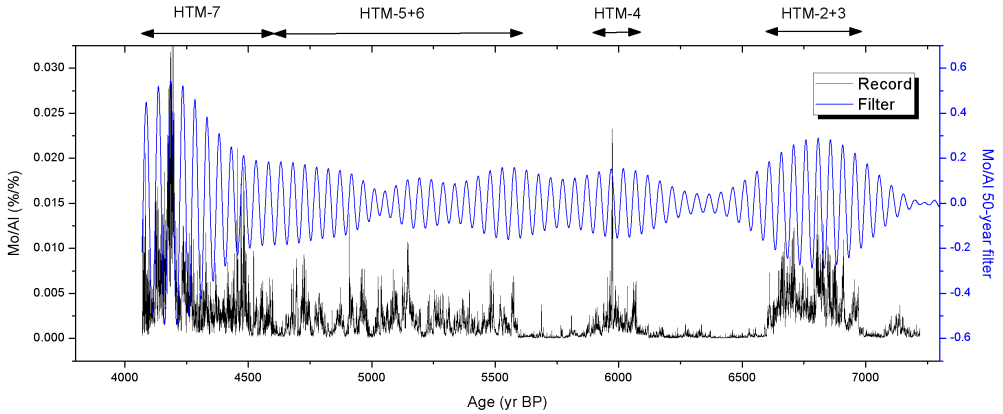

Figure 3.17: Comparison between the HTM F80 Mo/Al record (black) and its filtered 50-year periodicity (blue).

Apart from a weak 56-year cycle, no significant cyclicity was found in the molybdenum record at SR5 during the HTM (Figure 3.18). This 56-year cycle is strongest during the later part of SR5-1 and the first few hundreds of years of SR5-2. The same applies to the uranium and vanadium records, although in addition a weaker 44-year cycle is suggested by their power spectra.

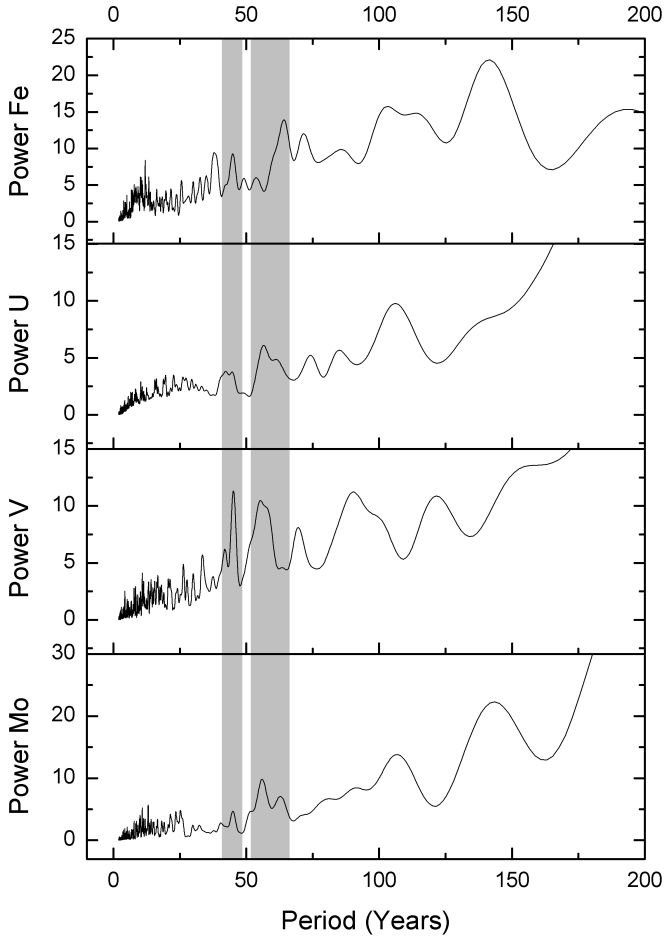

Figure 3.18: Power spectra for iron, uranium, vanadium and molybdenum at SR5 during the HTM. Grey bands indicate cyclic periods shared between (some of) the elements.

Despite suggestion by the power spectrum of the iron record of possible influence of a 54-year and 20-year cycle at F80 and a 45-year and 38-year cycle at SR5 no good relation can be found between the filters of these

cycles and their iron records, nor with the timing of events as suggested by the molybdenum records (Figure 3.19). However, when performing spectral analysis on HTM-5+6 specifically (Figure 3.20), good correlation can be found between Mo/Al and Fe/Al on both a 59-year and a 28-year periodicity (Figure 3.21).

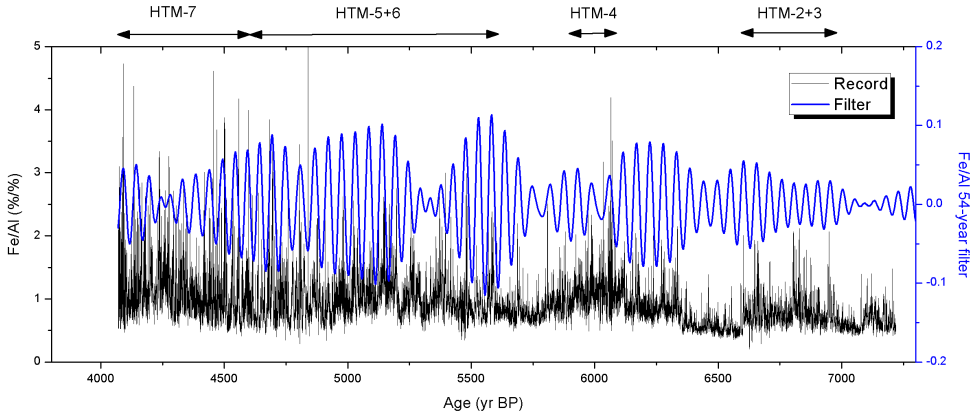

Figure 3.19: Comparison between the HTM F80 Fe/Al record (black) and its filtered 54-year periodicity (blue).

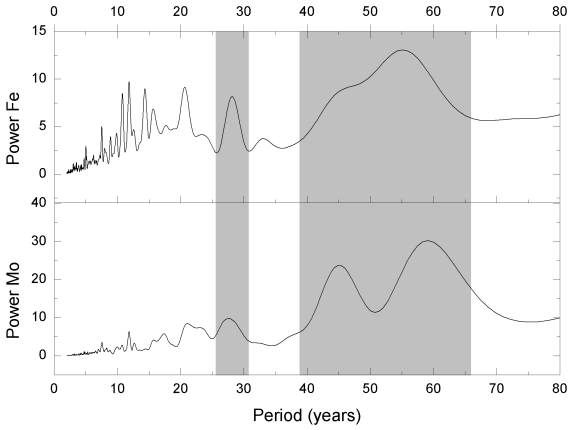

Figure 3.20: Power spectra for Mo/Al and Fe/Al at F80 during HTM-5+6. Grey bands indicate cyclic periods shared by the two elements.

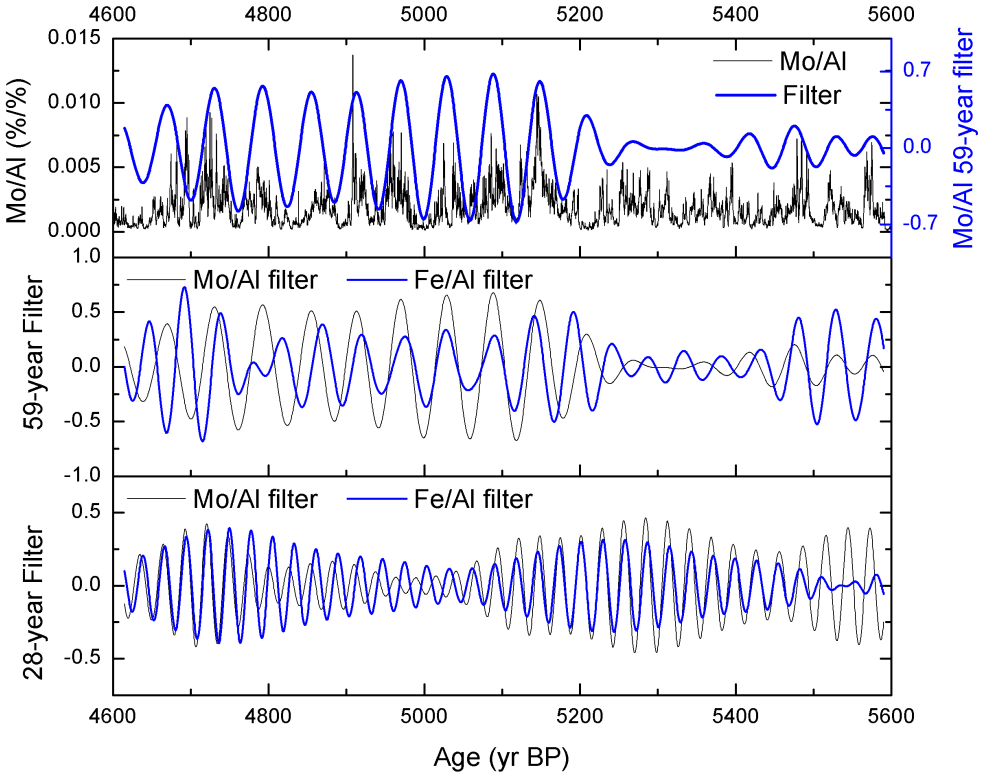

Figure 3.21: (Top) Comparison between the Mo/Al record of the HTM-5+6 at F80 (black) and its 59-year filter (blue). (Middle and bottom) Comparison between the 59-year (middle) and 28-year (bottom) frequency filters of the Mo/Al and Fe/Al records of the HTM-5+6 at F80.

Cyclicities during the MCA at F80 tend to be of higher frequency than during the HTM at F80, with the molybdenum record being dominated by a 45-year cycle and a weaker 27-year cycle (Figure 3.22). Although this 45-year cycle is not present in the vanadium and uranium records, there is relatively good correlation between these two records and their filtered 27-year cycles. Cyclicities of 38 and 26 years in the iron record are mostly related to the iron enrichments before, during and after the pre-MCA hypoxic event.

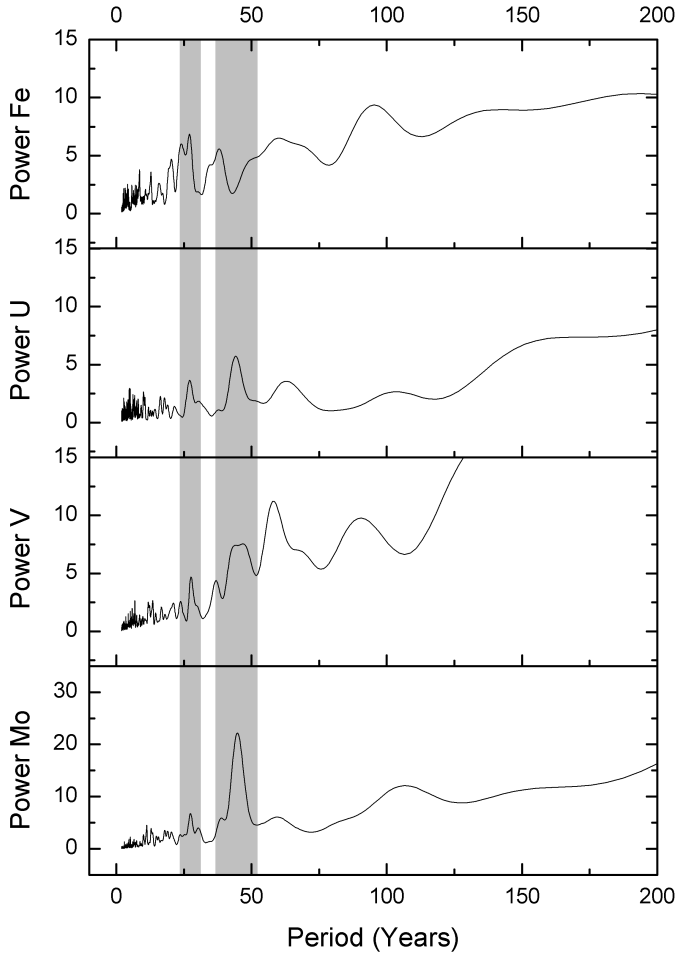

Figure 3.22: Power spectra for iron, uranium, vanadium and molybdenum at F80 during the MCA. Grey bands indicate cyclic periods shared between (some of) the elements.

4 Discussion

4.1 Techniques

4.1.1 Laser Ablation-Inductively Coupled Plasma-Mass Spectrometry

Although the LA-ICP-MS method has been successively applied for many different purposes since its first use in 1985 (Gray, 1985) many possible biases exist that need to be accounted for. It should be noted that a standard is used to calibrate the measurements from the sample. This is achieved by calculating the sensitivity of the LA-ICP-MS system to each element using the known concentrations in the standard and correcting for this calculated sensitivity in the sample measurements.

The main problem here is probably the inconsistency of matrix type between the sample and the standard. While the standard is very homogeneous, the matrix of the sample changes considerably within the ∼3.5 cm block length typically analysed (Figure 4.1). This has an impact in several different ways. First, changing densities throughout the sample may influence the relative ablation of different elements. Second, changing sediment types (as the possible cause of the changing matrix) may influence the ease with which the material ablates. Laser ablation of one material in the sediment may be easier than of another material, introducing possible biases through changing elemental fractionations. However, even in the theoretical case of a constant sample matrix possible biases may arise when the matrix of the sample is different than the matrix of the standard, since the matrix may also play a role in the sensitivity of the LA-ICP-MS system to the different elements analysed. As such, calibrating a sample for elemental sensitivities using a standard with a different matrix may, in itself, be erroneous.

Theoretically the best solution to these matrix problems would be to create a group of standards that all have a certain matrix typical for a certain sediment type. In practice this has many drawbacks though, not least of all the fact that the very nature of these matrices is that they are heterogeneous, making it hard to use as a standard. There is one possible use for such a standard though, where the elemental sensitivities calculated from the NIST-610 standard can be assessed using the second standard. A possible workaround may exist, especially for the biases due to density differences, where the resin used for the resin-embedding of the sample is spiked with a

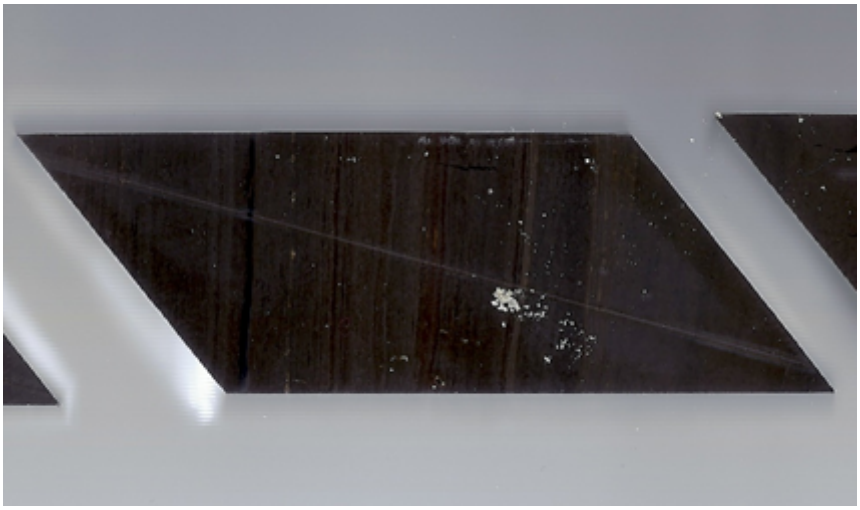

Figure 4.1: Scan of one of the resin-blocks used from the MCA, showing changing sediment types on small scales, suggesting possible matrix changes. The block itself is ∼4.5 cm in diameter.

certain element not natural to the source area of the sample. Since a decrease in sample density will be inversely visible in the resin as an increase in resin density, the concentration of such an element could be used as an indication of the density of the sample.

4.1.2 Calibration of the LA-ICP-MS (trace) elemental records

Without a sufficiently good standard for calibration to elemental sensitivities of the measured elemental concentrations on the sample the resulting element-to-aluminium fractions will have a certain error margin. Although further calibration to the discrete samples measured using ICP-OES has been performed, here too some problems arise. As an example, the method for averaging of the LA-ICP-MS-derived element-to-aluminium ratios has a substantial impact on the calibration. The two main candidates here were application of an arithmetic mean and of a geometric mean (Figure 4.2). Furthermore, the whole concept of such a calibration of LA-ICP-MS to ICP-OES, as performed for this study, is mathematically false (Equation 4.1). The discrete samples take the ratio of the mean of the element to the mean of aluminium, while the binned means take the mean of the ratios of the element to aluminium. However, these two expressions are not the same.

$$\frac{mean(A)}{mean(B)} = \frac{A_1 + A_2 + \ldots + A_n}{B_1 + B_2 + \ldots + B_n} \neq \frac{A_1/B_1 + A_2/B_2 + \ldots + A_n/B_n}{n} = mean\frac{A}{B} \tag{4.1}$$

Despite all these problems the impact on further analyses is very small, since mostly they only influence the quantification of the different element-to-aluminium ratios while the trends and cyclicities stay the same. The only exception to this is the possible bias of calcite layers. Since aluminium concentrations will be significantly lower in a calcium carbonate-based matrix, using aluminium as an internal normaliser possibly introduces significant peaks in all other elements when passing a calcite layer. However, not many of these layers appear in the LA-ICP-MS (trace) elemental records.

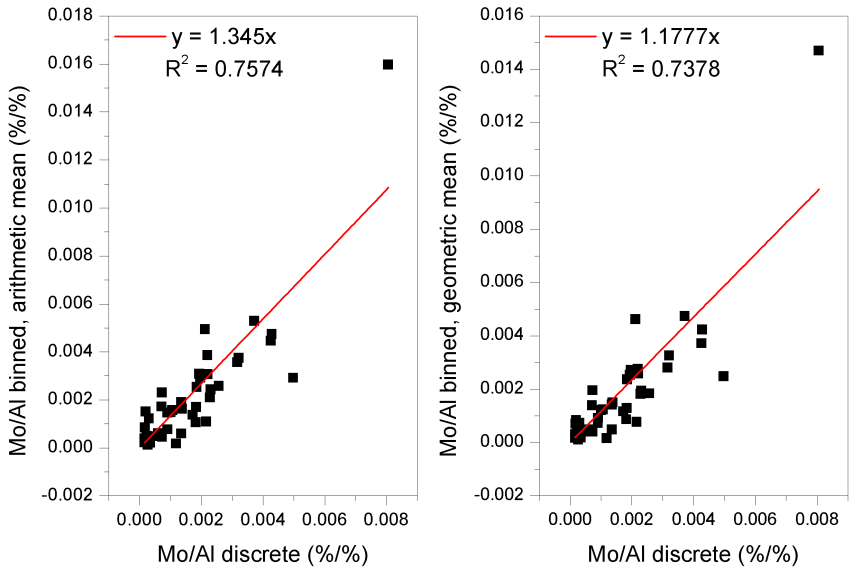

Figure 4.2: Comparison between arithmetic (left) and geometric (right) binned means, correlated to the discrete samples of the MCA at F80.

4.2 Critical assessment of Mo/Al peak counting as a dating technique

4.2.1 Mo/Al peak counting

4.2.1.1 Validation of Mo/Al peak counting approach: modern hypoxic interval Age models for the modern intervals at F80, LL19 and BY15 have been constructed based on the assumption that Mo/Al ratios will display strong seasonality, with more intense enrichments during spring and summer algal blooms. There are several lines of evidence supporting the validity of this assumption. First, the chemical behaviour of molybdenum in the water column and in the sediments suggests possible coupling with organic matter supply (Helz *et al.*, 1996). Molybdenum could be trapped by and adsorbed onto organic aggregates settling to the sediment-water interface, increasing the incoming flux of molybdenum. In addition, Tribovillard *et al.* (2006) have shown that molybdenum can be scavenged by organic matter either through O–S groups attaching to the molybdenum species, or through metal-rich particles carried by the organic matter. These processes will enhance burial of molybdenum during the spring and summer algal blooms, leading to a seasonal signal in the molybdenum record.

A second indication of the validity of the assumption of a seasonal signal in the Mo/Al record involves seasonal variability in the deposition of aluminium. Due to decreased productivity, aluminium content of the total sedimentary matter is expected to be higher during autumn and winter than during spring and summer (e.g., Deuser *et al.*, 1981; Pohl *et al.*, 2004). Hence, both enhanced Mo sequestration, and dilution of the incoming detrital matter by organic material, act to elevate the Mo/Al ratio during the summer season. Indeed, strong anticorrelation can be found between raw aluminium counts and Mo/Al ratios during the modern hypoxic interval (Figure 4.3).

Finally, the validity of the assumption of seasonal molybdenum variability can be tested by comparison with the bottom water oxygen records. At all three sites (F80, LL19 and BY15) the bottom water oxygen records indicate a shift to euxinic conditions around 1980. This suggests that more permanent molybdenum enrichments should start around that time. If a strong seasonal signal is present in the molybdenum record, this signal should be able to be used to "count back" from the time the core was taken (i.e., 2013) year by year, back to the moment molybdenum enrichments started (i.e., 1980). For sites F80 and LL19 this is indeed the case, with 34 peaks in Mo/Al

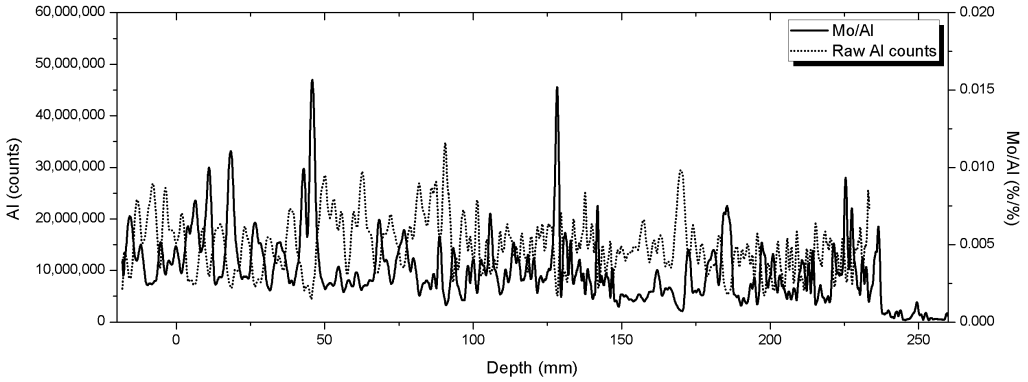

Figure 4.3: 30-point moving averages of Mo/Al ratios (solid line) and raw Al counts (dotted line) for the top ∼30 cm of F80, showing strong anti-correlation.

corresponding to 34 troughs in raw Al counts (Figure 4.3). At BY15 only 30 such peaks can be identified. However, when assuming the top of the core has been lost (i.e., the record runs up to 2009), correlation can be found between suggested Mo/Al, and especially U/Al, ratios and inflow events as indicated in the bottom water oxygen record (Figure 3.15).

4.2.1.2 Application of Mo/Al peak counting to construct age models for older intervals Given the strong seasonal signal in the molybdenum record of the modern events at F80, LL19 and BY15, the identification of annual Mo/Al peaks has been used in the construction of an age model for the older events at F80. In an effort to mitigate any possible subjective influences on the determination of the age model, spectral analysis was used to identify the frequency in the depth domain of Mo/Al relating to the yearly variability of molybdenum. The resulting sedimentation rate records were then used to construct the age model.

Several problems arise when performing this procedure to reconstruct an age model. Although objectivity of the method is high, the arbitrary selection of 1-cm slices for spectral analysis can introduce problems when a shift in conditions and/or sedimentation rate occurs within this slice. Although the three conditions described in the methods section are set up in part to catch these biases, some may still pass. This is especially likely when changes in sedimentation rate happen gradually, leading to a wide base of the peak of

the candidate frequency. More abrupt changes will result in two separate peaks with narrow bases, which are easier to filter out.

The question may arise whether these 1-cm slices are actually representative of the overall situation, especially since the conditions may block several consecutive slices. This could lead to the 1-cm slice dictating the sedimentation rate of up to 15 cm of sediment while these other slices could contain valuable information. As an example, the sedimentation rates as reconstructed for points A and B (see Figure 4.4) determine sedimentation rates for the ∼15 cm in between these points, since no other points between A and B passed the filter. As such, any variability between these points is not incorporated. The same applies to point C and the subsequent point, since these two points determine the sedimentation rate for ∼10 cm of core.

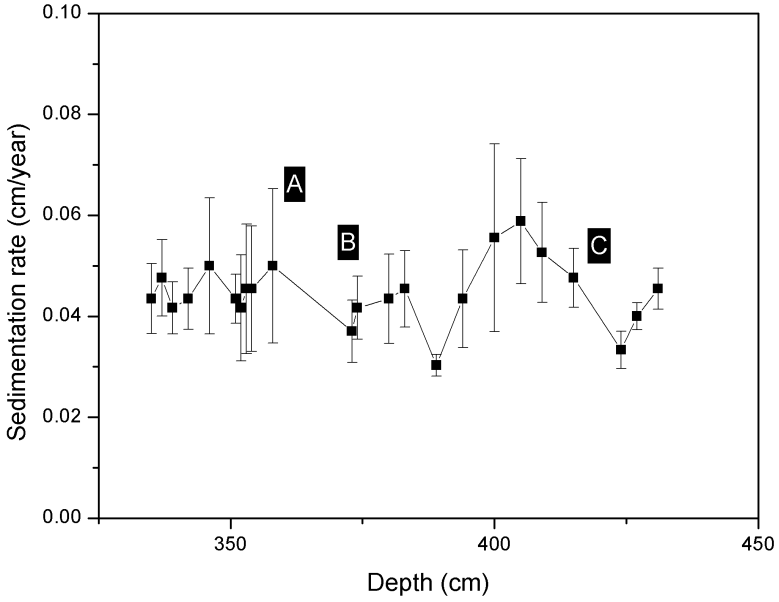

Figure 4.4: Reconstructed sedimentation rate during the HTM at F80. Three points have been identified for clarification in the text (A, B, C).

Finally, since a prerequisite of the observed seasonality in Mo/Al is the presence of euxinic conditions close to the sediment-water interface (Tribovillard *et al.*, 2006), more oxygenated intervals of the record with constant near-zero Mo/Al levels cannot be used for determination of sedimentation rate. This introduces a potential bias towards good constraint of sedimenta-

tion rates during hypoxic events without proper constraint on sedimentation rates outside these events (e.g., before and after HTM-4).

4.2.1.3 Possible future improvements to dating approach One improvement that can be made when using spectral analysis on the Mo/Al record for reconstructing timescales is to restrict the analysis to individual events. Although this will result in a floating timescale rather than a fixed one, this will remove the bias of euxinic over oxygenated intervals. In addition, a fourth condition could be added, removing any candidate frequencies with broad peaks (verified by filtering that frequency range over the sliced part of the record).

4.2.2 Sedimentation rates

4.2.2.1 Influence of detrital versus non-detrital material on sedimentation rates Sedimentation rates calculated by the Mo/Al peak counting approach can be used to estimate the total input of non-detrital (biogenic and authigenic) material through time. In this method, a constant flux of detrital material is assumed and the contribution of the major biogenic and authigenic phases are summed (Equation 4.2). The resulting relationship between sedimentation rate and the flux of non-detrital material can be used to assess the extent to which bulk sedimentation rate is dictated by accumulation of biogenic and authigenic material. In principle, if no relationship is observed it can be stated that the input of detrital material exerts the primary control on sedimentation rates. Mo/Al is used to estimate organic matter (OM)/Al using the constant A. A is determined by regressing Mo/Al to organic carbon (Figure 4.5). From the gradient, Mo/Al can be converted to C_{org}, and C_{org} to OM assuming organic matter (CH_2O) $= 2.5 * C_{org}$. Furthermore, B (=2.7) estimates the concentration of rhodochrosite from Mn, C (=1.88) estimates the concentration of pyrite from S, and D (=2.14) estimates the concentration of opal (SiO_2) from biogenic silica. All parameters are normalised to Al.

$$non\text{-}detrital\ component/Al = A*Mo/Al + B*Mn/Al + C*S/Al + D*BSi/Al \quad (4.2)$$

When regressing Mo/Al to C_{org}, good correlation is found with an R^2 of 0.92, indicating on average that C_{org} equals to $Mo/Al * 261.98 + 0.396$ (Figure 4.5).

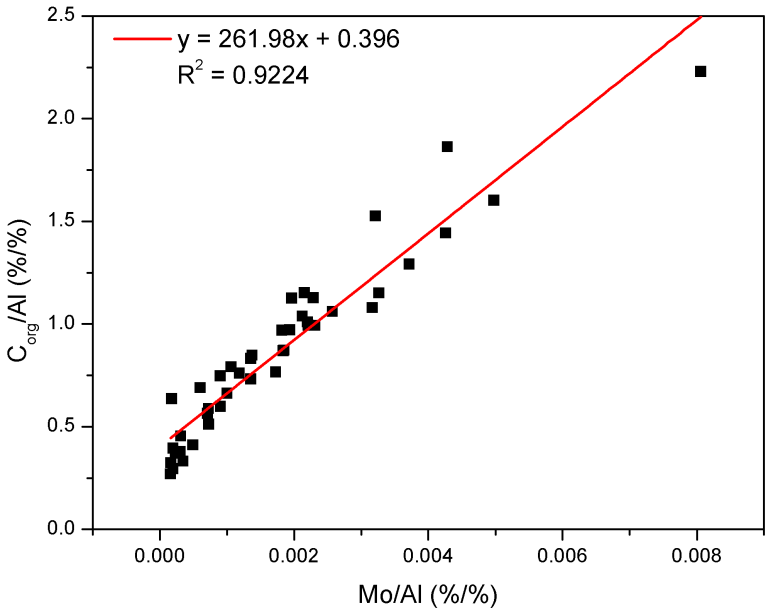

Figure 4.5: Correlation between the Mo/Al and Corg/Al discrete sample records at F80 during the HTM.

This leads to an expression for OM/Al (Equation 4.3).

$$A * Mo/Al = OM/Al = 2.5 * 261.98 * Mo/Al + 0.396 \quad (4.3)$$

Applying equations 4.2 and 4.3 to the discrete samples for F80 and the biogenic silica record produces a record of the total non-detrital component of incoming material at this site. Correlation of this record to the sedimentation rate record estimated by Mo/Al peak counting (Figure 4.4) is very weak with an R^2 of 0.0086 (Figure 4.6). This indicates that the initial assumption of a constant flux of detrital material to F80 was false, and that the detrital component must have varied substantially over the course of the record.

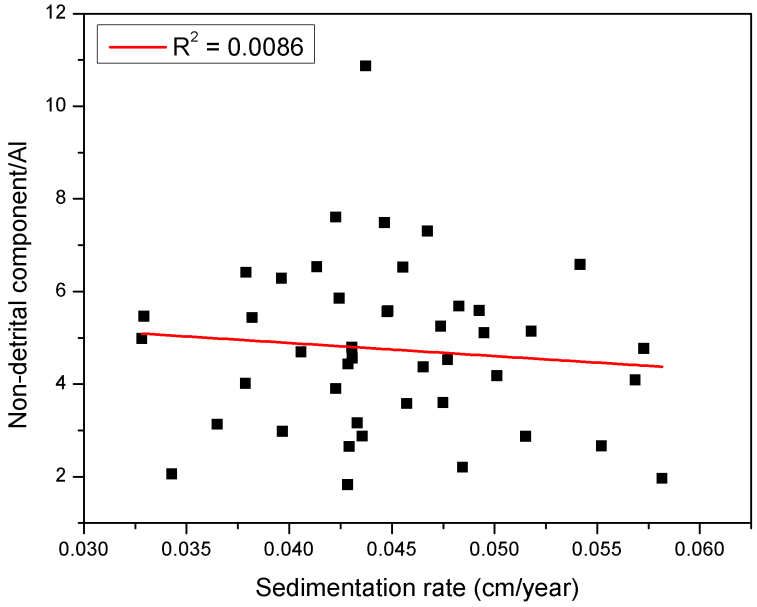

Figure 4.6: Correlation between reconstructed sedimentation rate and reconstructed non-detrital component of sedimentation for the HTM at F80.

4.2.2.2 Comparison of methods for inferring sedimentation rates

Several methods can be used to reconstruct sedimentation rates for past hypoxic events at F80 and SR5. Here a comparison will be given between reconstructions of sedimentation rates during specific events based on paleomagnetic secular variation (PSV), spectral analysis tuning and the peak-counting technique used for the modern event. The PSV-method was used to date a reference core in the Gotland basin (Lougheed *et al.*, 2012) to which the F80 record was tuned by comparison of the respective Loss on Ignition (LOI) and C_{org} profiles of the two cores (Jilbert and Slomp, 2013a). The peak-counting technique has been used to date the modern hypoxic event at F80, LL19 and BY15. This method is based on the assumption that a strong seasonal signal is present in the Mo/Al record, allowing counting of Mo/Al peaks to provide a timescale. It could however also be used to reconstruct a floating timescale for individual, older hypoxic events. The spectral analysis tuning is an attempt to expand the peak-counting technique to the older hypoxic intervals of the MCA and the HTM. This is achieved by identifying

the frequency of the yearly cyclicity in the Mo/Al record in a wavelet diagram and/or a power spectrum and using that frequency as an indication of sedimentation rates. Given a strong seasonal signal in the molybdenum record the peak-counting technique will yield the most precise result if used on a single, continuous and short hypoxic event, and will therefore be used to assess the other methods.

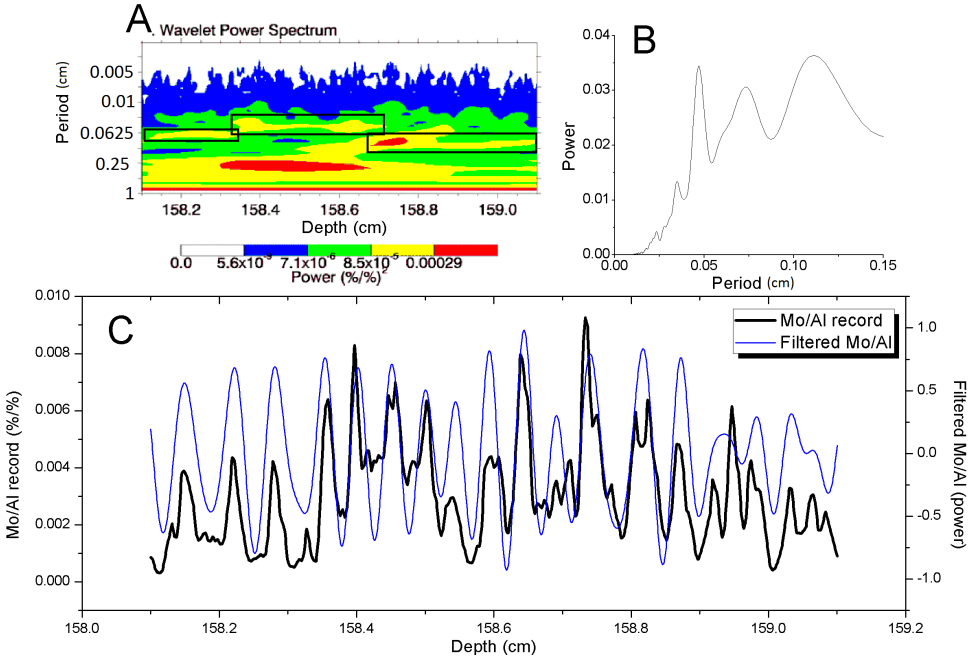

Figure 4.7: (A) Wavelet analysis of a selected interval within MCA-2a, suggesting a yearly periodicity shifting from 0.08 cm to 0.04 cm to 0.06 cm, indicated by the black boxes. (B) Spectral analysis of the selected interval, confirming yearly periodicities of 0.048 and 0.074 cm. (C) Filtered series (blue) of the selected interval (black). The filtered periodicity is between 0.04 and 0.085 cm.

The spectral analysis method has been divided into two submethods. The first uses power spectra of 1-cm slices over the whole Mo/Al record to identify sedimentation rates, while the second submethod applies this procedure exclusively to an hypoxic interval of no more than 1 cm long. Wavelet analysis of such an hypoxic interval (in this case MCA-2a) suggests changing sedimentation rates throughout the interval between ∼0.08 and 0.04 cm

year^{-1} (Figure 4.7a). Spectral analysis on the interval indeed reveals periodicities of 0.048 and 0.074 cm year^{-1}, with a small bump at 0.061 cm year^{-1} (Figure 4.7b). Filtering over these frequencies yields an approximation of sedimentation rate as estimated using the spectral analysis method (Figure 4.7c).

Based on the PSV age model, sedimentation rates during the MCA were slightly higher than during the HTM (Figure 4.8). Although the three techniques based on peak counting agree with this assessment, error bars during the MCA are large compared to the HTM. Especially during the HTM, the PSV dating method seems to consistently estimate sedimentation rates around 0.015 cm yr^{-1} lower than the peak-counting methods. This is probably caused by the lower frequency boundary for the spectral analysis-based reconstructions being higher than the PSV-based sedimentation rates. The PSV-based sedimentation rates are interpolations between a few datapoints, and should therefore be interpreted as average sedimentation rates over longer timescales.

Although points from the three peak-counting techniques generally fall within each other's error bars, the wide spread (especially during the MCA) shows that this technique for creating an age model needs more improvement before it can be confidently used to date Baltic Sea sediment cores. For this reason the PSV age model has been used to date the trace elemental records discussed in this report. It should be noted, however, that the spectral analysis dating method shows very good agreement with the peak-counting technique. For this reason the spectral analysis dating method is a good candidate to provide high-resolution floating timescales for individual hypoxic events.

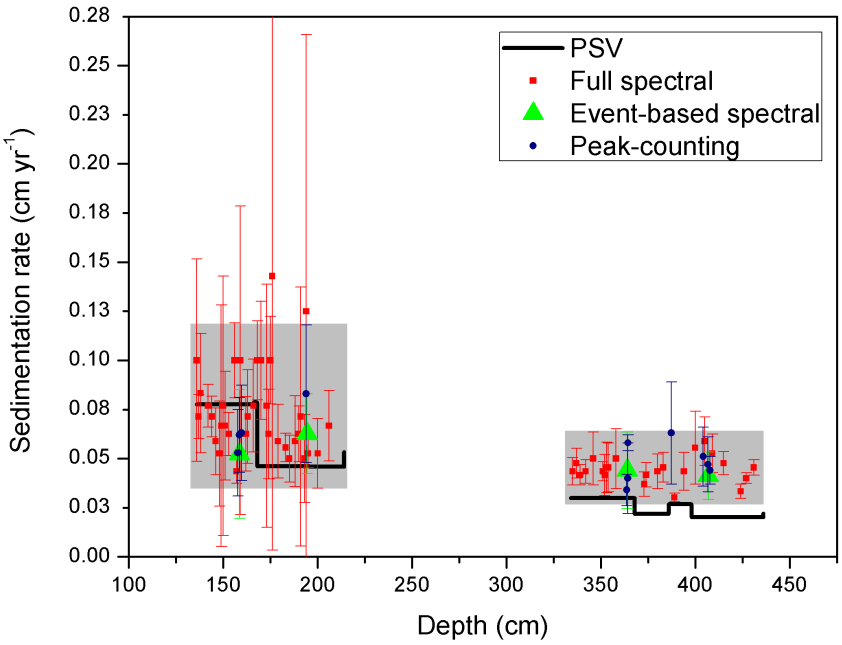

Figure 4.8: Reconstructed sedimentation rates for the MCA and the HTM at F80 based on the PSV age model (black), the spectral analysis age model (red) and spectral analysis (green) and peak-counting (blue) on specific hypoxic intervals. Grey boxes indicate the upper and lower frequency boundaries for the spectral analysis-based reconstructions.

4.3 Euxinia and redox conditions recorded in Baltic Sea high-resolution (trace) elemental records

4.3.1 Validity of molybdenum as redox proxy

In order to be able to use molybdenum as a proxy for paleoredox conditions, it must be verified that molybdenum was never depleted from the local system due to, for example, reservoir effects (Algeo and Lyons, 2006). Depletion would occur if the input of molybdenum was too low compared to the fixation of Mo in the sediments. The fact that Mo/Al enrichments at F80 keep increasing throughout the HTM, the MCA and the modern hypoxic event (Figure 3.1) suggests that depletion of molybdenum does not play a role here. Furthermore, good correlation can be found between Mo/Al and the Br/P ratio (as a high-resolution equivalent of C/P; Figure 4.9a), further strengthening the idea that molybdenum can be used to reconstruct redox conditions at F80.

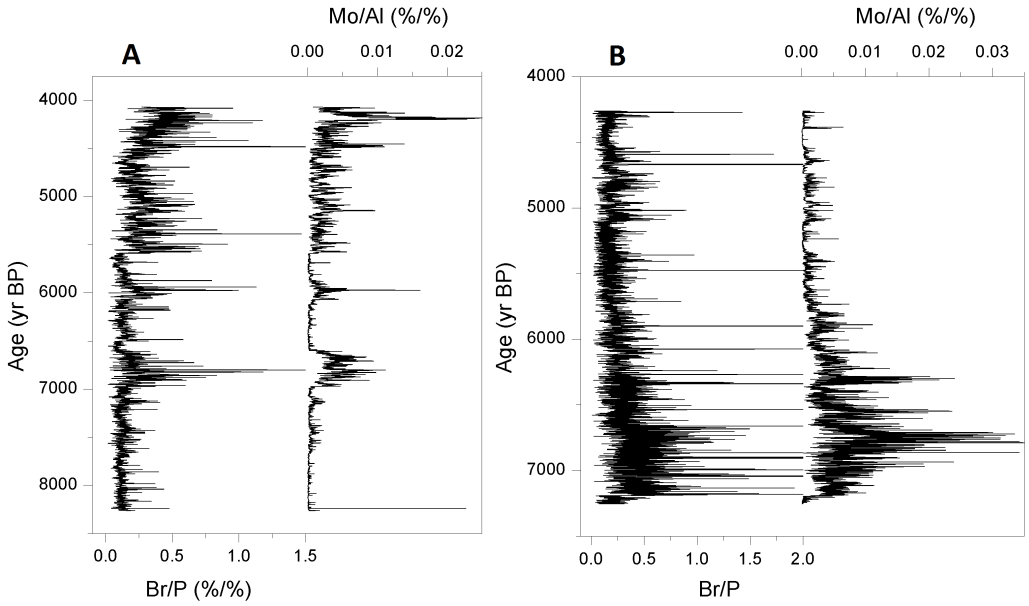

Figure 4.9: Br/P and Mo/Al ratios throughout the HTM at F80 (A) and SR5 (B).

Due to the consistent yearly enrichments in Mo/Al at sites F80, LL19 and BY15 during the modern hypoxic event it can be assumed that here,

too, molybdenum has not been depleted. However, during the HTM at SR5 a decoupling is visible between the Mo/Al and Corg discrete samples (Figure 3.2). This could suggest that depletion of molybdenum played a role in this basin during the HTM. Weak correlation between Mo/Al and Br/P ratios at SR5 again suggests that Mo/Al depletion may have occurred here during the HTM (Figure 4.9b).

4.3.2 Reorganisation of hypoxic events

Although the discrete samples profile of Mo/Al suggests seven hypoxic events during the HTM at F80 (Figure 3.1), the LA-ICP-MS record indicates only five of these are present. Since HTM-3 is not reflected in the high-resolution molybdenum record it can be merged with HTM-2. In addition, the minimum in the discrete samples profile of molybdenum between HTM-5 and HTM-6 is not unique and should therefore not be considered as a boundary between (main) hypoxic events. Although molybdenum enrichments during HTM-1 are very low (up to 0.003 Mo/Al) a small event is visible here confirming HTM-1 as a (weak) hypoxic event.

4.3.3 Baltic Sea hypoxic intervals throughout the Holocene

Throughout the HTM at F80 a gradual increase in Mo/Al ratios indicates bottom water oxygen levels were, on average, decreasing throughout these 4.5 kyr (Figure 3.1). This is not only visible in the strengths of individual events (with a weak HTM-1 and strong HTM-7) but also in the frequency of events. As an example, the first few events are separated by several centuries of oxygenated conditions, while F80 becomes permanently euxinic from HTM-5.

After termination of HTM-7 at F80 around 4.1 ka BP several millennia passed where bottom waters were oxic as evidenced by the near-zero Mo/Al values (Figure 3.1). Around 1.05 ka BP the hypoxic events of the MCA started with the onset of MCA-1. However, half a millennium before MCA-1 a short hypoxic event occurred (the pre-MCA event; Figure 3.10). Due to a very strong seasonal signal the duration of this hypoxic event can be counted as 15 years using the Mo/Al peak-counting technique, although true onset of the event is hard to determine due to small enrichments before the pre-MCA event. It should be noted that the PSV-based age model used for the results is off here, claiming lower sedimentation rates (see Section 4.2).

In contrast to the very gradual increase in Mo/Al enrichments over several millennia during the HTM, the MCA is characterised by a more rapid onset, after which Mo/Al is continuously enriched until the final termination ∼450 years later.

Although Mo/Al enrichments gradually increased during the HTM at F80, the opposite was true at SR5 in the Bothnian Sea (Figure 3.2). Here, SR5-1 was the most intense event, after which each subsequent event was weaker than the preceding one. Two factors could have played a role here, explaining this discrepancy between F80 and SR5. One of these factors is the build-up of a sill between the Bothnian Sea and the Baltic Sea. Due to the resulting shallower passage between the basins less hypoxic and salty deep waters could reach the Bothnian Sea, causing a weakening of the halocline in this basin. This may have contributed to the weakening of events at SR5 throughout the HTM. In addition to this, reservoir effects may have influenced the amount of molybdenum available for storage in the sediments. If transport of molybdenum to bottom waters was slower than its precipitation, molybdenum would become depleted in the deeper waters. In such a case, even strong events would lead to the precipitation of only limited amounts of molybdenum.

4.3.4 Causes of onsets and terminations of Baltic Sea hypoxia

A combination of two different factors could lead to perturbations in bottom water oxygen concentrations. First, increased nutrient loading could lead to increased primary productivity in the surface waters. The resulting increased flux of organic matter to deeper waters then causes oxygen stress, since bacteria will use remaining oxygen to degrade the organic matter. Second, a decrease in deep water ventilation rates could cause stagnation of the bottom waters.

4.3.4.1 Nutrient loading as driver of Baltic Sea hypoxia Increased primary productivity due to increased availability of nutrients leads to an enhanced flux of organic matter to deeper waters, potentially causing oxygen stress in Baltic Sea bottom waters. There are two possible sources for such an increased flux of nutrients. First, an external flux can be composed of (river) runoff into the sea, introducing terrestrial nutrients to the system. As a second possibility, internal remobilisation of phosphorus from the sediments may cause increased nutrient loading in the surface waters (e.g., Jilbert and

Slomp, 2013b). These internal and external forcings may act together (e.g., external input of nutrients triggering internal remobilisation of phosphorus).

4.3.4.1.1 Internal forcings on Baltic Sea nutrient loading Since phosphorus is ultimately the limiting nutrient in the Baltic Sea (Jilbert and Slomp, 2013a), internal remobilisation of phosphorus could have a significant impact on sea surface primary productivity. Phosphorus is mainly transported to sediments as organic P. Concentrations of phosphorus in the water column are mainly dependent on the rate of phosphorus release or uptake from reduction or creation of iron-oxyhydroxides, the rate of phosphorus regeneration from organic matter, and the rate of change of the hypoxic area (Jilbert *et al.*, 2011). Given a hypoxic area constant in size, the water column phosphorus concentration will be determined by the difference in phosphorus uptake by iron-oxyhydroxides outside the hypoxic area, and phosphorus release through remineralisation of organic matter in the water column and surface sediments inside the hypoxic area (Jilbert *et al.*, 2011).

Preferential remineralisation of phosphorus from organic matter increases with increasing anoxia (Algeo and Ingall, 2007), which results in decreasing NH_4^+/HPO_4^{2-} sediment efflux ratios with increasing depth and hence with increasing anoxia (Jilbert *et al.*, 2011). As a consequence, increased oxygen stress will lead to increased sedimentary N/P and C/P ratios. Given that bromine may be used as a proxy for marine organic matter content in the sediment (Ziegler *et al.*, 2008), the LA-ICP-MS Br/P record can be used as a high-resolution equivalent to the discrete-sample C_{org}/P_{tot} ratios. Onset of the modern hypoxic event at two of the three analysed sites is characterised by an increase in Br/P ratios, confirming the increased preferential remineralisation of phosphorus from organic matter under more reducing conditions at these sites (Figure 4.10). At BY15 this increase in background Br/P ratios does not occur. High-frequency (seasonal) variations further indicate that the degree of preferential remineralisation of phosphorus from organic matter changes throughout the year, with highest Br/P ratios correlating with Mo/Al peaks (i.e., most reducing conditions).

The size of the hypoxic area will rarely be constant, with phases of contraction following phases of expansion and vice-versa. During expansion of the hypoxic area between 1994 and 2000 strong positive correlation was found between the size of the hypoxia area and total pool of HPO_4^{2-} in the water column (Conley *et al.*, 2002). Due to an expanding hypoxic area, both

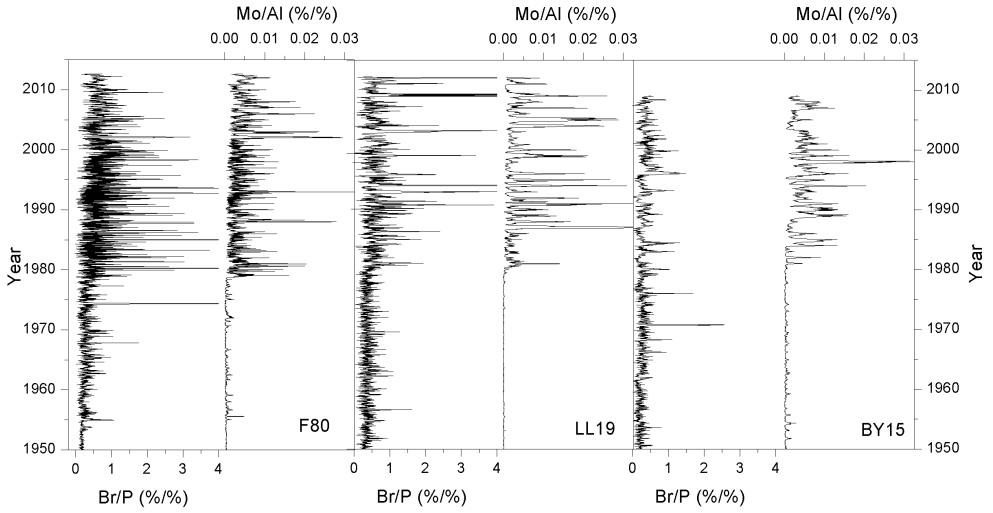

Figure 4.10: Br/P and Mo/Al records for the modern hypoxic event at F80 (left), LL19 (middle) and BY15 (right). Note the lack of enrichments in Br/P at BY15.

remineralisation of phosphorus and release of iron-bound phosphorus from previously oxic sites act together to increase water column phosphorus concentrations. A net trend towards higher water column phosphorus concentrations was also found during the contraction phase between 1970 and 1993, although less severe. This suggests that release of phosphorus from remineralisation outweighs uptake of phosphorus by iron-oxyhydroxides even when the hypoxic area is decreasing in size. Transport of iron from shallow to deeper sites may contribute to this (Jilbert *et al.*, 2011).

Onsets of hypoxic events may therefore be accompanied by positive feedbacks in the phosphorus cycle, where an initial decrease in bottom water oxygen concentrations may reduce iron-oxyhydroxides. Any phosphorus bound to these Fe-oxyhydroxides would be remobilised, leading to increased primary productivity, further increasing oxygen stress. An initial increase in hypoxia area may therefore be sustained by release of iron-bound phosphorus from the previously less reducing sites.

Given the observed increase in Br/P ratios due to increased preferential remineralisation of phosphorus during the modern hypoxic event (Figure 4.10), the influence of this internal forcing can also be assessed for hypoxic events during the MCA and HTM. Slightly increased Br/P ratios can be seen

during all hypoxic events at F80 during the HTM (Figure 4.9a) as well as during MCA-1 and MCA-2 (Figure 4.11). No Br/P enrichments above background levels are present for the pre-MCA event. This may be because the conditions before onset of that hypoxic event were already quite unstable (as evidenced by the numerous Mo/Al peaks in the centuries before and after the event; Figure 3.10), essentially "drowning" the Br/P enrichments of the pre-MCA event in the background noise.

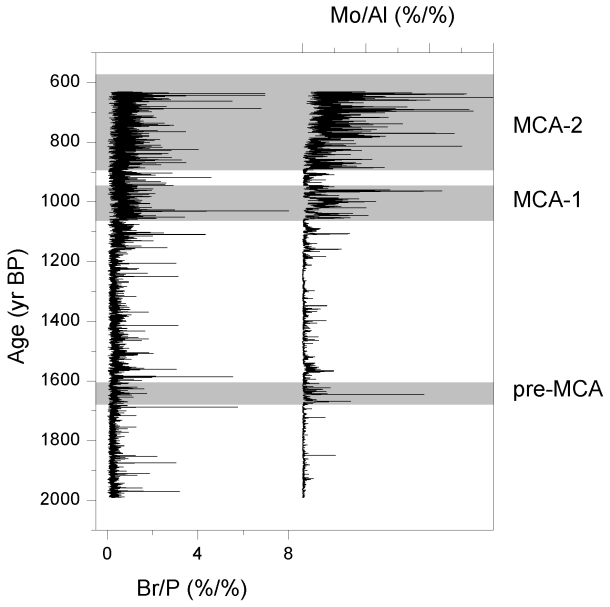

Figure 4.11: Br/P and Mo/Al records of the MCA at F80.

The sudden termination of HTM-7 at F80 (Figure 3.1) may be related to the closing of the sill between the Baltic Sea and the Bothnian Sea. While closing of this sill blocked salty deep waters from entering the Bothnian Sea, surface waters were still able to flow north. Any phosphorus carried to the north by surface waters would eventually be buried in the less reducing sediments of the Bothnian Sea, causing this basin to be a sink for phosphorus (Slomp *et al.*, 2013). The gradual shallowing of the sill between the Baltic and Bothnian seas may also explain the weak correlation between the Mo/Al and Br/P records during the HTM at SR5 (Figure 4.9). Although some correlation is still present during SR5-1, this is not the case for the rest of the HTM. Input of phosphorus from the Baltic Sea may have dampened the signal of preferential remineralisation of phosphorus in the Bothnian Sea.

In short, internal cycling of phosphorus is an important forcing for Baltic Sea hypoxia, having played a role in the modern hypoxic event (Jilbert *et al.*, 2011), and likely also during the MCA and HTM. Although correlation between Mo/Al and Br/P during the HTM at SR5 is not as strong as it is at F80, this does not exclude internal phosphorus cycling — rather, this is probably caused by depletion of molybdenum. However, an initial perturbation of the system is needed for internal cycling of phosphorus to start.

4.3.4.1.2 External forcings on Baltic Sea nutrient loading Input of new nutrients from, for example, river runoff may act as the initial perturbation needed to set in motion the positive feedback inherent in the sedimentary phosphorus. External input of nutrients may be influenced by climatological parameters (i.e., precipitation rates over the Baltic Sea catchment area). Anthropogenic input of nutrients as forcing of Baltic Sea hypoxia should not be excluded though (Zillén and Conley, 2010).

Increased precipitation rates over the Baltic Sea catchment area could enhance the flux of nutrients to the sea. A pollen-based climate reconstruction of the Baltic Sea catchment area (Seppä and Birks, 2001) shows almost no correlation between Baltic Sea hypoxia and precipitation in the catchment area. High precipitation rates do occur in the catchment area of the Baltic Sea before the onset of HTM-1 at F80 (circa 7.5 ka; Figure 4.12). These high precipitation rates may have enhanced nutrient loading in the Baltic Sea. Increased nutrient loading due to increased precipitation rates in the Baltic Sea catchment area may therefore have contributed to the onset of hypoxic events during the HTM. This was probably enhanced by release of phosphorus previously bound to iron-oxyhydroxides (Sohlenius *et al.*, 2001). See section 4.3.7 for a more in-depth analysis of the influence of regional climate on Baltic Sea hypoxia.

Onset of the modern hypoxic event as well as the hypoxic events of the MCA have been linked to anthropogenic influences (Zillén and Conley, 2010). The onset of MCA-1 at 900 AD coincides with a radical improvement of the plough in northern Europe (Gies and Gies, 1994). This improvement allowed for large-scale deforestation and subsequently lead to a significant rise in population and agricultural productivity. Related increased input of nutrients to the Baltic Sea may have triggered the onset of the hypoxic events of the MCA. Interestingly, termination of the last hypoxic event of the MCA (1350 AD) falls within the timeframe of the first spread of the plague and asso-

ciated decrease in population in Germany and Scandinavia (Walløe, 1995). As an example, the total population of Sweden dropped from 1,100,000 to 347,000 between 1300 AD and 1413 AD, a decrease of around 68% (Zillén and Conley, 2010). Likewise, total population of Germany dropped by 55% over the same timespan (Simms, 1976). These large drops in population were accompanied by a decrease in agricultural productivity, decreasing nutrient input to the Baltic Sea (Zillén and Conley, 2010). However, the process of farm abandonment and population decrease may be too slow to explain the very rapid decrease in hypoxia at the end of the MCA (Figure 3.1). For this reason either a strong positive feedback mechanism needs to be involved, or another forcing was responsible for the termination of the MCA hypoxic period.

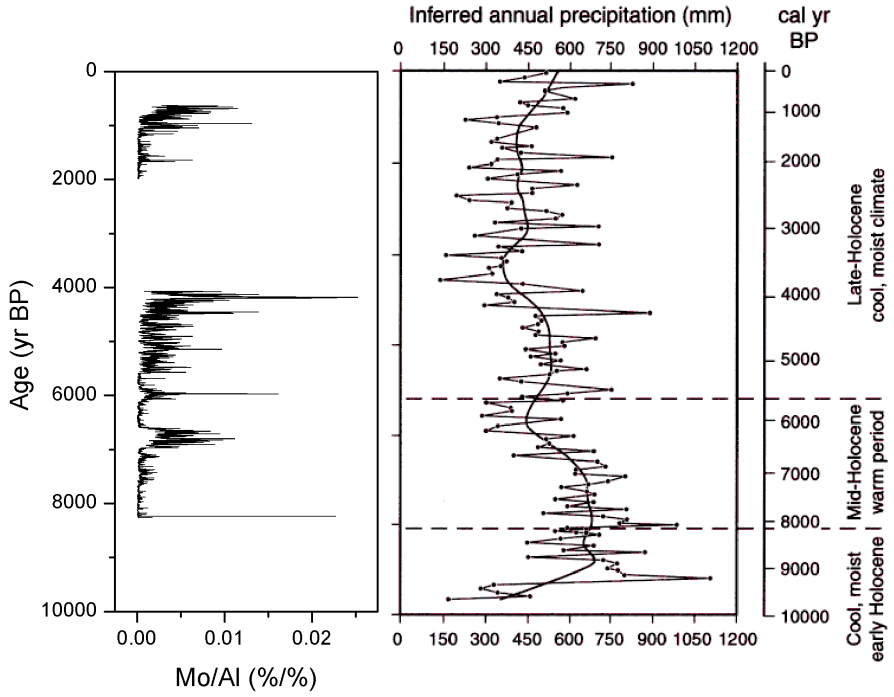

Figure 4.12: Precipitation rates in the Baltic Sea catchment area (Seppä and Birks, 2001), showing increased precipitation around the onset of the HTM. Right graph taken from Seppä and Birks (2001).

A small collection of varve thickness records from Finnish lakes (Ojala and Alenius, 2005; Haltia-Hovi *et al.*, 2007) shows no relationship with the Mo/Al

record at F80 (Figure 4.13), reinforcing the possibility that anthropogenic nutrient loading played an important role in the onset and termination of the hypoxic events of the MCA. Varve thickness has been interpreted as mainly driven by precipitation and summer temperatures (Haltia-Hovi *et al.*, 2007) while the x-ray density record has been linked to mineral matter influx, and hence precipitation (Ojala and Alenius, 2005). Although the occurrence of the pre-MCA hypoxic event indicates that the system was already close to anoxia several centuries before, human involvement may have sped up the transition to very intense hypoxic events that took several millennia during the HTM.

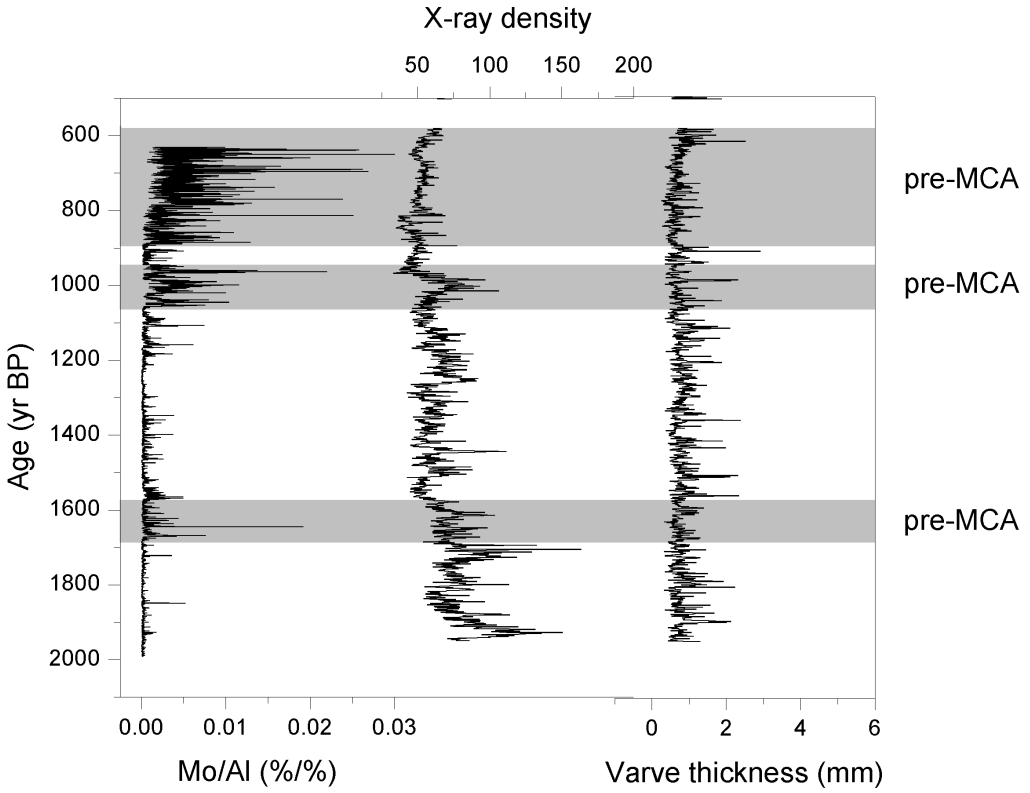

Figure 4.13: Comparison between the Mo/Al record at F80 (left) to X-ray densities from a core from Lake Nautajarvi (middle; Ojala and Alenius, 2005) and varve thicknesses from a core from Lake Lehmilampi (right; Haltia-Hovi et al., 2007). Grey bands indicate the hypoxic events as found in the LA-ICP-MS Mo/Al record at F80.

Starting in 1950, around 30 years before onset of the modern hypoxic event, Baltic Sea dissolved nutrient loads started increasing rapidly (Gustafsson *et al.*, 2012a). Following the 1980 mitigation measures on anthropogenic nutrient loading through, for example, fertilisers, surface nitrate concentrations stopped increasing. Surface phosphate concentrations kept rising after 1980, possibly because the external load reduction was more than compensated by phosphorus and nitrogen outflux from the sediments (Gustafsson *et al.*, 2012a).

To conclude, anthropogenic nutrient loading probably played an important role in the occurrence of both the modern hypoxic event and the hypoxic events of the MCA. Modern hypoxia is probably sustained by a strong outflux of phosphorus (and nitrogen) from the sediments due to liberation of iron-bound phosphorus and preferential remineralisation of organic phosphorus (Jilbert *et al.*, 2011). The same process probably sustained the hypoxic events of the MCA as well, since the Br/P enrichments found for the modern event (Figure 4.10) are also present during the MCA (Figure 4.11). Although no anthropogenic influences caused onset of the hypoxic events during the HTM, here too Br/P enrichments during hypoxic events indicate the importance of the liberation of phosphorus from the sediments (Figure 4.9a). High precipitation rates during the start of the HTM may have increased nutrient loading in the Baltic Sea, possibly contributing to the initial trigger for Baltic Sea hypoxia.

4.3.4.2 Stratification of the water column as driver of Baltic Sea hypoxia Apart from varying nutrient loading, changes in stratification of the water column may also contribute to the onset and termination of hypoxic events. Stratification of the Baltic Sea water column is mainly caused by a strong halocline, separating the surface waters of salinity 7–8 and deeper waters of salinity 11–13. Water column profiles of salinity and oxygen are strongly anti-correlated in the Baltic Sea, with relatively high salinity and low oxygen concentrations in deeper waters (Fonselius, 1981). Exchange between the two water masses separated by the halocline is limited (Gustafsson and Stigebrandt, 2007), leading to long residence times of Baltic Sea deep waters. Stratification is maintained by Major Baltic Sea Inflow events (MBI) introducing high-salinity deep waters (e.g., Matthäus and Franck, 1992). Increased fresh-water input (from river runoff or precipitation) as well as increased wind speeds may deepen the halocline (Meier *et al.*, 2011).

While Baltic Sea inflow events will introduce oxygen to deep Baltic Sea waters on the short term, the long term effect is enhanced stratification due to increased deep-water salinity. In the years following a MBI event, the halocline may be gradually weakened, decreasing the total hypoxic area (Jilbert *et al.*, 2011). Upon another inflow event, the halocline strengthens again, allowing an increased hypoxic area (Gustafsson, 2000). Because of this a rapid expansion of the hypoxia area (following an inflow event) may be followed by a gradual decline (in the period between inflow events), until another inflow event expands the hypoxia area again.

Major Baltic Sea inflow events occur during the winter, when easterly winds persist for around 20 days to "empty" the basin, followed by strong westerly winds of, again, around 20 days to "fill" the basin (Lass and Matthäus, 1996). Frequency of MBIs during the twentieth century was high, with one MBI every one to several years (Markus Meier *et al.*, 2006). Since 1980, the frequency of MBIs has dropped significantly, with only three significant inflow events since then (1983, 1993 and 2003).

Despite correlation between MBIs and Mn/Al records of several sites during the modern event (Figures 3.13, 3.14 and 3.15), the Mn/Al record cannot easily be used as a proxy for Baltic Sea inflow events during the MCA and HTM (Lenz *et al.*, 2014). Under anoxic conditions, a large pool of Mn^{2+} may build up in the bottom waters. Upon introduction of oxygen through an inflow event, this manganese can precipitate as Mn-oxides. When anoxic conditions return, these Mn-oxides are dissolved again. The high concentrations of manganese in alkaline pore waters then facilitate the precipitation of manganese-carbonates. The occurrence of manganese-carbonate layers can therefore be used as an indication of an oxic period during normally anoxic conditions (Calvert and Pedersen, 1996). However, sufficiently sulphidic bottom waters may cause high rates of Mn-oxide reduction following an inflow event, prohibiting the formation of manganese carbonates (Lenz *et al.*, 2014). This may, for example, be visible in the last few centuries of the MCA hypoxic period at F80 (Figure 4.14).

In addition to sufficiently sulphidic conditions potentially prohibiting the formation of manganese carbonates, the size of the hypoxic area is also of influence on the amount of manganese available for precipitation (Jilbert and Slomp, 2013b). During more oxic intervals, the source-to-sink ratio (S/B; Raiswell and Anderson, 2005) for manganese is much larger than during anoxic intervals (Figure 4.15). Here, the source area is defined as sites shallower than the redoxcline and the sink area as sites deeper than the re-

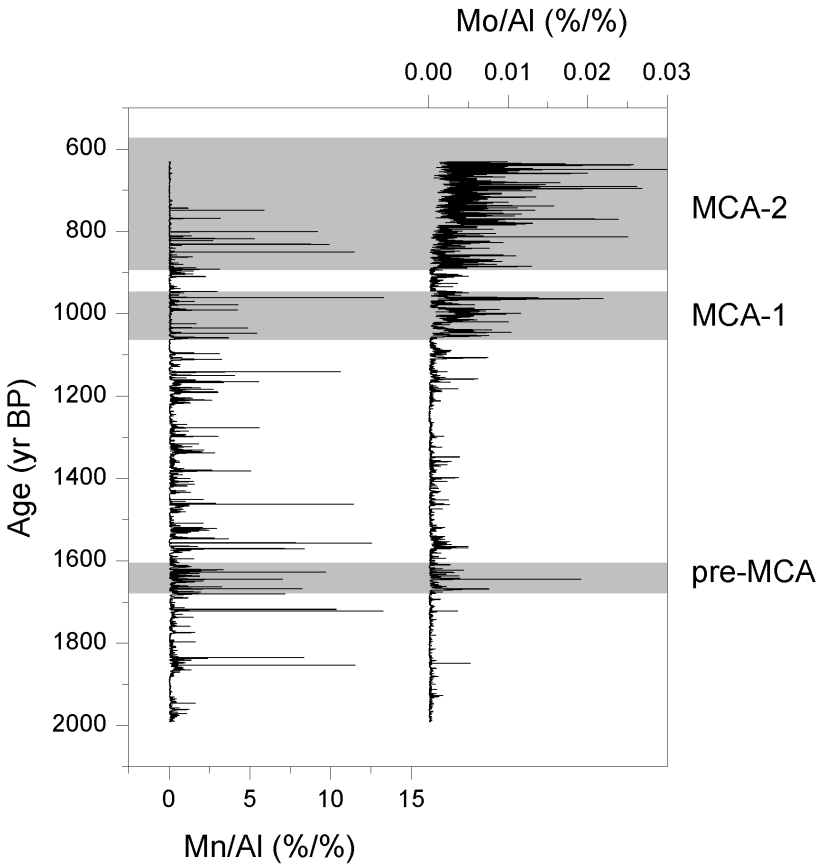

Figure 4.14: Mn/Al record for the MCA at F80. The Mo/Al record has been added for reference. Note the lack of manganese peaks in the last century of the hypoxic period.

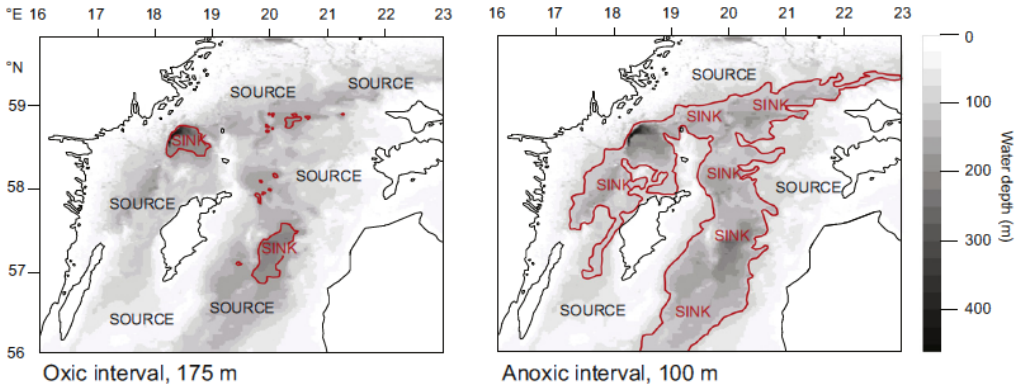

Figure 4.15: Indication of source and sink areas corresponding to a deep (175m) redoxcline (i.e., oxic intervals; left) and a shallow (100m) redoxcline (i.e., anoxic intervals; right). Figure taken from Jilbert and Slomp (2013b).

doxcline. The redoxcline for oxic and anoxic intervals was proposed at 175m and 100m water depth, respectively (Jilbert and Slomp, 2013b). A large source area compared to sink area (e.g., during a more oxic interval) leads to high rates of transport of manganese to these sink sites (such as F80). A smaller hypoxic area therefore facilitates higher concentrations of bottom water Mn^{2+} than a large hypoxic area would. This may explain the decrease in intensity of Mn/Al peaks at F80 since 1990 (Figure 3.1).

Stratification of the water column through relatively high salinity has been proposed as an explanation for the occurrence of the hypoxic events during the HTM (Gustafsson and Westman, 2002). Decreasing hypoxia throughout the HTM at SR5 may be due to decreasing salinity in this basin, reducing the strength of the halocline (Widerlund and Andersson, 2006). However, no relationship was found between Baltic Sea hypoxia during the last two millennia and changes in salinity (Zillén and Conley, 2010). Regardless, persistent stratification of the water column is needed to facilitate hypoxia in deeper waters.

4.3.4.3 Combinations of different forcings as triggers of hypoxic events Combining the analyses of sections 4.3.4.1 and 4.3.4.2, an identification of contributing factors to hypoxia can be made for the different hypoxic periods in the Baltic Sea. The hypoxic events during the HTM were probably triggered by an increase in deep-water salinities following the transition of the Baltic Sea from a freshwater lake to a brackish sea (Gustafsson and Westman, 2002). Related stratification of the water column would have facilitated the onset of hypoxia. Liberation of iron-bound phosphorus from the sediments probably played an important role as well (Sohlenius *et al.*, 2001). This notion is reinforced by the good correlation between the Mo/Al and Br/P records during the HTM at F80 (Figure 4.9a). In addition to this internal flux of nutrients, high precipitation rates over the Baltic Sea catchment area may have caused significant external nutrient loading through river runoff.

Since no relation has been found between changes in salinity and occurrence of hypoxia during the last two millennia (Zillén and Conley, 2010), onset of the hypoxic events of the MCA were probably triggered by increased nutrient loading in the surface waters. An increased anthropogenic flux of nutrients to the Baltic Sea seems a likely candidate, since northern European populations grew significantly around the onset of MCA-1 (Gies and Gies,

1994) and diminished by over 50% around the final termination of the MCA hypoxic events (Walløe, 1995). The termination of the MCA hypoxic period may have been too rapid to be explained by the demise of northern Europe's population alone though.

Good correlation between the Mo/Al and Br/P records at F80 during the MCA underlines the importance of internal cycling of phosphorus during medieval hypoxic events (Figure 4.11). It should be noted that, although the Baltic Sea was largely oxic during the millennia before MCA-1, the occurrence of the pre-MCA event shows that the system was already close to hypoxia. As such, anthropogenic nutrient loading may have been the final trigger needed to shift the Baltic Sea to hypoxia. Twentieth century external nutrient loading increased from 1950 to 1980, at which point mitigation efforts halted this increasing flux (Gustafsson *et al.*, 2012a). Increasing dissolved phosphorus concentrations in the Baltic Sea after 1980 can be ascribed to the internal cycling of phosphorus.

Long-term responses of the Baltic Sea ecosystem are probably related to many different forcings, both terrestrial and marine, and both climatic and anthropogenic, as well as their complex relationships (Zillén and Conley, 2010). Several different forcings seem to have to work together for a hypoxic event to occur. As an example, increased stratification due to the shift to a brackish sea and increased external nutrient input due to high precipitation rates and liberation of iron-bound phosphorus probably triggered the hypoxic events of the HTM. Increased anthropogenic input of nutrients may have triggered the onset of the hypoxic events of the MCA, but the system was already close to hypoxia in the millennia before.

4.3.5 Rapidity of onsets of hypoxic events

The onsets of most discussed events are characterised by rapid enrichments in Mo/Al, increasing from background levels to significantly higher values within a few years. After this initial onset, Mo/Al enrichments keep gradually increasing over the course of several decades (e.g., Figure 3.6). Despite this rapid onset in Mo/Al enrichments, most events during the HTM do feature very weak, progressively intensifying enrichments before these sudden onsets (e.g., HTM-2, HTM-4, HTM-5+6). These periods of slightly intensifying hypoxia before onset of an event typically last around 50 years. They are more pronounced in the V/Al record than in the Mo/Al record (e.g., Figure 3.6), indicating that this could be related to the site being anoxic for

a few decades before turning euxinic. The decade before onset of the modern hypoxic event at BY15 is characterised by a gradual increase in V/Al as well, concurrent with bottom water oxygen concentrations of around zero mol L-1 (Figure 3.15).

The main species of molybdenum in seawater is molybdate (MoO_4^{2-}). Fixation of molybdenum in surface sediments requires presence of H_2S. Under euxinic conditions, each oxygen atom in molybdate is sequentially (and rapidly) replaced by a sulphur atom, to produce thiomolybdates (MoS_4^{2-}; Helz *et al.*, 1996). These thiomolybdates are then fixed to the sediments in one of three different ways: they are scavenged by either iron sulphides (Vorlicek *et al.*, 2004), metal-rich particles (mainly iron) or sulphur-rich organic molecules (Helz *et al.*, 1996). Regardless of the scavenging process, the presence of sulphur is needed to produce thiomolybdate from molybdate. For this reason, fixation of molybdenum in surface sediments is mainly limited to euxinic conditions (Calvert and Pedersen, 1993).

Reduction of vanadium, unlike molybdenum, occurs in two steps. Under mildly reducing conditions, $V(V)$ is reduced to $V(IV)$. The VO^{2+} formed by this reduction process is hydrolysed to $VO(OH)_3^-$ or the insoluble $VO(OH)_2$ (Van der Sloot *et al.*, 1985). Surface adsorption may cause $VO(OH)_3^-$ to be removed from anoxic bottom waters as well (Emerson and Huested, 1991). When free sulphides are present, $V(IV)$ is further reduced to $V(III)$. $V(III)$ then precipitates as V_2O_3 or $V(OH)_3$ (Wanty and Goldhaber, 1992). For this reason, enrichments of vanadium, although weaker, can occur before the onset of euxinic conditions. Weak enrichments in V/Al before onset of a hypoxic event in the Mo/Al record can therefore be an indication that the bottom water conditions were already mildly reducing before actual onset of the event.

The Br/P ratio can be used as a high-resolution equivalent of the discrete sample C_{org}/P_{tot} ratio. Since the C_{org}/P_{tot} ratio will increase with increasing hypoxia (Jilbert *et al.*, 2011) due to preferential regeneration of phosphorus (Algeo and Ingall, 2007), it can be used to assess the rapidity of the onset of a hypoxic event. The bottom water oxygen concentrations at BY15 were already close to euxinia during the decade running up to the modern hypoxic event (Figure 3.15). This is reflected in a crossplot between the LA-ICP-MS Br/P and Mo/Al records for this hypoxic event (Figure 4.16). Here, the hypoxic event is indicated in black and the decade before the hypoxic event in red. It follows that Br/P at BY15 enriched independently of Mo/Al in the decade before onset of the hypoxic event, indicating that preferential

regeneration of phosphorus was already increasing during this time. The difference between the decade before the hypoxic event and the hypoxic event itself is probably due to the non-linear response of Mo/Al fixation in the sediments to increasing oxygen stress, enriching rapidly upon the transition to more permanent euxinia.

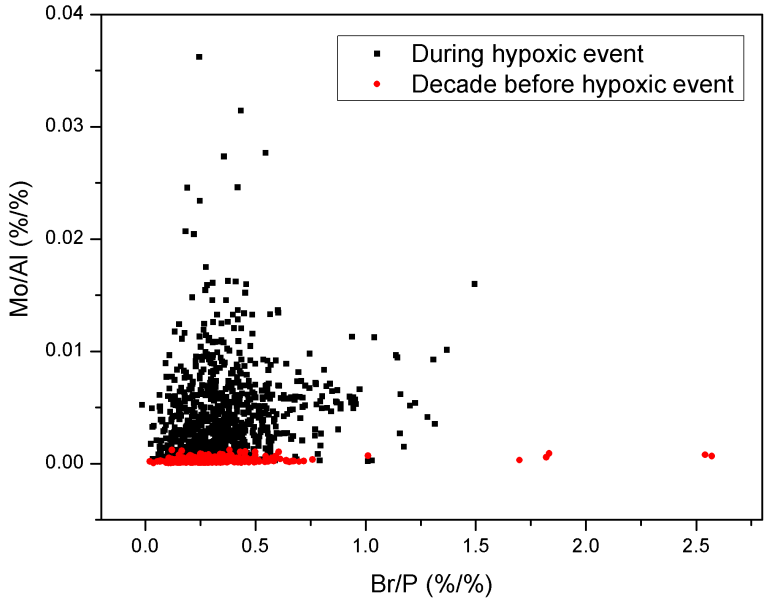

Figure 4.16: Crossplot of Mo/Al and Br/P for the modern hypoxic event at BY15. The hypoxic event is indicated by black, and the decade before onset of this event is indicated by red. Note the Br/P enrichments independent of Mo/Al during the decade before onset of the hypoxic event.

This notion of increasing Br/P ratios before onset of an event may be used to assess the bottom water oxygen evolution in the decades before older hypoxic events during the HTM and MCA. During the HTM, some increase in preferential regeneration of phosphorus is visible during the decades before most hypoxic events (e.g., HTM-2+3; Figure 4.17a). This indicates that, although onsets were rapid in the Mo/Al record, the transition of bottom water oxygen concentrations to euxinia may have been more gradual. The same gradual increases in bottom water oxygen concentrations may have occurred before the onsets of hypoxic events during the MCA (e.g., MCA-1; Figure 4.17b) and the pre-MCA hypoxic event (Figure 4.17c). Note that

absolute Br/P values during HTM-2+3 tend to be lower than those during hypoxic events of the MCA.

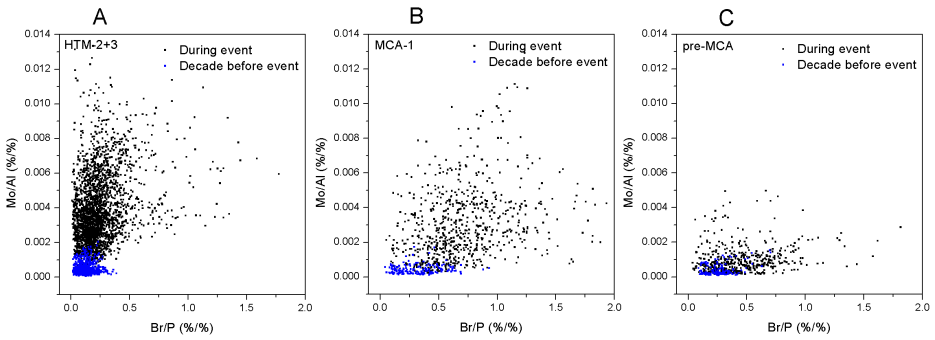

Figure 4.17: Crossplots between Br/P and Mo/Al for HTM-2+3 (A), MCA-1 (B) and the pre-MCA hypoxic event (C). The plots are split in the hypoxic events themselves (black) and the decade before that event (blue).

Rapid onsets of hypoxic events, going into euxinic conditions within a few years, may be caused by positive feedbacks in the phosphorus cycle. This feedback is based on the fact that phosphorus adsorbs strongly onto Fe-oxyhydroxides (Jensen *et al.*, 1995), and on preferential phosphorus regeneration from organic matter (Jilbert *et al.*, 2011). Phosphorus stored in the sediments under oxic conditions is mainly bound to Fe-oxyhydroxides. After an initial decrease in oxygen concentrations these Fe-oxyhydroxides will mobilise, releasing their phosphorus. The released phosphorus then allows for increased productivity, further decreasing deep water oxygen concentrations. Increased oxygen stress increases the preferential regeneration of phosphorus from organic matter, further enhancing the positive feedback.

Although onsets of events seem rapid in the Mo/Al record, with sudden enrichments within one year, this is more likely a reflection of the transition to permanent euxinia. As an example, onset of Mo/Al enrichments during the modern hypoxic event at BY15 start when bottom water oxygen conditions go to euxinia (Figure 3.15). During the decade before this transition, bottom water oxygen concentrations were close to zero, but no Mo/Al enrichments occurred. For this reason an assessment of the evolution of bottom water oxygen concentrations before and during the onset of a hypoxic event can best be made using information from the V/Al and Br/P records in addition

to Mo/Al.

4.3.6 Fe/Al as indicator of regional-scale hypoxic conditions

The size of the hypoxic area has changed considerably throughout the modern hypoxic event (Conley *et al.*, 2002). Fluctuations in the size of the hypoxic area may for example be influenced by the frequency and intensity of Baltic Sea inflow events (Jilbert *et al.*, 2011). A good candidate for reconstructing variations in location and size of the total hypoxic area in the Baltic Sea may be the LA-ICP-MS Fe/Al record.

Under both sufficiently oxic and sufficiently euxinic conditions iron will precipitate in the sediments as Fe-oxyhydroxides or nanoparticulate ferrihydrites, and pyrite, respectively (Raiswell and Canfield, 2012). For this reason, only a specific "window of opportunity" in bottom water oxygen concentrations exists for iron to mobilise from the sediments (Lyons and Severmann, 2006): the bottom water oxygen concentrations need to be too high for formation of pyrite, but too low for formation of Fe-oxyhydroxides. When sediments fall within this window of opportunity, iron may mobilise, forming a lateral "shuttle" from these sites to deeper parts of the sea (Lyons and Severmann, 2006). For this reason, the intensity of Fe/Al peaks at a hypoxic site may be used to assess the size of the hypoxic area (Figure 4.18).

The shelf sediments will act as a source area for iron, with the hypoxic area acting as its sink (see also Figure 4.15). A larger hypoxic area (i.e., larger sink area) will cause iron from the source area to be more spread out, decreasing iron shuttling to individual sites. This may in turn lead to decreased iron enrichments. When the sink area is small compared to the source area, large amounts of iron can be shuttled to these hypoxic sites, potentially leading to more significant enrichments. It may therefore be possible to use the intensity of Fe/Al enrichments at individual sites to assess the size of the hypoxic area.

During HTM-5, iron correlates well with the molybdenum record (Figure 3.7). During the latter part of HTM-5 and during HTM-6 this relationship is weaker. In between the "micro-events" of HTM-5+6 iron is still significantly enriched, with only slightly lower Fe/Al levels than during these events (e.g., Figure 3.8). Because of the location of F80 in the Baltic Sea the site can only act as a sink for iron, and any enrichments at F80 can be assumed to originate from the source area. The occurrence of constant iron enrichments at F80 indicates that the source-to-sink ratio (based on the

size of the hypoxic area) varied significantly even in the periods between the micro-events, suggesting that the size of the hypoxic area kept fluctuating even during those relatively more oxic periods. Variations in the hypoxic area are also visible in the termination of the final hypoxic event during the HTM (HTM-7). Here, shortly after the rapid decrease in molybdenum enrichments, a final peak in Fe/Al appears (Figure 3.1). This may be due to a decrease in hypoxic area leading to a decreased sink area and increased source area for iron.

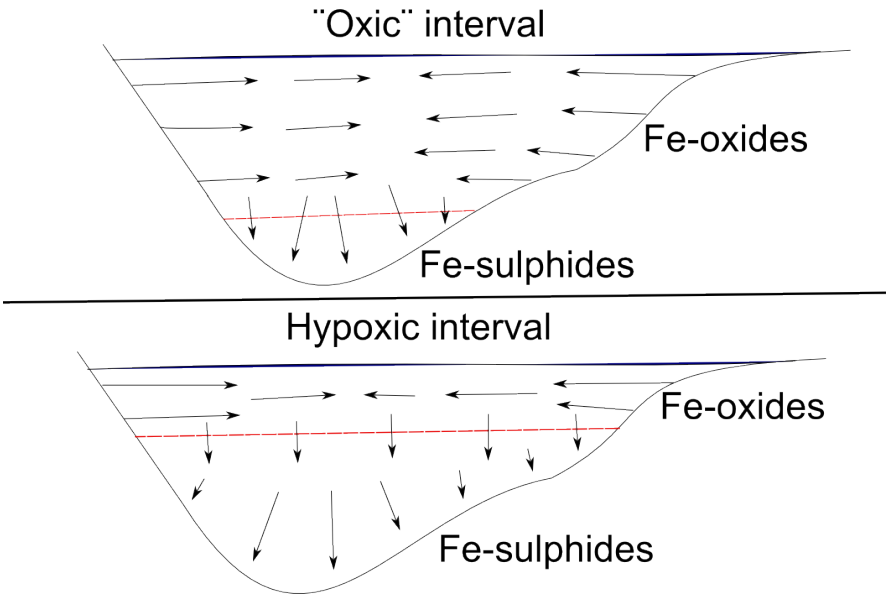

Figure 4.18: Schematic representation of the iron shuttle.

Significant iron enrichments occurred coincident with the onset of Mo/Al enrichments at the start of the pre-MCA event at F80, probably due to a rapid release of iron-oxyhydroxides from sediments following the ∼2 millennia of oxic bottom water conditions during which iron-oxyhydroxides could form (Figure 3.1; Figure 3.10). Although good correlation is present between the Mo/Al and Fe/Al records during MCA-1, some variability is present in the Fe/Al record on top of the Mo/Al record. This could indicate that the size of the hypoxic area fluctuated regularly throughout this hypoxic event. During MCA-2 the Fe/Al record more closely follows variations in the Mo/Al record (Figure 3.12).

Modern hypoxic event Fe/Al enrichments at F80 start ∼10 years before

those at LL19 (Figure 4.19). A possible reason for this is that, while LL19 was still sufficiently oxic, deeper parts of the source area for F80 were already transitioning to more euxinic bottom water oxygen conditions, turning that area into a sink for laterally transported iron. In contrast to F80, site LL19 is not only a sink for iron but also a source. Enrichments from 1981 indicate that at this point the hypoxic area had expanded sufficiently for LL19 to move out of the window of opportunity. It now acted as a sink for iron from more shallow sites that, due to the expanding hypoxic area, were now within this window of opportunity. In 1991 Fe/Al enrichments in both F80 and LL19 stopped simultaneously, possibly because the source-to-sink ratio had decreased so much that small amounts of mobilised iron were spread out over a large hypoxic sink area. Fe/Al enrichments at BY15 continued a bit longer, until reaching background levels in 1999. A small peak in Fe/Al at all sites occurs around the 2003 inflow event, indicating a small surge in transport of iron to deeper sites.

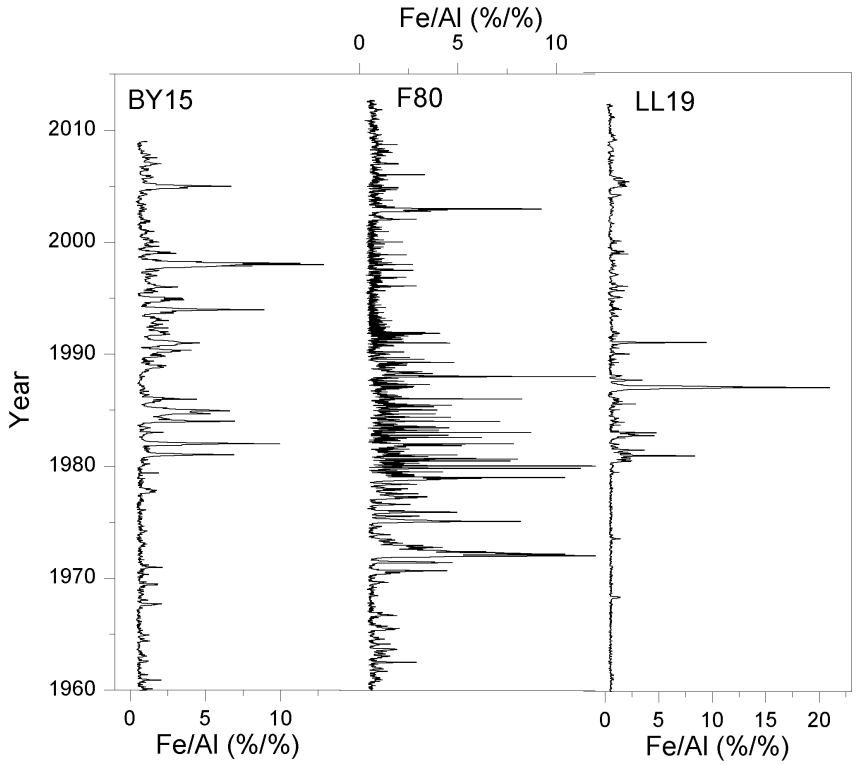

Figure 4.19: Fe/Al profiles for the modern hypoxic interval at BY15 (left), F80 (middle) and LL19 (right).

4.3.7 Multi-decadal to centennial cycles and patterns in Baltic Sea hypoxia

Many multi-decadal to centennial (to millennial) patterns seem to have occurred in Baltic Sea hypoxia during the Holocene. One example of such a pattern is the gradual intensification of Mo/Al enrichments starting around the onset of HTM-5 and continuing until the final termination of HTM-7 at F80 (Figure 3.1). During HTM-5+6 a ∼59-year and 28-year cyclicity is present in both the Fe/Al and Mo/Al records of F80 (Figure 3.21), characterised by micro-events lasting a few decades with less reducing intervals of at maximum two decades in between (Figure 3.8). Another interesting pattern is the speed at which maximum hypoxia is reached. During the HTM, there are almost four millennia between onset of HTM-1 and the most intense hypoxia of HTM-7. On the other hand, the increase to maximum hypoxia

took only 500 years during the MCA (1 kyr if taking the pre-MCA event into account), while maximum hypoxia during the modern hypoxic event was reached within decades.

These different trends, patterns and cycles are probably caused by a combination of internal variability of, and climatological influences on the Baltic Sea.

4.3.7.1 Internal variability Although frequency of hypoxic events at F80 increased markedly throughout the HTM, duration of these events is more variable. The transition from the short and relatively weak HTM-4 to the intense and long HTM-7 (Figure 3.1) is marked by numerous rapid excursions during HTM-5+6, each going back to pre-event background levels, although the system does not fully recover in between these "micro-events" (Figure 3.8). This period of rapid alternations between oxic and hypoxic conditions may be related to periodic contractions of an on average gradually expanding hypoxic area throughout HTM-5 to HTM-7. These contractions may be related to changes in the frequency of Baltic Sea inflow events, possibly enhanced by the positive feedbacks inherent in the iron-bound phosphorus.

While there are four millennia between the onset of HTM-1 and the most intense hypoxia during the HTM, this same transition to maximum hypoxia took only 500 years during the MCA, and only decades during the modern hypoxic event. This could perhaps be caused by differences in external loading and differences in the amount of phosphorus stored in the sediments. If the process of storing phosphorus in the sediments is sufficiently slow, the onset of the modern hypoxic event may have been controlled more by external input of phosphorus than liberation of phosphorus, compared to the MCA.

4.3.7.2 Climatological variability Many climatological variables have been shown to affect Baltic Sea hypoxia, such as temperature (Stal *et al.*, 2003), precipitation (Meier *et al.*, 2011) and wind stress (Meier, 2005). In addition, mean climate state over northern Europe (Seppä and Birks, 2001) as well as larger-scale climatic processes such as the North Atlantic Oscillation (NAO; Jilbert and Slomp, 2013) may affect hypoxia in the Baltic Sea. The influence of precipitation on Baltic Sea hypoxia is two-fold. As a direct effect, an increased flux of fresh water into the Baltic Sea (either through direct precipitation or through increased river runoff) will deepen the halo-

cline and enhance stratification (Meier *et al.*, 2011). As a secondary effect, increased river runoff may lead to enhanced external nutrient loading, leading to higher rates of primary productivity. It has been suggested that wind stress is the main physical forcer of stratification, rather than inflow events (Meier, 2005), since increased wind stress leads to increased mixing through transport of energy into the water column.

Temperature may affect Baltic Sea hypoxia in several ways. Higher sea surface temperatures can dissolve less gases than lower sea surface temperatures. In this way, temperature may directly influence the flux of oxygen from the atmosphere to the surface waters. However, increased sea surface temperatures in the Baltic Sea tend not to penetrate down into the water column very far (Gustafsson *et al.*, 2012b). Although Baltic Sea hypoxic events all occurred during warmer periods (i.e., the Holocene Thermal Maximum, the Medieval Climate Anomaly, and twentieth century global warming) no correlation has been found between hypoxia and temperature on a global scale (Diaz and Rosenberg, 2008). Stal *et al.* (2003) proposed that the depth of the thermocline may influence productivity of cyanobacteria, with increased productivity under higher temperatures.

Climate variability has been suggested as a possible driver for hypoxic events during the HTM and the MCA (Jilbert and Slomp, 2013a). One such climatic factor may be the North Atlantic Oscillation (NAO), where shifts in its mean phase over centennial timescales may have caused variations in hypoxia over these same timescales. Comparison with a varved lake record in the northern Alps (Lake Bourget; Arnaud *et al.*, 2012) suggests that the hypoxic events during the HTM and the MCA may be linked by the same forcing (Figure 4.20). Arnaud *et al.* (2012) measured down-core titanium content as a proxy of total terrigenous abundance, which tracks the accumulation of detrital material transported by rivers. On centennial timescales, good correlation can be found between the titanium record of Lake Bourget and the timing of hypoxic events at F80 according to the molybdenum record. As an example, timing of positive excursions in the titanium record are, within the error margins of the age models, coincident with hypoxic events HTM-2+3, HTM-4, the first half of HTM-5+6, HTM-7 and all events during the MCA. No such correlation is present for the modern event.

Changes in the titanium record have been interpreted to be caused by changes in precipitation due to climatic variability (Arnaud *et al.*, 2012). Furthermore, a general trend of increasing titanium enrichments seems to be present throughout the Holocene, with relatively low enrichments during

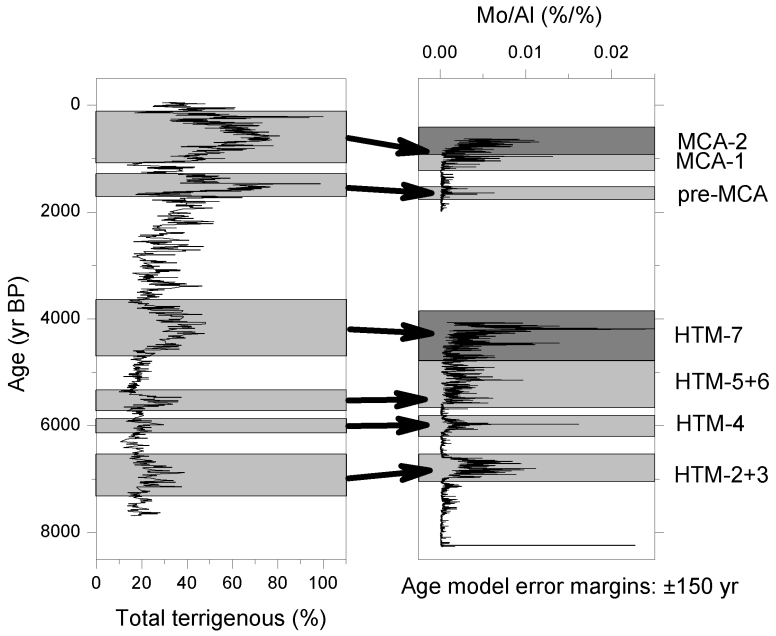

Figure 4.20: Comparison between total terrigenous component at Lake Bourget (left) to Mo/Al at site F80 (right), with arrows indicating possibly concurrent events.

the HTM and significantly higher values during the MCA. However, such intimate coupling between events in the HTM and MCA does not have to be present in the Baltic Sea. Since Lake Bourget is not in the catchment area of the Baltic Sea, the fact that the same trends are present throughout the Holocene indicates that hypoxic events are probably (at least partly) forced by external climatic variations and not by internal processes. This could for example be due to increased storminess over northern Europe, possibly extending southward to the northern Alps. Meier (2005) showed that changes in wind stress over the Baltic Sea may have been more important to stratification than salt-water inflows on longer timescales. Variations in storminess may have caused increased precipitation rates over both the Baltic Sea and the northern Alps, further explaining the observed correlation. The period of no Mo/Al enrichments between the HTM and the MCA can be explained by a decrease in deep-water salinity causing decreased strength of the halocline. If this process was stronger than the climate forcing found by Arnaud *et al.* (2012), no hypoxic events would occur.

A high-resolution study of titanium in Lake Mondsee (northern Austria; Swierczynski *et al.*, 2013) shows (weak) agreement between the F80 Mo/Al record and the Lake Mondsee titanium record on decadal timescales (i.e., timescales of the micro-events; Figure 4.21). Possible phase shifts cannot be deduced due to errors in the age models. The combination of a sharp increase in molybdenum levels and a sharp decrease in titanium levels around 4450 ka suggests that the two records may be anti-correlated. However, correlation of the two records is statistically not very significant. As with Lake Bourget, Lake Mondsee is not within the catchment area of the Baltic Sea, giving rise to the small possibility that the short-term micro-events of HTM-5+6 may be externally triggered rather than internally.

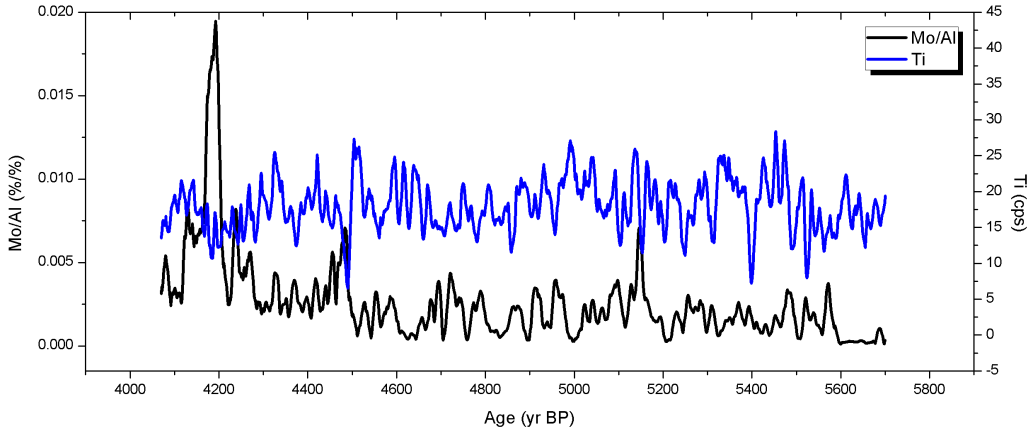

Figure 4.21: Comparison between Mo/Al at site F80 (black) and Ti at Lake Mondsee (blue) for the duration of HTM-5+6 and HTM-7. Weak anticorrelation may be present.

Especially interesting is the strong multidecadal signal in both records. Three main periodicities of this multidecadal signal are shared between the two records, spanning from a 48-year cycle to a 59-year cycle and a 98-year cycle (Figure 4.22). A possible forcing for this may be the Atlantic Multidecadal Oscillation (AMO), which affects precipitation patterns in northern Europe through subtle variations in North Atlantic sea surface temperatures (Schlesinger and Ramankutty, 1994). This may not only have affected flood frequencies and runoff rates in the northern Alps, but also the input of fresh water and nutrients through increased river runoff.

Possible anti-correlation between the records may be explained by out-

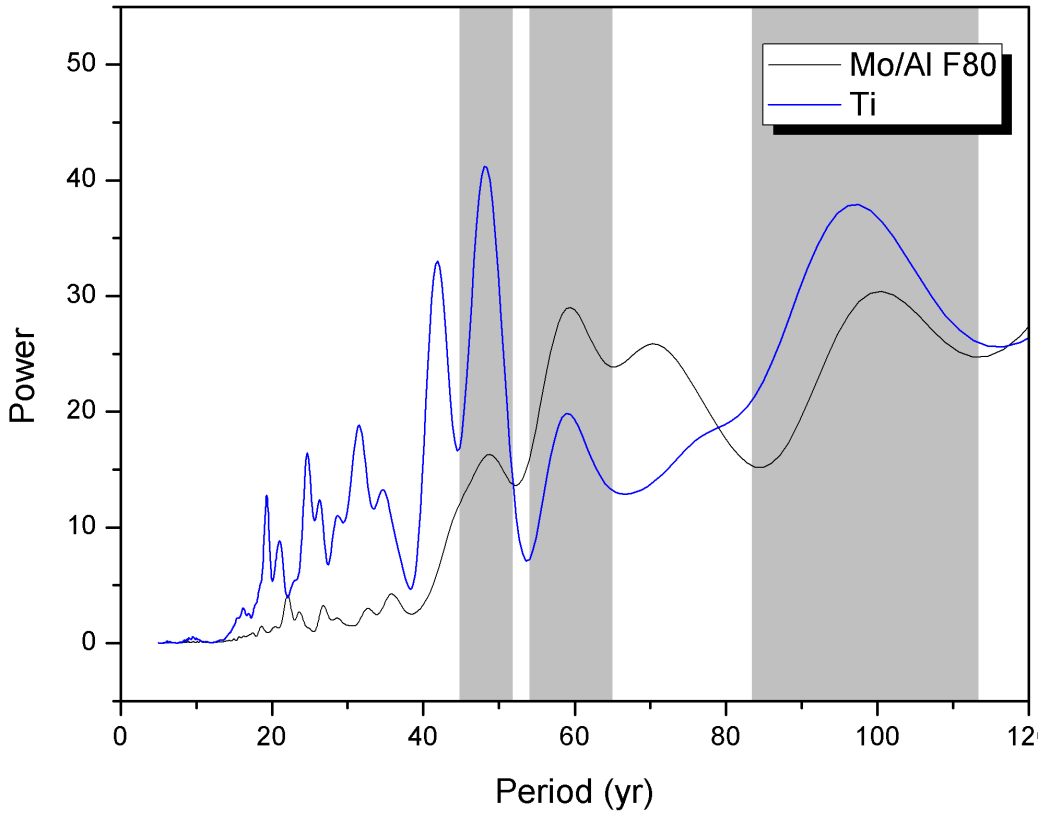

Figure 4.22: Power spectra of the Mo/Al record during HTM-5+6 at F80 (black) and the titanium record in the northern Alps during the same period (blue).

of-phase episodes of increased storminess between northern Europe and increased precipitation in central and southern Europe due to the North Atlantic Oscillation (NAO). The NAO is based on the pressure difference between the subtropical high pressure area and the subpolar low pressure area over the Atlantic Ocean. If the pressure difference is high (positive NAO or NAO+) westerlies over Europe will be relatively strong, leading to above-normal temperature and storminess over northern Europe and below-normal temperature and precipitation over central Europe. Since positive correlation is expected with storminess for the Baltic Sea Mo/Al records (through increased stratification following increased Baltic Sea inflow events, and increased nutrient loading from increased river runoff) and with precipitation

in the northern Alps titanium records (through enhanced input of terrigenous material), this may explain the possible anti-correlation observed in Figure 4.21.

During the MCA, the sill separating the Baltic Sea and the Bothnian Sea had developed enough to keep salty deep waters from entering the northern Bothnian Sea. As a result, the Bothnian Sea remained oxic with almost no Mo/Al enrichments since the end of the HTM (Figure 3.2). This closing of the sill may also have influenced ventilation rates through both basins. Indeed, a small shift to higher frequency variations can be seen when comparing the power spectrum of the HTM at F80 (Figure 3.16) to that of the MCA (Figure 3.22). This small shift to higher frequencies may have been a result of shorter ventilation times in both basins due to their separation.

4.4 Evolution of Baltic Sea hypoxia during the Holocene

Although the focus of most paleoreconstructions of the Baltic Sea often lies on hypoxia and hypoxic events, normal conditions consist of well oxygenated deep waters. Due to the important role of the halocline in stagnation of the water column, hypoxia did not occur in the Baltic Sea when it was still a freshwater lake. Mobilisation of iron-bound phosphorous during the transition of the Baltic Sea from a freshwater lake system to a brackish sea has been suggested as a possible cause for increased sea surface productivity during the HTM (Sohlenius *et al.*, 2001). The increased productivity combined with stratification of the water column due to salty deep water input probably caused the onset of the series of hypoxic events during the HTM. High precipitation rates over the catchment area of the Baltic Sea may have played a role as well (Sepp and Birks, 2001).

Hypoxia in the Baltic Sea gradually became more and more intense throughout the HTM, reaching the most intense period nearly 4 kyr after the initial onset (Figure 3.1). At the same time, the Bothnian Sea deep waters experienced the exact opposite trend, with gradually decreasing intensity of hypoxia throughout the HTM (Figure 3.2). The process linking these two basins is probably the shallowing of the sill between the Baltic and Bothnian seas. The shallower sill would have prevented more salty deep waters from entering the Bothnian Sea, eventually ending the hypoxia in this basin. Upon re-oxygenation of the Bothnian Sea it probably became a sink for phosphorous, ending hypoxia in the Baltic Sea as well.

During the HTM, a gradual increase in precipitation rates had started

over the northern Alps, probably related to larger-scale climatic processes. The effect of these processes is also visible in the Mo/Al record of the HTM at F80, where wetter periods over the northern Alps correlate with hypoxic events in the Baltic Sea (Figure 4.20). Coupling of northern European and central European climates probably became more significant around the onset of the HTM (∼8.2 kyr), with a shift from dominant westerly air flow to a meridional flow pattern and frequent southerly air flows (Seppä and Birks, 2001). After termination of the hypoxic periods of the HTM precipitation rates in the northern Alps kept increasing although no hypoxic events occurred in the Baltic Sea for approximately 2.5 kyr. Decreased stratification due to low deep water salinities probably acted against climatic forcing, keeping the Baltic Sea oxygenated.

Increasing salinity in deeper waters due to increased frequency and intensity of Baltic Sea inflow events may have set in motion the hypoxic events during the MCA. The occurrence of the pre-MCA event, 500 years before the onset of the more intense hypoxic events of the MCA, may be related to a stronger halocline. Human influences in the form of rapid population growth and increased agricultural productivity in northern Europe may have accelerated the increase in hypoxia throughout the MCA through enhanced nutrient loading. While the rapid onset of more intense hypoxia around 900 AD may be related to population growth, the equally rapid decline in 1350 AD may (in part) have been caused by outbreak of the plague in northern Europe, and its associated decimation of population. This final termination may have been too rapid to be completely explained by decreasing human populations though.

While human influence on the hypoxic events during the MCA can hardly be confidently deduced, its impact on the modern hypoxic event is thought to be substantial, mainly in the form of input of nutrients from land. However, the fact that the timing of the onset of the modern hypoxic event coincides with the shift from high- to low frequency Baltic Sea inflow events shows that the role of nature should not be underestimated. Despite mitigation efforts on the input of nutrients to the Baltic Sea hypoxia remains intense (Gustafsson *et al.*, 2012). Modern hypoxia is probably maintained by internal recycling of nutrients (Jilbert *et al.*, 2011).

5 Conclusions

5.1 Techniques and age model

Although the LA-ICP-MS line-scanning method is a strong tool for resolving trace elemental enrichments at a high resolution, some problems persist. These problems mainly influence the quantification of the results and have, therefore, little to no effect on spectral analyses and qualitative comparisons to other records. They can, however, significantly hinder element-to-element analyses, which should always be kept in mind. These problems mainly relate to the difference in matrix between the sample and the standard, which could, in part, be solved by spiking the resin with a certain element not natural to the sample source region.

Construction of an age model using Mo/Al peak counting has been successfully applied to the modern hypoxic event at three different sites. This indicates that the peak-counting technique is a good candidate for dating of hypoxic events. However, applying this idea to the whole MCA and HTM is not precise enough, mainly because more oxygenated intervals may not contain a yearly Mo/Al signal. For this reason the method is (for now) limited to creating a floating timescale for a single hypoxic event. The existing age model for F80 based on paleomagnetic secular variation may underestimate sedimentation rates during hypoxic events, suggesting that sedimentation rates during events are higher than during oxygenated intervals.

5.2 Hypoxic events in the Baltic Sea during the Holocene

Over the course of the Holocene, the Baltic Sea has tipped into and out of hypoxia on several occasions. Three main periods of hypoxia can be discerned, starting with the Holocene Thermal Maximum (HTM) between 8 ka and 4.1 ka. Other hypoxic periods are the Medieval Climatic Anomaly (MCA) between 900 AD and 1350 AD and the modern hypoxic event. Two main forcings may influence hypoxia in the Baltic Sea. First, increased nutrient loading could lead to increased surface productivity, increasing deep-water oxygen stress through enhanced oxidation of organic matter. In addition, stratification of the water column could significantly increase deep-water residence times, creating oxygen stress through lack of supply from surface waters.

Increased sea surface nutrient loading may originate both from within

the Baltic Sea as well as be external. External input of nutrients could be related to precipitation rates governing river runoff as well as agricultural activity and deforestation in the catchment area. Internal nutrient loading is caused by (1) the liberation of iron-bound phosphorus following a shift to more reducing conditions and (2) increasing preferential regeneration of phosphorus from organic matter with increasing euxinia. The liberation of iron-bound phosphorus may set in motion a positive feedback loop, where an initial trigger causes hypoxia to spread. Once a site becomes hypoxic, the iron-oxyhydroxides reduce, releasing phosphorus. The resulting increasing sea surface nutrient loading then leads to increased productivity, and subsequent enhanced oxygen stress in deeper waters.

On average, oxygen stress gradually increased throughout the HTM in the Baltic Sea, reaching most severe hypoxia a few decades before final termination of this hypoxic period. Onset of this hypoxic period is probably related to the transition of the Baltic Sea from a freshwater lake to a brackish sea. The resulting stratification due to increasing deep-water salinities probably facilitated hypoxic conditions. High precipitation rates in the catchment area as well as liberation of iron-bound phosphorus probably contributed to eutrophication of the surface waters.

While oxygen stress gradually increased in the Baltic Sea during the HTM, it may have gradually decreased during this same time period in the Bothnian Sea, possibly due to the build-up of a sill separating the deeper water masses of these two basins. This would have led to decreased stratification of the Bothnian Sea due to decreased salt-water inflows, re-oxygenating the basin. At this point, the Bothnian Sea became a sink for phosphorus from the Baltic Sea, which may have caused the final termination of hypoxia in the Baltic Sea a few centuries later.

Although the MCA is characterised by more rapid Mo/Al enrichments than the HTM, with most severe hypoxia reached just 500 years after initial onset, the presence of a small hypoxic event another 500 years before that shows that the system was already instable by that time. The two millennia between the HTM and the MCA are characterised by oxic conditions, probably because stratification was weaker during this period. The occurrence of the pre-MCA hypoxic event shows that stratification was already strong enough to allow hypoxia long before hypoxia really started. This indicates that multiple different forcings have to act together to cause hypoxia in the Baltic Sea. Onset of hypoxia in the Baltic Sea was probably triggered by increased nutrient loading through enhanced agricultural productivity and

deforestation in northern Europe following (and facilitating) a dramatic increase in total population. Termination of the MCA hypoxic period correlates with a ∼50% drop in northern European population due to the Black Death. However, related farm abandonment and decreased agricultural productivity alone does not fully explain the rapidity of the termination. This suggests that, if a decrease in human population is the cause of the termination of hypoxia during the MCA, a strong positive feedback must have played a role as well.

A few decades before onset of the modern hypoxic event, external nutrient loading to the Baltic Sea started increasing rapidly, probably related to fertiliser runoff. Despite mitigation efforts in the early eighties, sea surface phosphorus concentrations kept increasing, due to both liberation of iron-bound phosphorus and preferential regeneration of organic phosphorus. Preferential regeneration of phosphorus may not have played a large role at BY15, which is one of the deeper sites, evidenced by a lack of increasing Br/P ratios following the onset of the modern hypoxic event.

Although onsets of most hypoxic events seem rapid in the Mo/Al records, small enrichments in V/Al and Br/P in the decade(s) before the hypoxic events show that bottom water oxygen concentrations may have decreased more gradually. The oxygen record at BY15 shows that oxygen concentrations were near-zero for around one decade before onset of the modern hypoxic event. However, since euxinic conditions are required for precipitation of molybdenum in the sediments, no molybdenum enrichments are present during this decade. Br/P versus Mo/Al crossplots do show some preferential regeneration of phosphorus related to increasing oxygen stress in the decade before onset of the modern hypoxic event. The same Br/P enrichments are present in the decade before many hypoxic events throughout the Holocene.

Timing of hypoxic events throughout the Holocene has been correlated with a titanium record from a lake in the northern Alps. This record has been interpreted as a precipitation record through input of terrigenous material. A possible link between this lake and the Baltic Sea may be a shift in atmospheric circulation over northern Europe around 8.2 ka, from dominant westerlies to a more meridional overturning with frequent southerlies. Although precipitation rates over the northern Alps keep increasing between the HTM and the MCA, such increase in hypoxia is not found in the Baltic Sea. This may be due to a low salinity gradient in the Baltic Sea during these millennia, suppressing the climate forcing.

Starting with the onset of HTM-5, oxygen conditions in the Baltic Sea

gradually became more and more euxinic until the end of HTM-7, probably related to an – on average – expanding total hypoxic area. The occurrence of "micro-events" throughout HTM-5+6 may be caused by temporary contractions in the hypoxic area during its gradual increase on a multi-decadal timescale. Such multi-decadal variability has been found in another lake record from the northern Alps, with possible anti-correlation between the two records. This could be explained by variability in the North Atlantic Oscillation causing out-of-phase fluctuations in storminess between northern Europe, and temperature and precipitation in central and southern Europe.

5.3 Suggestions for the future

The construction of high-resolution LA-ICP-MS (trace) elemental records of sediment cores has many promising applications. Thanks to the high resolution, individual hypoxic events can be analysed in high detail, allowing identification of yearly Mo/Al peaks and summer-winter contrasts. Significant improvement can still be made in the construction of age models of such cores using some form of the peak-counting technique. Important aspects for improvement are increasing objectivity of the method and possibly expansion of floating timescales for individual events to full age models.

Increasing the number of analysed sites may improve assessments of regional-scale variations in hypoxic area. Upon improvement of the calibration procedure, qualitative element-to-element analyses can be performed more confidently. Causes of internal variability within the Baltic Sea may improve understanding of short-term variability in hypoxia throughout the Holocene. These causes may be found by, for example, modelling studies or more detailed studies into the iron-bound phosphorus feedback mechanism.

The cause of terminations of hypoxic events, arguably the aspect of hypoxia most relevant to society, is still unresolved. Although some geo-engineering solutions have been proposed to counter the modern hypoxic event, these are generally not practical options. More investigation into the terminations of older hypoxic events may help understanding of the conditions needed to end current hypoxia in the Baltic Sea. However, conditions during the HTM and MCA may have been significantly different from present-day.

6 Acknowledgements

First and foremost, I would like to thank Tom Jilbert for his excellent supervision for the duration of my thesis. I appreciate the time and effort he has put into helping me on both the practical and theoretical aspects. Thanks as well to Caroline Slomp for taking the time to use regular meetings to give me nudges in the right direction. I had a great time on the Aranda taking sediment cores and am happy I could experience such a cruise. Finally, I would like to thank Bo Gustafsson for providing me with water column oxygen data from the Baltic Environmental Database for all analysed sites.

7 References

Algeo, T.J., Maynard, J.B., 2004. Trace-element behaviour and redox facies in core shales of Upper Pennsylvanian Kansas-type cyclothems. Chemical Geology 206, 289–318.

Algeo, T.J., Lyons, T.W., 2006. Mo-total organic carbon covariation in modern anoxic marine environments: Implications for analysis of paleoredox and paleohydrographic conditions. Paleoceanography 21, PA1016.

Algeo, T.J., Ingall, E., 2007. Sedimentary Corg:P ratios, paleocean ventilation, and Phanerozoic atmospheric pO_2. Palaeogeography, Palaeoclimatology, Palaeoecology 256, 130–155.

Anderson, R.F., Fleisher, M.Q., LeHuray, A.P., 1989. Concentration, oxidation state, and particulate flux of uranium in the Black Sea. Geochimica et Cosmochimica Acta 53, 2215–2224.

Arnaud, F., Révillon, S., Debret, M., Revel, M., Chapron, E., Jacob, J., Giguet-Covex, C., Poulenard, J., Magny, M., 2012. Lake Bourget regional erosion patterns reconstruction reveals Holocene NW European Alps soil evolution and paleohydrology. Quaternary Science Reviews 51, 81–92.

Barnes, C.E., Cochran, J.K., 1991. Geochemistry of uranium in Black Sea sediments. Deep-Sea Research 38, S1237–S1254.

Berglund, B.E., Sandgren, P., Barnekow, L., Hannon, G., Jiang, H., Skog, G., Yu, S.-Y., 2005. Early Holocene history of the Baltic Sea, as reflected in coastal sediments in Blekinge, southeastern Sweden. Quaternary International 130, 111–139.

Berrang, P.G., Grill, E.V., 1974. The effect of manganese oxides scavenging on molybdenum in Saanich Inlet. Marine Chemistry 2, 125–148.

Bertine, K.K., 1972. The deposition of molybdenum in anoxic waters. Marine Chemistry 1, 43–53.

Breit, G.N., Wanty, R.B., 1991. Vanadium accumulation in carbonaceous rocks: a review of geochemical controls during deposition and diagenesis. Chemical Geology 91, 83–97.

Calvert, S.E., Pedersen, T.F., 1993. Geochemistry of recent oxic and anoxic marine sediments: implications for the geological record. Marine Geology 113, 67–88.

Calvert, S.E., Pedersen, T.F., 1996. Sedimentary geochemistry of manganese: implications for the environment of formation of manganiferous black shales. Economic Geology 91, 36–47.

Collier, R.W., 1984. Particulate and dissolved vanadium in the North Pacific Ocean. Nature 309, 441–444.

Conley, D.J., Humborg, C., Rahm, L., Savchuk, O.P., Wulff, F., 2002. Hypoxia in the Baltic Sea and basin-scale changes in phosphorus biogeochemistry. Environmental Science & Technology 36, 5315–5320.

Conley, D.J., Björck, S., Bonsdorff, E., Carstensen, J., Destouni, G., Gustafsson, B.G., Hietanen, S., Kortekaas, M., Kuosa, H., Meier, H.E.M., Mller-Karulis, B., Nordberg, K., Norkko, A., Nürnberg, G., Pitkänen, H., Rabalais, N.N., Rosenberg, R., Savchuk, O.P., Slomp, C.P., Voss, M., Wulff, F., Zillén, L., 2009a. Hypoxia-related processes in the Baltic Sea. Environmental Science & Technology 43, 3412–3420.

Conley, D.J., Bonsdorff, E., Carstensen, J., Destouni, G., Gustafsson, B.G., Hansson, L.A., Rabalais, N.N., Voss, M., Zillén, L., 2009b. Tackling hypoxia in the Baltic Sea: is engineering a solution? Environmental Science & Technology 43, 3407–3411.

Cruse, A.M., Lyons, T.W., 2004. Trace metal records of regional paleoenvironmental variability in Pennsylvanian (Upper Carboniferous) black shales. Chemical Geology 206, 319–345.

Deuser, W.G., Ross, E.H., Anderson, R.F., 1981. Seasonality in the supply of sediment to the deep Sargasso Sea and implications for the rapid transfer of matter to the deep ocean. Deep Sea Research Part A. Oceanography Research Papers 28, 495–505.

Diaz, R.J., Rosenberg, R., 2008. Spreading dead zones and consequences for marine ecosystems. Science 321, 926–929.

Emerson, S.R., Huested, S.S., 1991. Ocean anoxia and the concentration of molybdenum and vanadium in seawater. Marine Chemistry 34, 177–196.

Erickson, B.E., Helz, G.R., 2000. Molybdenum(VI) speciation in sulfidic waters: stability and lability of thiomolybdates. Geochimica et Cosmochimica Acta 64, 1149–1158.

Fonselius, S., 1981. Oxygen and hydrogen sulphide conditions in the Baltic Sea. Marine Pollution Bulletin 12, 187–194.

Fonselius, S., Valderrama, J., 2003. One hundred years of hydrographic measurements in the Baltic Sea. Journal of Sea Research 49, 229–241.

Francois, R., 1988. A study on the regulation of the concentrations of some trace metals (Rb, Sr, Zn, Pb, Cu, V, Cr, Ni, Mn and Mo) in Saanich Inlet sediments, British Columbia, Canada. Marine Geology 83, 285–308.

Fryer, B.J., Jackson, S.E., Longerich, H.P., 1995. The design, operation and role of the laser-ablation microprobe coupled with an inductively cou-

pled plasma–mass spectrometer (LAM-ICP-MS) in the earth sciences. The Canadian Mineralogist 33, 303–312.
Gies, F., Gies, J., 1994. Cathedral, forge, and waterwheel. New York: HarperCollins, ISBN-13: 978–0060925819.
Gray, A.L., 1985. Solid sample introduction by laser ablation for inductively coupled plasma source mass spectrometry. Analyst 110, 551–556.
Gustafsson, B.G., 2000. Time-dependent modelling of the Baltic entrance area. 2. Water and salt exchange of the Baltic Sea. Estuaries 23, 253–266.
Gustafsson, B.G., Westman, P., 2002. On the causes for salinity variations in the Baltic Sea during the last 8500 years. Paleoceanography 17, 12-1–12-14.
Gustafsson, B.G., Stigebrandt, A., 2007. Dynamics of nutrients and oxygen/hydrogen sulde in the Baltic Sea deep water. Journal of Geophysical Research: Biogeosciences 112, G02023.
Gustafsson, E., 2012. Modelled long-term development of hypoxic area and nutrient pools in the Baltic Proper. Journal of Marine Systems 94, 120–134.
Gustafsson, B.G.., Schenk, F., Blenckner, T., Eilola, K., Markus Meier, H.E., Müller-Karulis, B., Neumann, T., Ruoho-Airola, T., Savchuk, P., Zorita, E., 2012. Reconstructing the Development of Baltic Sea Eutrophication 18502006. AMBIO 41, 534–548.
Haltia-Hovi, E., Saarinen, T., Kukkonen, M., 2007. A 2000-year record of solar forcing on varved lake sediment in eastern Finland. Quaternary Science Reviews 26, 678–689.
Helz, G.R., Miller, C.V., Chamock, J.M., Mosselmans, J.L.W., Pattrick, R.A.D., Gamer, C.D., Vaughan, D.J., 1996. Mechanisms of molybdenum removal from the sea and its concentration in black shales: EXAFS evidences. Geochimica et Cosmochimica Acta 60, 3631–3642.
Huerta-Diaz, M.A., Morse, J.W., 1992. Pyritisation of trace metals in anoxic marine sediments. Geochimica et Cosmochimica Acta 56, 2681–2702.
Jensen, H.S., Mortensen, P.B., Andersen, F.O., Rasmussen, E., Jensen, A., 1995. Phosphorus cycling in a coastal marine sediment, Aarhus Bay, Denmark. Limnology and Oceanography 40, 908–917.
Jilbert, T.J., de Lange, G., Reichart, G.-J., 2008. Fluid displacive resin embedding of laminated sediments: preserving trac metals for high-resolution paleoclimate investigations. Limnology and oceanography: methods 6, 16–22.
Jilbert, T.J., Slomp, C.P., Gustafsson, B.G., Boer, W., 2011. Beyond the Fe-P-redox connection: Preferential regeneration of phosphorus from organic

matter as a key control on Baltic Sea nutrient cycles. Biogeosciences 8, 1669–1720.

Jilbert, T.J., Slomp, C.P., 2013a. Rapid high-amplitude variability in Baltic Sea hypoxia during the Holocene. Geology 41, 1183–1186.

Jilbert, T.J., Slomp, C.P., 2013b. Iron and manganese shuttles control the formation of authigenic phosphorus minerals in the euxinic basins of the Baltic Sea. Geochimica et Cosmochimica Acta 107, 155–169.

Kabel, K., Moros, M., Porsche, C., Neumann, T., Adolphi, F., Andersen, T.J., Siegel, H., Gerth, M., Leipe, T., Jansen, E., Sinninghe Damsté, J.S., 2012. Impact of climate change on the Baltic Sea ecosystem over the past 1,000 years. Nature Climate Change 2, 871–874.

Kochenov, A.V., Korolev, K.G., Dubinchuk, V.T., Medvedev, Y.L., 1977. Experimental data on the conditions of precipitation of uranium from aqueous solutions. Geochemistry International 14, 82–87.

Korolev, D.F., 1958. The role of iron sulphides in the accumulation of molybdenum in sedimentary rocks of the reduced zone. Geochemistry International 4, 452–463.

Laskar, J., Fienga, A., Gastineau, M., Manche, H., 2011. La2010: A new orbital solution for the long term motion of the Earth. Astronomy & Astrophysics 532, A89.

Lass, H.-U., Matthäus, W., 1996. On temporal wind variations forcing salt water inflows into the Baltic Sea. Tellus A 48, 663671.

Lenz, C., Behrends, T., Jilbert, T., Silveira, M., Slomp, C.P., 2014. Redox-dependent changes in manganese speciation in Baltic Sea sediments from the Holocene Thermal Maximum: An EXAFS, XANES and LA-ICP-MS study. Chemical Geology 370, 49–57.

Leri, A.C., Hakala, J.A., Marcus, M.A., Lanzirotti, A., Reddy, C.M., Myneni, S.C.B., 2010. Natural organobromine in marine sediments: New evidence of biogeochemical Br cycling. Global biogeochemical cycles 24, GB4017.

Lyons, T.W., Severmann, S., 2006. A critical look at iron paleoredox proxies based on new insights from modern euxinic marine basins. Geochimica et Cosmochimica 70, 5698–5722.

Markus Meier, H.E., Feistel, R., Piechura, J., Arneborg, L., Burchard, H., Fiekas, V., Golenko, N., Kuzmina, N., Mohrholz, V., Nohr, C., Paka, V.T., Sellschopp, J., Stips, A., Zhurbas, V., 2006. Ventilation of the Baltic Sea deep water: A brief review of present knowledge from observations and models. Oceanologia 48, 133–164.

Matthäus, W., Franck, H., 1992. Characteristics of major Baltic inflows–a statistical analysis. Continental Shelf Research 12, 1375–1400.

McManus, J., Berelson, W.M., Klinkhammer, G.P., Hammond, D.E., Holm, C., 2005. Authigenic uranium: relationship to oxygen penetration depth and organic carbon rain. Geochimica et Cosmochimica Acta 69, 95–108.

Meier, H.E.M., Feistel, R., Piechura, J., Arneborg, L., Burchard, H., Fiekas, V., Golenko, N., Kuzmina, N., Mohrholz, V, Nohr, C., Paka, V.T., Sellschopp, J., Stips, A., Zhurbas, V., 2006. Ventilation of the Baltic Sea deep water: A brief review of present knowledge from observations and models. Oceanologia 48, 133–164.

Meier, H.E.M., Eilola, K., Almroth, E., 2011. Climate-related changes in marine ecosystems simulated with a three-dimensional coupled biogeochemical-physical model of the Baltic Sea. Climate Research 48, 31–55.

Middelburg, J.J., de Lange, G.J., van der Weijden, C.H., 1987. Manganese solubility control in marine pore waters. Geochimica et Cosmochimica Acta 51, 759–763.

Morford, J.L., Emerson, S.R., 1999. The geochemistry of redox sensitive trace metals in sediments. Geochimica et Cosmochimica Acta 63, 1735–1750.

Ojala, A.E.K., Alenius, T., 2005. 10 000 years of interannual sedimentation recorded in the Lake Nautajärvi (Finland) clastic-organic varves. Palaeogeography, Palaeoclimatology, Palaeoecology 219, 285–302.

Omstedt, A., Hansson, D., 2006. The Baltic Sea ocean climate system memory and response to changes in the water and heat balance components. Continental Shelf Research 26, 236–251.

Pedersen, T.F., Price, N.B., 1982. The geochemistry of manganese carbonate in Panama Basin sediments. Geochimica et Cosmochimica Acta 46, 59–68.

Pohl, C., Löffler, A., Hennings, U., 2004. A sediment trap flux study for trace metals under seasonal aspects in the stratified Baltic Sea (Gotland Basin; 57deg 19.20'N; 20deg 03.00'E). Marine Chemistry 3–4, 143–160.

Raiswell, R., Canfield, D.E., 2012. The iron biogeochemical cycle past and present. Geochemical Perspectives 1. Rajendran, A., Dileepkumar, M., Bakker, J.F., 1992. Control on manganese and iron in Skagerrak sediment (northeastern North Sea). Chemical Geology 98, 111–129.

Reissmann, J.H., Burchard, H., Feistel, R., Hagen, E., Lass, H.U., Mohrholz, V., Nausch, G., Umlauf, L., Wieczorek, G., 2009. Vertical mixing in the Baltic Sea and consequences for eutrophication–a review. Progress in Oceanography 82, 47–80.

Richards, F.A., 1965. Anoxic basins and fjords. Chemical Oceanography 611–643. London, New York, Academic Press, 1965–(OCoLC)609135016.

Rudnicki, M.D., Elderfield, H., 1993. A chemical model of the buoyant and neutrally buoyant plume above the TAG vent field, 26N, Mid-Atlantic Ridge. Geochimica et Cosmochimica Acta 57, 2939–2958.

Ruttenberg, K.C., 1993. Reassessment of the Oceanic Residence Time of Phosphorus. Chemical Geology 107, 405–409.

Savchuk, O.P., Wulff, F., Hille, S., Humborg, C., Pollehne, F., 2008. The Baltic Sea a century ago — a reconstruction from model simulations, verified by observations. Journal of Marine Systems 74, 485–494.

Schlesinger, M.E., Ramankutty, N., 1994. An oscillation in the global climate system of period 65–70 years. Nature 367, 723–726.

Seppä, H., Birks, H.J.B., 2001. July mean temperature and annual precipitation trends during the Holocene in the Fennoscandian tree-line area: pollen-based climate reconstructions. The Holocene 11, 527–539.

Simms, A., 1976. Deserted medieval villages and fields in Germany. Journal of Historical Geography 2, 223–238.

Sohlenius, G., Erneis, K.C., Andren, E., Andren, T., Kohly, A., 2001. Development of anoxia during the Holocene fresh-brackish water transition in the Baltic Sea. Marine Geology 177, 221–242.

Spencer, D.W., Brewer, P.G., 1971. Vertical advection diffusion and redox potentials as controls on the distribution of manganese and other trace metals dissolved in waters of the Black Sea. Journal of Geophysical Research 76, 5877–5892.

Swierczynski, T., Lauterbach, S., Dulski, P., Delgado, J., Merz, B., Brauer, A., 2013. Mid- to late Holocene flood frequency changes in the northeastern Alps as recorded in varved sediments of Lake Mondsee (Upper Austria). Quaternary Science Reviews 80, 78–90.

Todd, J.F., Elsinger, R.J., Moore, W.S., 1988. The distributions of uranium, radium and thorium isotopes in two anoxic fjords; Framvaren Fjord (Norway) and Saanich Inlet (British Columbia). Marine Chemistry 23, 39.–415.

Tribovillard, N., Algeo, T.J., Lyons, T., Riboulleau, A., 2006. Trace metals as paleoredox and paleoproductivity proxies: an update. Chemical Geology 232, 12–32.

Vaquer-Sunyer, R., Duarte, C.M., 2008. Thresholds of hypoxia for marine biodiversity. Proceedings of the National Academy of Sciences 105, 15452–15457.

Van Cappellen, P., Ingall, E.D., 1997. Redox stabilization of the atmosphere and oceans and marine productivity. Science 275, 406–408.

Van der Sloot, H.A., Hoede, D., Wijkstra, J., Duinker, J.C., Nolting, R.F., 1985. Anionic species of V, As, Se, Mo, Sb, Te and W in the Scheld and Rhine estuaries and the Southern Bight (North Sea). Estuarine Coastal Shelf Science 21, 633–651.

Vorlicek, T.P., Kahn, M.D., Kasuza, Y., Helz, G.R., 2004. Capture of molybdenum in pyrite-forming sediments: role of ligand-induced reduction by polysulfides. Geochimica et Cosmochimica Acta 68, 547–556.

Walløe, L., 1995. Plague and Population–Norway 1350-1750. Norwegian Academy of Science and Letters, Oslo, 1–48.

Wanty, R.B., Goldhaber, M.B., 1992. Thermodynamics and kinetics of reactions involving vanadium in natural systems: Accumulation of vanadium in sedimentary rocks. Geochimica et Cosmochimica Acta 56, 1471–1483.

Wehrli, B., Stumm, W., 1989. Vanadyl in natural waters: adsorption and hydrolysis promote oxygenation. Geochimica et Cosmochimica Acta 53, 69–77.

Widerlund, A., Andersson, P.S., 2006. Strontium isotopic composition of modern and Holocene mollusc shells as a palaeosalinity indicator for the Baltic Sea, Chemical Geology 232, 5466.

Zheng, Y., Anderson, R.F., van Geen, A., Fleisheir, M.Q., 2002. Preservation of non-lithogenic particulate uranium in marine sediments. Geochimica et Cosmochimica Acta 66, 3085–3092.

Ziegler, M., Jilbert, T.J., de Lange, G.J., Lourens, L.J., Reichart, G.J., 2008. Bromine counts from XRF scanning as an estimate of the marine organic carbon content of sediment cores. Geochemistry, Geophysics, Geosystems 9, Q05009.

Zillén, L., Conley, D.J., Andrn, T., Andrén, E., Björck, S., 2008. Past occurrences of hypoxia in the Baltic Sea and the role of climate variability, environmental change and human impact. Earth Science Reviews 91, 77–92.

Zillén, L., Conley, D.J., 2010. Hypoxia and cyanobacteria blooms — are they really natural features of the late Holocene history of the Baltic Sea? Biogeosciences 7, 2567–2580.

Zillén, L., Lenz, C., Jilbert, T., 2012. Stable lead (Pb) isotopes and concentrations–a useful independent dating tool for Baltic Sea sediments. Quaternary Geochronology 8, 41–45.